AN INVESTIGATION OF THE MECHANICAL IMPLICATIONS OF SACROPLASTY USING FINITE ELEMENT MODELS BASED ON TOMOGRAPHIC IMAGE DATA

by

Dennis Earl Anderson

Thesis submitted to the Faculty of
Virginia Polytechnic Institute and State University
in partial fulfillment of the requirements for the degree of

MASTER OF SCIENCE

in

Engineering Mechanics

John Cotton, Chair
Michael Madigan
J. Wallace Grant

April 25, 2005
Blacksburg, Virginia

Keywords: finite element modeling, sacroplasty, bone cement, CT images

AN INVESTIGATION OF THE MECHANICAL IMPLICATIONS OF SACROPLASTY USING FINITE ELEMENT MODELS BASED ON TOMOGRAPHIC IMAGE DATA

by
Dennis Earl Anderson
Committee Chairman: John Cotton
Engineering Mechanics

(Abstract)

Sacral insufficiency fractures are an under-diagnosed source of acute lower back pain. A polymethylmethacrylate (PMMA) cement injection procedure called sacroplasty has recently been utilized as a treatment for sacral insufficiency fractures. It is believed that injection of cement reduces fracture micromotion, thus relieving pain. In this study, finite element models were used to examine the mechanical effects of sacroplasty.

Finite element models were constructed from CT images of cadavers on which sacroplasties were performed. The images were used to create the mesh geometry, and to apply non-homogeneous material properties to the models. Models were created with homogeneous and non-homogeneous material properties, normal and osteoporotic bone, and with and without cement.

The results indicate that the sacrum has a 3D multi-axial state of strain. While compressive strains were the largest, tensile and shear strains were significant as well. It was found that a homogeneous model can account for around 80% of the variation in strain seen in a non-homogeneous model. Thus, while homogeneous models provide a reasonable estimate of strains, non-homogeneous material properties have a significant effect in modeling bone. A reduction in bone density simulating osteoporosis increased strains nearly linearly, even with non-homogeneous material properties. Thus, the non-homogeneity was modeled similarly in both density cases. Cement in the sacrum reduced

strains 40-60% locally around the cement. However, overall model stiffness only increased 1-4%. This indicates that the effects of sacroplasty are primarily local.

Acknowledgements

I would like express my appreciation to Dr. Cotton, my advisor and committee chairman, for his support while writing this thesis. In addition to providing general direction and advice, he also helped solve computer-related issues throughout the process. Of particular note, he took the time to set up the Bonemat code for our purposes.

My thanks to Pearse Morris of the Division of Radiologic Sciences at Wake Forest University School of Medicine for providing the CT images used as source data for the models. My thanks to Drs. Grant and Madigan for serving on my committee. I would also like to thank my parents, James and Darla, for their love, encouragement, and friendship.

Table of Contents

List of Figures

List of Tables

List of Equations

Chapter 1: Introduction

The mechanical responses of the human skeletal system to various conditions are of clinical interest. However, being biological structures, bones have geometric and material complexities that make them difficult to analyze. Because of this, the finite element method has frequently been used to model components of the skeletal system.

This thesis describes an examination of the sacrum using the finite element method. Finite element models were created using computed tomography (CT) images as source information for both the geometry and material properties. The primary goal of the model was to quantify the effect of injecting polymethylmethacrylate (PMMA) cement into the sacrum, a procedure termed a sacroplasty.

This chapter presents background information that is relevant to a finite element examination of sacroplasty. Important features of sacral anatomy are described. The background of the sacroplasty is summarized, including its relation to the more common vertebroplasty. Previous finite element models relevant to this research are reviewed and the use of CT images in finite element modeling is discussed.

1.1 The Sacrum

The sacrum is a roughly triangular bone located at the base of the vertebral column. It serves an important function in the human skeleton, in that it serves as a foundation for both the vertebral column and the pelvic girdle. The sacrum forms the posterior wall of the pelvic cavity, and is curved, with the anterior surface being concave. The sacrum is formed from five sacral vertebrae that fuse together. Due to this composite nature, the geometry of the sacrum is relatively complicated.

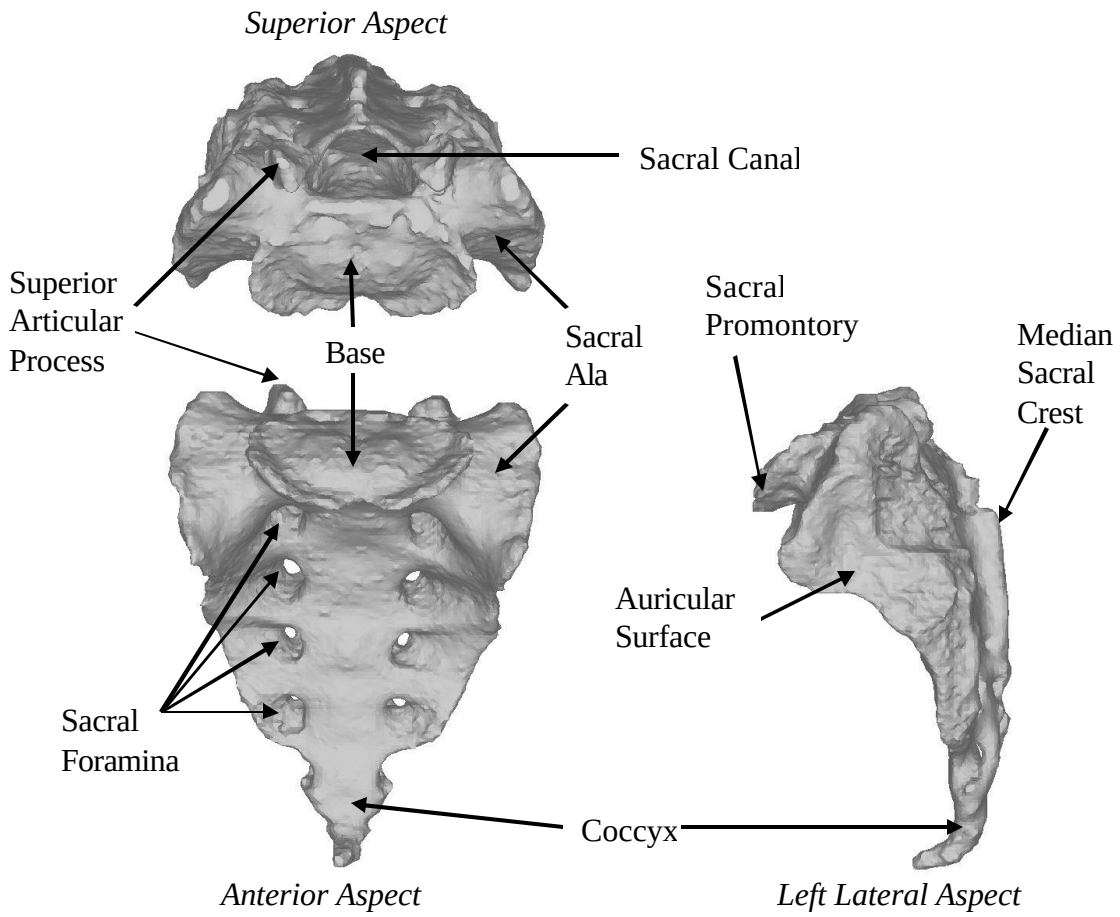

Figure 1.1: Anatomy of the sacrum

Important anatomic features of the sacrum, illustrated in Figure 1.1, are as follows. The superior surface of the first sacral vertebra, which articulates with the fifth lumbar vertebral body, is called the *base* of the sacrum. The anterior protruding edge is the sacral *promontory*. The *superior articular processes* are posterior of the base, and articulate with the inferior articular processes of the fifth lumbar vertebra. The transverse processes of the sacral vertebrae form the sacral lateral mass, or *sacral ala*. The sacrum articulates with the ilia at the *auricular surface* on each side. The rough areas posterior to the auricular surface provide attachment points for the sacroiliac ligaments. The *sacral canal* serves as a continuation of the spinal canal housing the spinal cord. The *sacral foramina* allow nerves and blood vessels to communicate from anterior and posterior sides, and with the sacral canal. The *median sacral crest* runs down the center of the posterior of the sacrum. At the inferior end, the sacrum articulates with the *coccyx*. (Williams, 1989, Tortora, 1984)

Similar to the vertebrae, the sacrum is comprised largely of cancellous bone with an external shell of cortical bone. Cancellous bone, also called trabecular or spongy bone, is characterized by open spaces, often filled with red marrow. The structure of cancellous bone is a lattice-work of interconnected plates and rods called trabeculae. By comparison cortical, or compact, bone is relatively solid. The difference between cancellous and cortical bone may be defined by the amount of porosity, or open space, present. In general, the porosity of cortical bone is 5 – 30%, while that of cancellous bone ranges from 30 – 90% (Carter, 1977).

1.2 Sacral Insufficiency Fractures

Stress fractures in bone are fractures due to repetitive sub-critical loads, and are divided into two types, fatigue fractures and insufficiency fractures (Pentecost, 1964). The distinction depends on whether the fracture occurs in normal bone (fatigue fracture) or bones with reduced mineralization and elasticity (insufficiency fracture). Fatigue fractures of the sacrum have been described in the literature occurring in runners, a pregnant woman, and military recruits (Weber, 1993). On the other hand, sacral insufficiency fractures are observed in conjunction with osteoporosis, osteopenia, and calcium metabolism disorders (Weber, 1993). Other risk factors include corticosteroid therapy, radiation therapy in the pelvic region, and arthritis (Babayev, 2000). Given these risk factors, sacral insufficiency fractures are most likely to appear in the elderly.

Sacral insufficiency fractures were first described as a specific clinical condition by Lourie (1982). The vast majority of cases occur in women, comprising 93% of the cases in the literature reviewed by Weber (1993). Insufficiency fractures are usually located lateral to the sacral foramina, parallel to the sacroiliac joint, as opposed to traumatic fractures, which usually occur near the sacral foramina or sacral canal (Weber, 1993). Sacral insufficiency fractures usually present clinically as pain in the pelvis, lower back, or buttocks, sometimes with pain extending to the lower limbs (Weber 1993, Grasland, 1996). Although the symptoms may be initiated by trauma, such as a fall, often sacral insufficiency fractures are not brought about by a particular traumatic event.

The literature makes it clear that diagnosis of sacral insufficiency fracture has been a problem. Due to the non-specific nature of these symptoms, sacral insufficiency fractures are frequently misdiagnosed (Grasland, 1996). The symptoms may suggest

other conditions such as lumbosacral radicular compression from disk disease, spinal stenosis or tumor (Lourie, 1982). Conventional radiography often does not show evidence of sacral insufficiency fractures, adding to the possibility of misdiagnosis. Bone scintigraphy is a much more sensitive diagnostic tool, as is computed tomography and magnetic resonance imaging (Babayev, 2000, Weber, 1993).

TREATMENT

The treatment for sacral insufficiency fractures specified in some of the literature consists of bed rest and analgesics, followed by a return to normal activities over a period of months (Grasland, 1996, Newhouse, 1992). However, Babayev (2000) argues against this, citing the adverse effects of extended immobility, especially when applied to the elderly. Extended bed rest has numerous deleterious effects, including decreased cardiac output and aerobic capacity, predisposition to pneumonia, muscle atrophy, bone loss, constipation, incontinence and pressure sores on the skin. The elderly are especially sensitive to these effects, as even a moderate decline in health may result in a significant loss of functional ability (Harper, 1988).

Taillandier (2003) studied the outcomes of pelvic fractures in sixty patients (average age 83 ± 7.1) and found that at one year the mortality rate was not significantly higher than the general population. However, only 36.6% had regained their pre-fracture level of self sufficiency. Reducing patient immobilization time could allow a better recovery rate.

Because sacral insufficiency fractures are usually stable and do not require operative intervention, Babayev (2000) recommends that treatment include early

mobilization with pain control. This approach does reduce the risks associated with bed rest, but really only calls for management of symptoms.

Recently a cement injection procedure, termed a sacroplasty, has been utilized in the treatment of sacral insufficiency fractures (Garant, 2002, Pommersheim, 2003). This procedure consists of the injection of polymethylmethacrylate (PMMA) cement into the sacrum. Such a procedure was first utilized to provide pain relief in patients with bone metastases (Dehdashti, 2000, Marcy, 2000). In the case of fractures, the cement serves as artificial support in the weakened bone. Thus, sacroplasty represents a proactive treatment option for sacral insufficiency fracture.

Garant (2002) reported a single case of sacral insufficiency fracture in a 63 year old woman and Pommersheim (2003) reported 3 cases, involving women aged 71, 74, and 76. All four patients suffered from severe lower back pain that affected their daily function. Two were bedridden, one used a wheelchair, and one used a walker. Following sacroplasty, symptoms improved immediately in all four cases. Followups in three patients reported them to be pain free and ambulatory. Thus, in the short term sacroplasty appears to be successful in treating sacral insufficiency fractures, with pain relief and improved function in daily activities (Pommersheim, 2003).

1.3 Vertebroplasty

The sacroplasty is a variation of the vertebroplasty technique, a treatment for vertebral compression fractures. The concepts of the sacroplasty and the vertebroplasty are essentially the same: percutaneous injection of cement into the core cancellous bone for crack stabilization and strength augmentation. However, the sacroplasty presents greater procedural difficulty, because the skeletal geometry at the level of the sacrum makes imaging and proper needle placement more difficult (Dehdashti, 2000, Garant, 2002, Pommersheim, 2003).

Because sacroplasty is a relatively new procedure, it has not been studied extensively. Comparitively, vertebroplasty has been well studied. The biomechanics of vertebroplasty have been the subject of numerous experimental studies and several finite element studies, as reviewed by Wilcox (2004). Because of the similarity between the procedures, an overview of vertebroplasty research is worthwhile when studying sacroplasty.

BACKGROUND

Vertebroplasty was first developed in the 1980s (Galibert, 1987, Bascoulergue, 1988) and has become a widespread treatment for pathologic vertebral compression fractures caused by the weakening of the vertebral bodies (Wilcox, 2004). Loss of strength of a vertebral body may be due to benign or malignant tumors, or to the loss in bone density associated with osteoporosis (Mathis, 2001). Vertebroplasty is an attractive treatment option for several reasons. These include successful relief of pain in 67 to

100% of cases, rapid results (pain relief within 1 day) and low complication rates (Mathis, 2001, Watts, 2001).

Several mechanisms have been suggested in the literature for the pain relief caused by vertebroplasty. These include destruction of nerve endings by the heat of the cement polymerization reaction or by the toxicity of the cement monomer. However, the more likely explanation appears to be that mechanical stabilization eliminates painful motion at the fracture site (Belkoff, 2001, Mathis, 2001, San Millan, 1999).

Three major variables in the vertebroplasty are the amount, placement and type of cement. The amount of cement injected has a significant effect, while the type of cement used does not (Wilcox, 2004). As little as 2 mL of cement may restore the fracture strength of the vertebral body, while 4-8 mL can restore pre-fracture stiffness (Belkoff, 2001). Distribution has been examined by comparing unilateral and bilateral injections of cement. Finite element analysis (Liebschner, 2001) suggests the bilateral approach is preferable because of the symmetry it provides, although experimental tests (Tohmeh, 1999) found no significant difference.

Vertebroplasty can greatly increase both vertebral strength and stiffness. However, evidence indicates that overstiffening of the vertebral body is not desirable. Post-vertebroplasty fracture of adjacent spinal levels has been observed clinically (Barr, 2000). Berlemann (2002) showed that vertebroplasty reduces the failure load of two-body spinal segments, with failure occurring in to the untreated body. Thus, vertebroplasty can adversely affect loads in adjacent vertebrae.

Patients who experience a vertebral compression fracture are at high risk of additional fractures (Wasnich, 1996), and the effects of vertebroplasty on adjacent

vertebrae can increase that risk. In addition to post-fracture treatment, vertebroplasty has also been used as a preventive treatment (Barr, 2000, Heini, 2000). In fact, Sun (2004) suggests that vertebroplasty is more effective as vertebral reinforcement than fracture repair. The same may be true of sacroplasty. However, the use of either sacroplasty or vertebroplasty as a purely preventive treatment would require improvements in fracture risk assessment.

RELATION TO SACROPLASTY

The similarities between vertebroplasty and sacroplasty are notable, and can provide some general insight into the sacroplasty. For example, pain relief due to mechanical stabilization of a fracture should be equally applicable in vertebrae or sacrum. However, specific information, such as the amount of cement used in vertebroplasty, is probably less relevant to the sacroplasty.

Despite the similarities in the procedures, it should be noted that the differences between sacrum and vertebrae are not negligible. For example, the loads undergone by sacrum and vertebrae are not directly comparable. The mechanical state in a vertebral body is primarily one of simple compression, as the adjacent bodies are roughly opposite each other. However, the sacrum articulates superiorly and laterally, left and right, as illustrated in Figure 1.2. Additionally, several muscles, such as the gluteus maximus, erector spinae and piriformis, attach directly to the sacrum. These things mean the loading situation for the sacrum is relatively complex. Thus, care should be taken not to over-exaggerate the connection between vertebroplasty and sacroplasty.

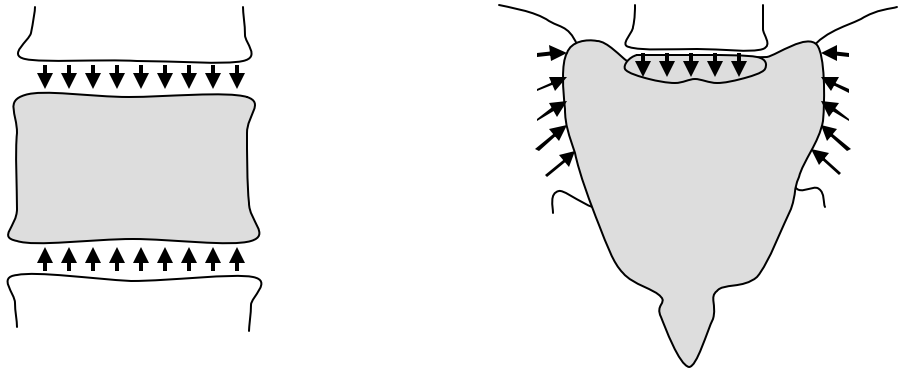

Figure 1.2: Loading of sacrum versus vertebral body. This simple comparison of loading on a vertebral body (left) and the sacrum (right) shows the greater complexity of sacral loads. Loads on the vertebral body can be described as simple compression, while the sacrum is likely to include significant shear components as well.

1.4 Finite Element Modeling

This section presents background information relevant to the finite element analysis of sacroplasty. Finite element models of particular interest were reviewed in the literature. These include finite element models of the sacrum and models examining vertebroplasty. The use of CT images as source data for creating finite element models was examined, including using CT data to derive material properties.

PRIOR FINITE ELEMENT MODELS

A search of the literature found few finite element models that include the sacrum. Dawson (1999) modeled the entire pelvis to examine loading during lateral impact fractures. Garcia (2000) modeled the entire pelvis, including sacrum, to examine the stability of pelvic ring fracture fixation methods. Ezquerro (2004) and Charriere (2003) created models that included the sacrum, which served as a base when examining lumbar spine biomechanics. However, the sacrum was incidental to the primary focus of these two studies. Although these studies provide a precedent for finite element modeling of the sacrum, none of them examine the sacroplasty procedure.

Vertebroplasty has been the subject of several finite element models (Kosmopoulos, 2004, Liebschner, 2001, Polikeit, 2003, Tack, 2001). However, they examine relatively diverse aspects of the vertebroplasty procedure. Liebschner (2001) examined the effects of cement volume and placement by inserting ‘cement’ cylinders into a model of a vertebral body. Tack (2001) also examined the effect of cement volume, along with the importance of patient bone mineral density (BMD) in determining

necessary injection volumes. Polikeit (2003) examined the effect of vertebroplasty on load transfer between levels with a two-vertebra model.

It should be noted that in all of these cases cancellous bone was modeled as a continuum material rather than as a structure of individual trabeculae. While the trabecular architecture has definite effects on material properties (Goldstein, 1987), creating a finite element model including actual trabeculae presents difficulties. First, defining the geometry of the trabeculae, although possible, requires a high-resolution CT scan (Augat, 1998). Second, modeling individual trabeculae on a whole-bone scale will result in very large models. Kosmopoulos (2004) modeled individual trabeculae in an examination of the effects of percent fill and cement modulus on vertebroplasty. However, this model was two-dimensional, based on a saggital plane section of a thoracic vertebra, and as such was naturally less extensive than a whole-vertebra model.

MODELING MATERIAL PROPERTIES

Computed tomography (CT) describes a procedure in which x-ray transmission measurements made at multiple angles around an object are used to reconstruct a section, or slice, of the object. Each local volume of interest, the size of which depends on scanner resolution, is called a voxel. The CT numbers measured for a voxel are related to the x-ray attenuation coefficient of the material in that volume. This allows differentiation between materials with different attenuation coefficients. Clinically, CT numbers are often expressed in Hounsfield units, in which the relative density of air is -1000 HU and the density of water is 0 HU (Goodenough, 2000). A three-dimensional

scan is formed by combining multiple adjacent slices. The CT image is essentially a three-dimensional array in which the CT numbers are stored.

CT images are commonly used in the creation of finite element models of bone. They provide accurate information on bone geometry, can be interpreted to provide mechanical properties, and allow the modeling of bones *in vivo* (Marom, 1990). All of the models reviewed used CT image information in developing the model geometry. However, only one (Dawson, 1999) used the brightness information of the CT image to calculate the material properties of the elements.

The material properties of cancellous bone vary greatly and depend on factors such as anatomic location and bone density (Goldstein, 1987). Thus cancellous bone is a non-homogeneous material, and may differ from point to point within the same bone. It is also known to be anisotropic, generally showing the greatest stiffness in the direction of the greatest functional loads. For example, cancellous samples from the vertebral bodies were found to have greater stiffness in the superior-inferior direction than anterior-posterior or medial-lateral (Augat, 1998). However, pelvic cancellous bone is "not highly anisotropic" (Dalstra, 1993) as compared to that in regions such as vertebrae or tibia with more constant loading directions.

In the current study, the material properties used were non-homogeneous, linear elastic and isotropic. Assuming isotropic materials is a simplification. However, with the exception of Liebschner (2001), none of the models examined in the literature attempted to include anisotropy in element material properties. On the other hand, with the exception of Dawson (1999), all use homogeneous material properties, generally differentiating only between cancellous and cortical bone. According to Dalstra (1995),

in a study of the pelvic bone, using homogeneous properties is not a bad assumption. However, non-homogeneous properties did provide better results, as the homogeneous models overestimated stresses.

By using the CT image as a source of information, an estimation of non-homogeneous material properties can be made. In experimental tests, linear relations between CT image numbers and cancellous bone density have proved to be statistically significant. Ciarrelli (1991) gives a coefficient of determination of $R^2 = 0.82$, while McBroom (1985) gives a value of $R^2 = 0.89$. A variety of empirical relations have been developed that relate bone density to elastic modulus. According to a review of this work by Martin (1991), the elastic modulus of cancellous bone is roughly proportional to the density squared, and to density cubed for cortical bone. Thus, CT image brightness can be converted to bone density, and bone density to elastic modulus, providing an estimate of material properties throughout the bone.

The most common strategy when creating non-homogeneous properties from CT images has been to assume that material variation within each element is negligible, and calculate an average value at each element (Taddei, 2004). First, the CT numbers within the element volume are averaged. Then the value for each element can be converted to elastic modulus using the CT to density and density to modulus relations. Thus each element is homogeneous, but the material properties vary among the elements.

Several different methods of calculating element averages from the CT numbers can be found in the literature. Merz (1996) took the material values nearest to each element node and averaged them. Zannoni (1998) used an average of all material values within the element. Cattaneo (2001) used a geometrically weighted average of the eight

CT grid values nearest the element centroid. Finally, Taddei (2004) used a numerical integration over the volume of the element, providing the best estimation of the element average, though with increased computational effort.

1.5 Summary of Research

Finite element models of the upper pelvis were created. Mesh geometry was defined from CT images of two cadavers on which sacroplasty had been performed. The CT images were then used to apply non-homogeneous material properties to the meshes. A primary mesh was created from each image. These were used as the basis for the models. The material properties applied to the mesh were modified to create models representing different situations of interest.

To check model convergence, two additional meshes were created from one image, using smaller element sizes. Identical homogeneous material properties were applied to the three different meshes. The results in the regions of interest were compared to determine the effect of mesh size.

The importance of using non-homogeneous properties was examined. Homogeneous models were created corresponding to each non-homogeneous model. A homogeneous model was created by changing the elastic modulus of all elements to the mean elastic modulus of the non-homogeneous model. The homogeneous models were compared with corresponding non-homogeneous models to determine the amount of variation due to non-homogeneous properties.

Because sacroplasty is likely to be performed on osteoporotic individuals, models simulating osteoporosis were also created. Osteoporosis was simulated by reducing the bone density calculated from the CT images. This reduced the elastic modulus values applied to the models. The effects of osteoporosis were examined by comparing the normal and reduced density cases.

The effects of cement, as the primary interest of this research, were examined by creating models to represent the cases with and without cement. The cases without cement were created by reducing the elastic modulus of the ‘cement’ elements to a value representing cancellous bone.

Comparisons between the various models were primarily based on the principal strains. This was done both on a whole model scale and locally. Local strain comparisons were performed in regions of interest defined in the locations of cement in the sacrum.

Chapter 2: Materials and Methods

In this chapter, the materials and methods utilized in the finite element examination of the sacrum are described. The CT images used as data sources are presented in Section 2.1. Section 2.2 describes the modeling process used to move from CT image data to a finite element model. Details of the specific models created and used in the finite element analysis are presented in Section 2.3. Descriptions of the analyses performed can be found in Section 2.4.

2.1 CT Images

Sacroplasty procedures were performed on multiple anatomic cadavers at Wake Forest University. The ages and medical conditions of the specimens are unknown, however they are not believed to have had osteoporosis. About 3-7 ml of cement, mixed with barium sulphate for opacity, was injected on each side of the sacrum (Morris, 2005).

CT scanning was performed using a GE scanner at Wake Forest University (Morris, 2005). The images show the pelvic region, roughly from the L5 vertebra to the proximal femur. Scans were performed both before and after the sacroplasty procedure. The images were received in the Dicom format, a standard format for medical imaging. Two post-procedure images, called “Male Post 03” and “Pelvis Post 05” were used in the creation of the finite element models. These will be referred to as Male Post 3, or MP3, and Pelvis Post 5, or PP5, in this thesis.

2.2 Model Development

Finite element models of the sacrum were created using CT images of the pelvic region as a source of information. To progress from a CT image to a finite element model required a number of steps, including:

- Image processing to define the relevant geometric data
- Creation and refinement of a finite element mesh from the geometric data
- Combining image data and the completed finite element mesh to calculate element material properties
- Defining and applying loads and boundary conditions

Figure 2.1 shows an outline of the process, and identifies the main steps and the software used in each step.

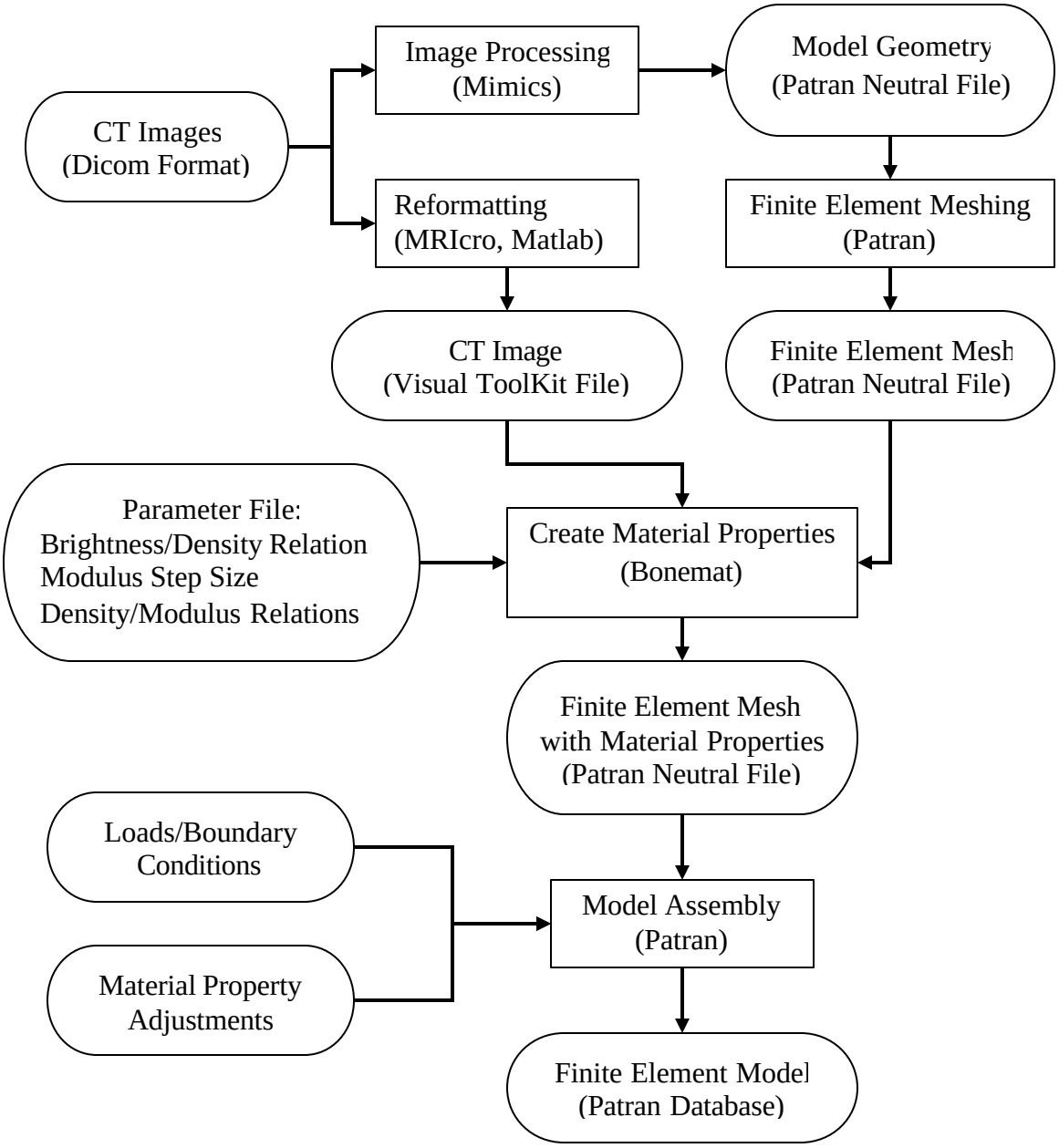

Figure 2.1: The modeling process. Major steps are shown in boxes, with the software used in parentheses. Inputs/outputs are shown in the rounded boxes, along with file types if applicable.

IMAGE PROCESSING

The first step in creating a model was to isolate the desired geometry, based on the CT image. In this case the sacrum, where the cement was injected, is central to the desired geometry. It was decided that including the entire pelvis in the model was unnecessary. The inferior portion of the pelvis was removed by “cutting” through the ilia, extending anteriorly from the greater sciatic notch (see Figure 2.2). The inclusion of the superior parts of the ilia serves to separate the locations of the injected cement (near the sacroiliac joint) from the applied boundary conditions, and additionally simplifies the application of boundary conditions.

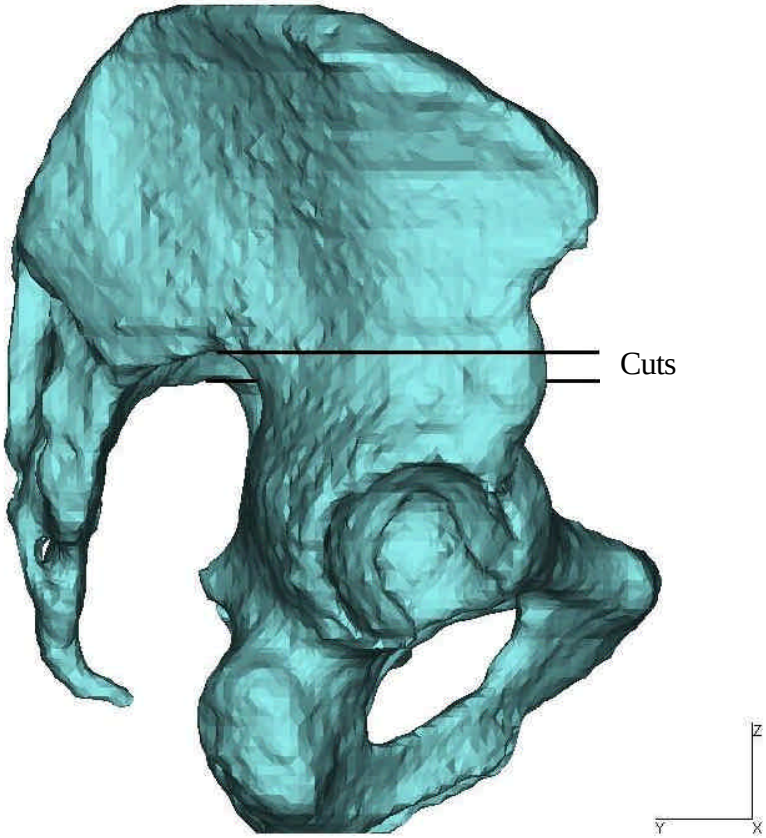

Figure 2.2: Removal of lower pelvis. Cuts in the ilia were in transverse planes, approximately level with the greater sciatic notch.

The program Mimics, (Materialise Software, Ann Arbor, Michigan, USA) was used to select the desired geometry for the model. The selected portions of the image are referred to as a mask. Thresholding, or selecting a range of brightness values, can quickly create a mask that includes only bony tissue. The L5 vertebra was manually separated from the sacrum mask and removed. The planar cuts through the ilia were also created manually. If needed, a reference plane can be created in Mimics to serve as a guide when creating the cuts. When the cuts were completed, the inferior portion of the pelvis was removed from the mask.

In addition to removing the soft tissue, the thresholding operation removes much of the cancellous bone because it is less dense than the cortical bone. This leaves holes and openings in the sacrum mask, where there is actually bone tissue. These were filled in using a combination of freehand drawing and fill operations. The resulting mask was ‘solid’, with all the bony tissue included.

While the geometry of the sacrum is relatively complex, a particular problem was presented by the sacral foramina and the sacral canal. When carried through to the finite element model, these features caused considerable difficulty. Thus it was decided to simplify the model geometry by filling the sacral foramina and the sacral canal. Similar simplifications were made by filling fissures along the posterior side of the sacroiliac joints. It was felt that the resulting deviation of the model from the actual bone geometry is justified by the decrease in meshing problems. Additionally, the use of image based material properties (discussed later) should mitigate the effects of these simplifications.

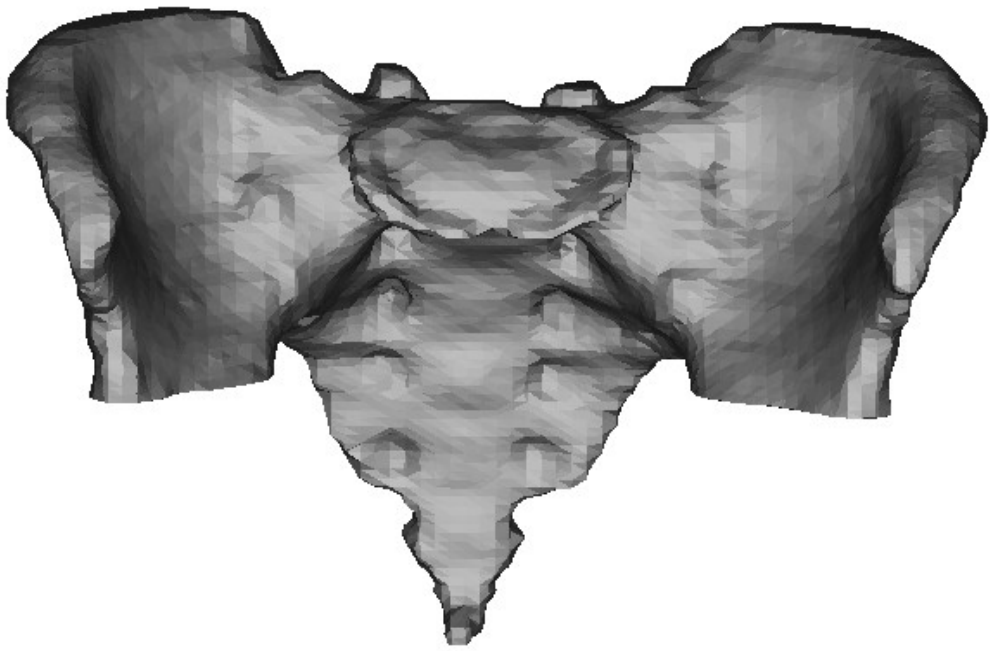

Figure 2.3: 3D surface representation used for model creation. This shows the geometry created in Mimics from the image Male Post 03. The final geometry included the entire sacrum and coccyx, as well as the superior portion of each ilia. The sacral canal and sacral foramina were filled in.

When image processing was complete, a 3D representation of the sacrum geometry was created in Mimics to serve as the basis of the finite element model geometry. Figure 2.3 shows an example of the 3D representation, which is actually a surface made up of triangular faces. The 3D surface representation created in Mimics was exported as a Patran neutral file, in which the geometry is represented by a mesh of triangular surface elements. This file was imported into Patran and used for finite element modeling.

FINITE ELEMENT MESHING

The finite element mesh was created using MSC.Patran, (MSC Software, Santa Ana, California, USA) based on the surface geometry imported from Mimics. The imported mesh provided a good representation of the geometry, but was not optimized for

finite element analysis. A new surface mesh was created in Patran using the Mesh on Mesh function, which creates a new mesh based on an existing one. During this operation, the global edge length was set, defining the approximate element size for the model.

The surface mesh created from the original geometry still contained poor elements, or elements which failed the element verification tests. The two main verification tests for triangular elements are Aspect and Skew. The Aspect test checks the ratio of element length and width. The Skew test checks the angular deviation of the element, which is zero for an equilateral triangle. Failed elements occur most frequently in areas where the surface geometry is complicated, which includes much of this model.

Mesh improvement was accomplished by methodically improving failed elements, beginning with the worst. There are a number of ways that elements can be improved. Most commonly, small areas were selected for automatic remeshing. Other methods used include manually redefining elements, or manually moving a node.

The completed surface meshes were used to create solid meshes of first order (linear) 4-node tetrahedral elements (Patran element type Tet4). These meshes model the geometry of the bones using three-dimensional elements, and served as the meshes for finite element analysis. Four different solid meshes were used in the analysis, as described in Section 2.3.

APPLYING MATERIAL PROPERTIES

Determining the element elastic modulus values from the CT images involved several steps. First, the average element brightness values based on the CT image brightness data were calculated. A linear relationship between image brightness and bone

density was used to estimate the density of each element. Finally, empirical relationships between bone density and the elastic modulus were used to assign an elastic modulus value to each element. The program for determining element stiffness values was based on the public domain Bonemat V2 code, developed by Taddei et al (2004), and available at http://www.tecno.ior.it/back2net/.

Three inputs were required for Bonemat V2, the CT image, the finite element mesh, and a parameter file. The CT images were originally in the Dicom format, which cannot be read by Bonemat V2. To allow Bonemat V2 to read the images, they were converted to Visual ToolKit (*.vtk) file format using the free medical image viewer MRIcro (Chris Rordan, www.mricro.com) and a custom program created in Matlab (The MathWorks Inc., Natick, Massachusetts, USA). The finite element mesh was output from Patran as a Patran neutral file, which is readable by Bonemat V2. The parameter file is a small text file that serves several functions. It identifies the input and output files, defines the brightness/density and density/modulus relations, and specifies the modulus step size and order of numerical integration to be used. An annotated description of the parameter file is found in Appendix 1.

The Bonemat V2 software computes a volume based average value of the CT image brightness for each element by integrating over the element volume. The average element brightness for an element *n* is calculated as shown in the following equation:

$$\overline{B}_n = \frac{\int_{V_n} B(x, y, z)dV}{\int_{V_n} dV} \qquad (1)$$

where $B(x,y,z)$ represents the CT image brightness field, and V_n represents the volume of element *n* (Taddei, 2004). Bonemat V2 evaluates Equation 1 numerically for each

element in the mesh. A fourth order numerical integration was specified in the parameter file.

Because the program could theoretically produce a different material property for each element, there is a way to control the number of material properties created. Elements with similar modulus values are grouped into a bin and assigned a single material property. The modulus step size, specified in the parameter file, controls the spacing of the bins. A modulus step size of 100 MPa was used, which resulted in the bins being spaced about 100 MPa apart.

CT images, with proper scanner calibration, can provide accurate information on apparent bone density (Zannoni, 1998). However, no information on scanner calibration was available. Thus, information from the literature was used to develop brightness to density relationships. To define the brightness-density line, two points on the line were determined. Empirical equations relating density to elastic modulus were taken from the literature.

The first point on the brightness-density line was defined using cortical bone density. Cortical bone is described as having a density from 1.7 to 2.0 g/cm^3 (An, 2000). The brightness value for cortical bone was estimated from examination of the CT image, and that value was assigned a density of 1.7 g/cm^3. The brightness values of the CT image are illustrated in Figure 2.4(a). Note that the brightness was represented by grayscale values from 0 to 255.

In determining the second point on the brightness-density line, a value for the elastic modulus of cancellous bone was required. A search of the literature found no such

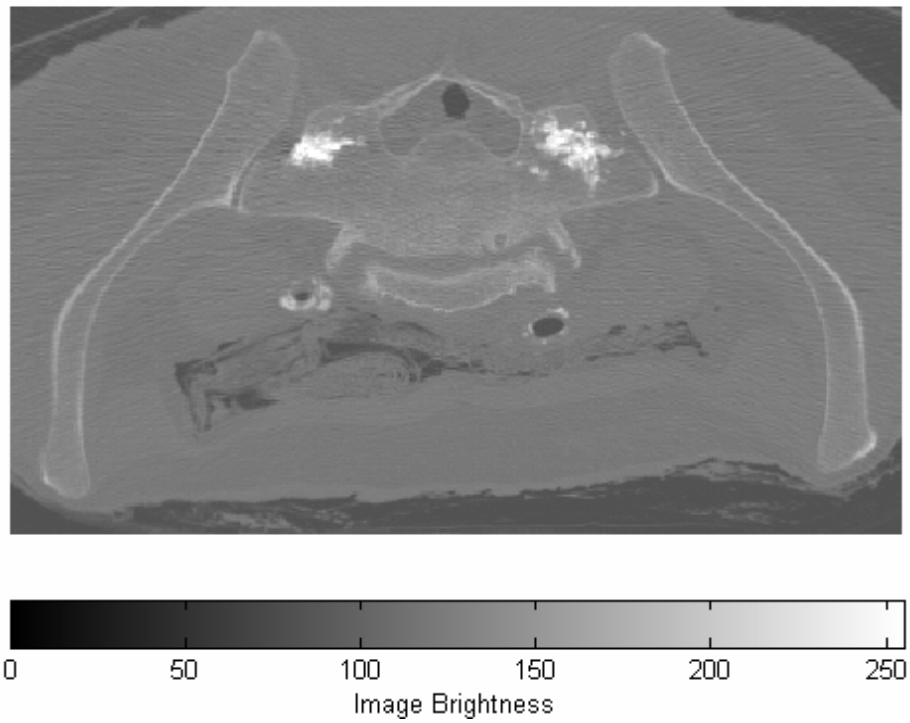

(a)

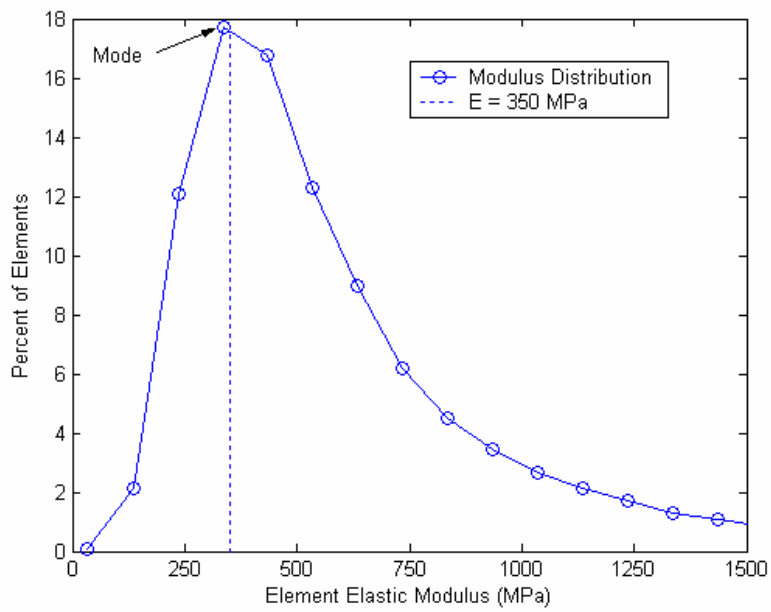

(b)

Figure 2.4: Determining the CT image brightness – bone density relationship. Two points were determined to define a line: (a) A brightness value of 200 found for cortical bone was assigned a density of 1.7 g/cm^3. (b) The second point was adjusted so the mode of the element modulus values created was near 350 MPa. The lines created are shown in Figure 2.5(a)

values reported for human sacral cancellous bone. In a survey by Goldstein (1987), compressive properties of trabecular bone were presented from a variety of studies. Table 2.1 presents values reported for anatomical locations near the sacrum. The conspicuous variation in these modulus values is due to several things, including anatomical location, testing method (e.g. strain rate, loading direction) and sample storage method (Goldstein, 1987). Without more specific information available, a value of 350 MPa was chosen to represent the average modulus of sacral cancellous bone in this study. While this may not be the true modulus of sacral cancellous bone, it falls well within the range of the values shown in Table 2.1.

Table 2.1: Published cancellous bone elastic modulus values from locations near the sacrum. These values were presented in a review by Goldstein (1987).

Source	Location	Storage	Modulus (MPa)
Evans and King (1961)	Proximal Femur	Embalmed	20.68 – 965
Schoenfeld et al. (1974)	Proximal Femur	Fresh	Avg. 344.7
Brown and Ferguson (1980)	Proximal Femur	Fresh Frozen	1000 – 9800
Martens et al. (1983)	Proximal Femur	Fresh Frozen	58 – 2248
Ciarelli et al. (1986)	Proximal Femur	Fresh Frozen	49 – 572
McElhaney et al. (1970)	Vertebral Body	Fresh	Avg. 151.7
Lindahl (1976)	Vertebral Body	Dried Defatted	1.1 – 139
Struhl et al. (1987)	Vertebral Body	Fresh Frozen	10 – 428
Ashman et al (1986)	Vertebral Body	Fresh	158 – 378
Keller et al (1987)	Vertebral Body	Fresh Frozen	15 – 30
Struhl et al. (1987)	Iliac Crest	Fresh Frozen	5 – 282

Because the sacrum and ilium are mostly cancellous bone by volume, a majority of the elements in the model should represent cancellous bone. Therefore, it was assumed that material value assigned the greatest number of elements, or the element modulus mode, should be approximately the average elastic modulus of cancellous bone, or 350 MPa. The second point defining the brightness-density line was adjusted so that the element modulus mode was near 350 MPa. This is illustrated in Figure 2.4(b).

It was desired to represent both normal and osteoporotic bone in the finite element models. Osteoporosis is defined by the World Health Organization as bone mineral density (BMD) more than 2.5 standard deviations below the young adult mean value (World Health Organization, 1994). In a study by Knapp et al (2004), lumbar spine BMD of a young, normal adult population was estimated to be 1.029 g/cm^2 (SD = 0.123). Applying the WHO definition, osteoporotic BMD would be 0.7215 g/cm^2 or below, a reduction of 30%. Thus, to represent osteoporosis, the density-brightness line for normal bone was reduced by 30%. The density brightness lines used for normal and osteoporotic cases are shown in Figure 2.5(a). The lines used for the two different CT images were essentially the same.

Empirical equations from the literature were used to define the elastic modulus based on the density. Two different density-modulus equations were used, one for cancellous bone (Hodgkinson and Curry, 1992), and one for cortical bone (Carter and Hayes, 1977). The relation developed by Carter and Hayes (1977) gives modulus as a function of both density and strain rate. For this analysis, a strain rate of 0.01/sec was assumed, making modulus a function of density alone. The resulting curves are shown in Figure 2.5(b). The curves described by the two equations intersect at a density of 0.981 g/cm^3. Below this density, the cancellous equation was used, and above it the cortical equation was used. (See Appendix 1 for details on equation input to Bonemat V2.)

A Poisson's ratio of 0.3 was used for all elements. Some models (Tack, 2001, Garcia, 2000, Polikeit, 2003, Ezquerro, 2004) have used multiple values for Poisson's ratio, such as 0.2 for cancellous bone and 0.3 for cortical bone. Other models (Dawson, 1999, Charriere, 2003, Kosmopoulos, 2004) have used a value of 0.3 for all bone. In this

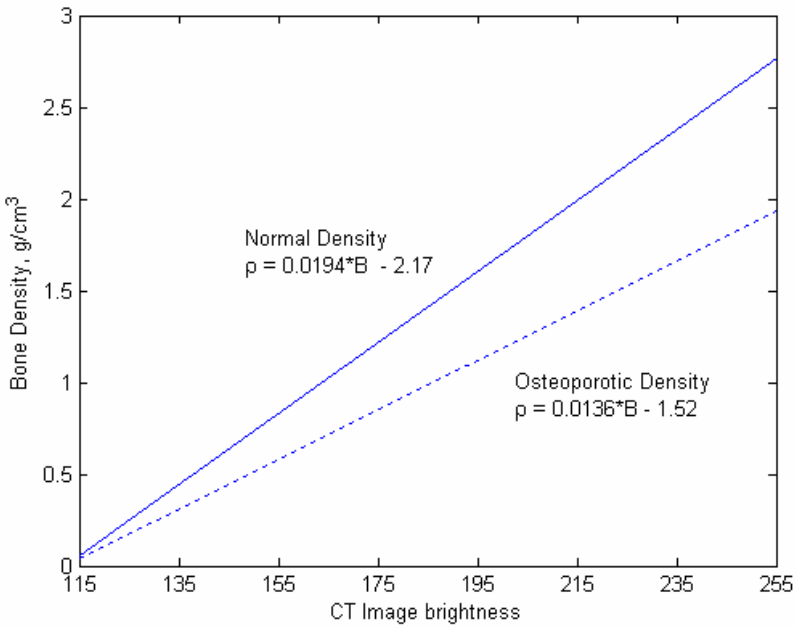

(a)

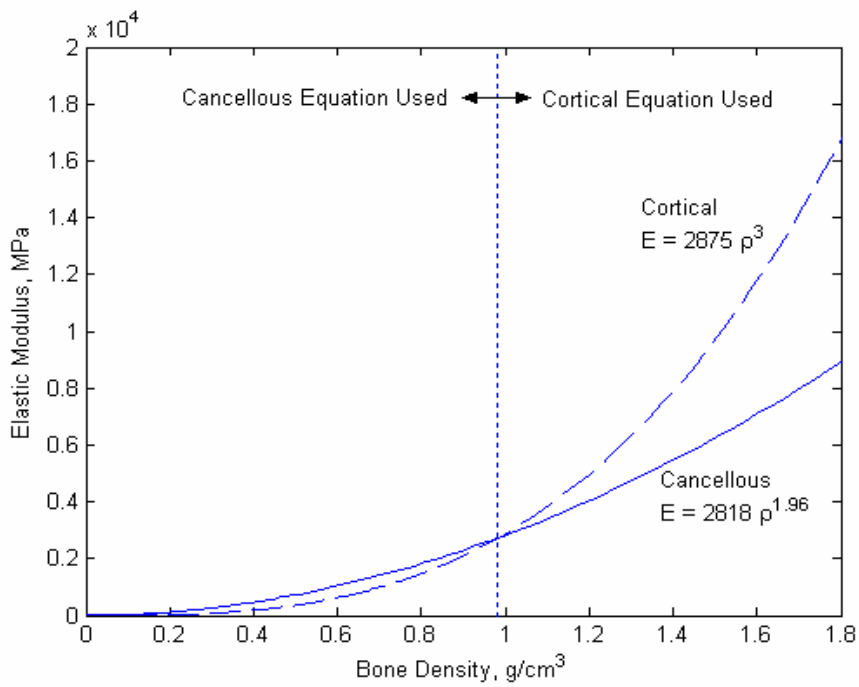

(b)

Figure 2.5: Conversion from CT image brightness to elastic modulus. (a) CT image brightness was converted to bone density using linear relationships. (b) Empirical curves were used to convert bone density to elastic modulus. The shift from cancellous to cortical bone occurred at 0.981 g/cm^3.

model the use of a uniform value makes sense because the elements do not necessarily represent cancellous or cortical bone exclusively.

EDITING ELEMENT MATERIAL PROPERTIES

Bone cement appears in the CT images more brightly than cortical bone, and so it is assigned a high density value by Bonemat V2. This resulted in the stiffness being over-estimated in areas containing cement. To address this, the elastic moduli in regions containing cement were reduced in Patran. A nominal elastic modulus value of 2500 MPa was assumed for cement, based on values for PMMA cement found in the literature (Giddings, 2001, Linden, 1991, Saha, 1984). Elements in regions of cement with higher elastic moduli were reassigned to the existing material value nearest 2500 MPa.

The use of pure cement properties could still overestimate the elastic modulus, because the actual material is a composite of the cancellous bone and cement. Although the addition of cement greatly increases the stiffness of cancellous bone, Baroud (2003) found that the resulting bone-cement composite is not as stiff as pure cement. Nonetheless, in modeling of vertebroplasty, pure cement properties have been used (Polikeit, 2003, Tack, 2004).

To create models with different material conditions, such as without cement, or homogenous, the material properties were modified in Patran. The procedure was similar to that used to correct the cement properties: selecting the elements to be changed, and reassigning the materials. Further details on the material properties of the models can be found in Section 2.3.

LOADING AND BOUNDARY CONDITIONS

Loads on the skeletal structure *in vivo* are complex, highly variable, and difficult to quantify. When applying loads to the model, one could try to include all the loads from the various muscles and ligaments. For example, Stolk (2001) included 19 different muscle forces when modeling the proximal femur. Loads applied to the model were simplified from the *in vivo* case, as is done for laboratory mechanical tests. Simonian (1996) performed mechanical testing of pelvic specimens when examining different methods of fixation for transforaminal pelvic fractures. In these tests, the still attached proximal femurs were secured in aluminum cylinders with potting compound and held fixed while a load was applied to the L4 vertebra.

In the model, a load of 1000 N was applied in a downward direction on the base of the sacrum. This load was chosen by Simonian (1996) as representative of the physiologic load on the sacrum. To distribute the load, it was divided and applied to multiple nodes on the base of the sacrum. For the “Male Post 03” models, the load was distributed evenly among 103 nodes. In the “Pelvis Post 05” models, the load was distributed among 50 nodes. However, in the models used for the convergence study, the load was applied to a single node to reduce loading variations as a possible source of error.

The lower ‘cut’ surfaces were fixed by setting nodal displacements on them to zero in three orthogonal directions. If actual mechanical tests similar to this model were performed, the lower parts of the ilia would probably be potted and clamped for testing. Thus, assuming zero displacement at these locations fits the mechanical testing scenario.

2.3 Finite Element Models

There were a number of variations of the models created to allow parametric analysis of the results. The models created include various combinations of CT image, mesh size, material homogeneity, inclusion of cement, and bone density. Figure 2.6 illustrates the parameters defining the specific the models created.

As noted previously, CT scans from two different subjects were used to create the models. The model development procedure used for each image was the same. Analyzing models with different geometry and material distributions allowed some insight into the amount of variation that can naturally be expected between individuals.

There were a total of four finite element meshes used in the models, shown in Figure 2.7. All four meshes were composed of four-node tetrahedral elements. A primary mesh was created from each image, referred to as “Normal” size. The “Normal” meshes were used for most of the models, and a variety of material conditions were applied to them. Two additional meshes created from the image Male Post 03 were used for convergence testing. For these, referred to as “Fine” and “Very Fine”, the global edge length values input to Patran were reduced, resulting in smaller element sizes. Table 2.2 gives details of the four meshes.

Models were created with both homogeneous and non-homogeneous material properties. Non-homogeneous properties were created using Bonemat V2 as described previously. Figure 2.8 shows the material property distributions of the non-homogeneous Male Post 03 models. The Pelvis Post 05 models showed similar behavior. Appendix 2 tabulates the material properties applied to all models.

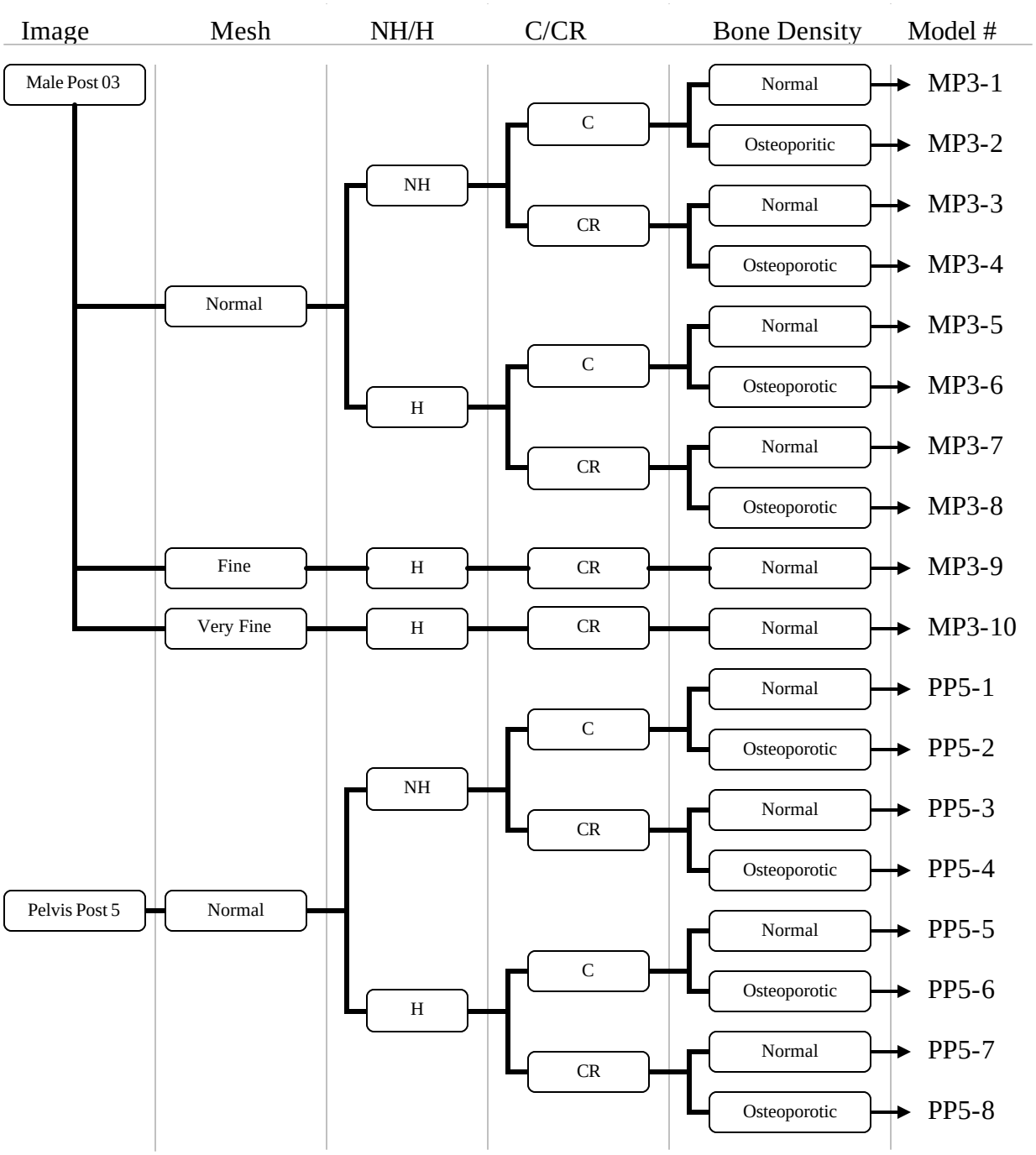

Figure 2.6: Summary of finite element models created. Differing aspects of the models were source CT image, size of mesh created, homogeneous (H) or nonhomogeneous (NH) material properties, whether cement was included (C) or removed (CR), and normal or osteoporotic bone density.

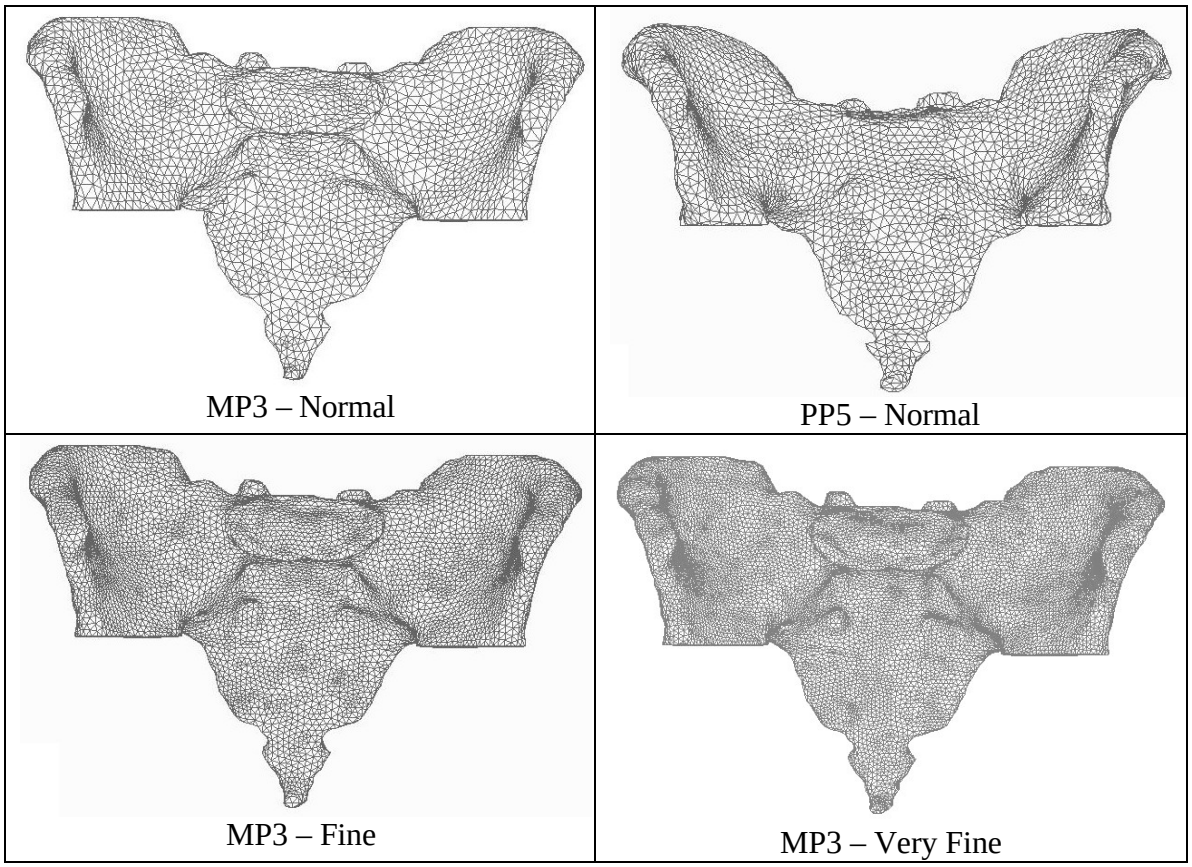

Figure 2.7: Finite element meshes created. Most analysis was performed with the Normal size meshes, from two different CT images. The two meshes with reduced element size (Fine and Very Fine) were used for convergence testing.

Table 2.2: Details of finite element meshes created

Mesh	Global Edge Length (mm)	# Elements	# Nodes
MP3-Normal	5	77,215	15,354
PP5-Normal	5	68,073	13,861
MP3-Fine	3.15	241,462	46,005
MP3-Very Fine	2.4	596,472	109,217

In preliminary tests, homogeneous models based on the non-homogeneous mean more closely matched the non-homogeneous results than homogeneous models based on the mode. Thus, homogeneous elastic modulus values were determined by taking the mean of the non-homogeneous elastic moduli over all the elements.

At the core of this study was determining the difference made by the inclusion of cement in the sacrum. As noted previously, the CT images included cement, and so the

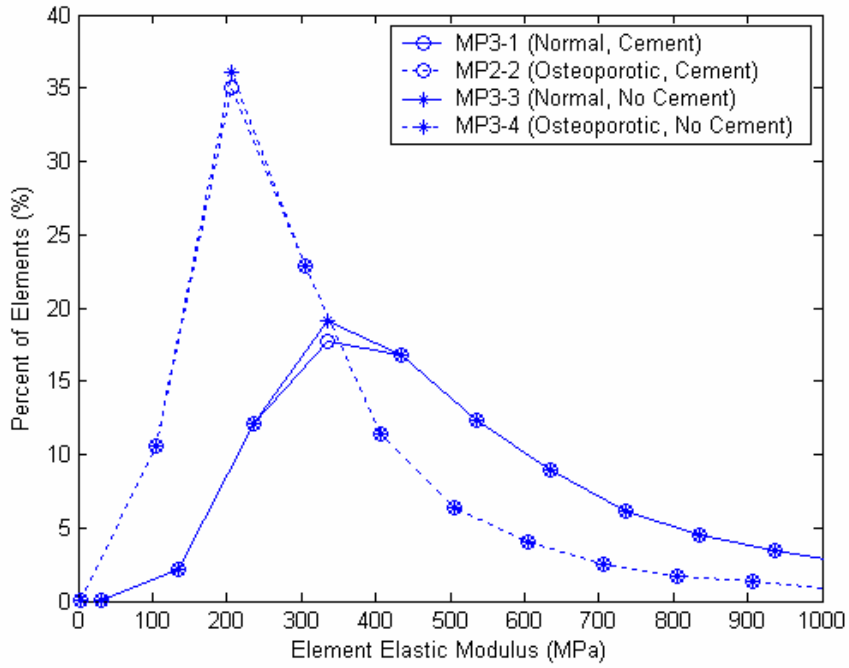

(a)

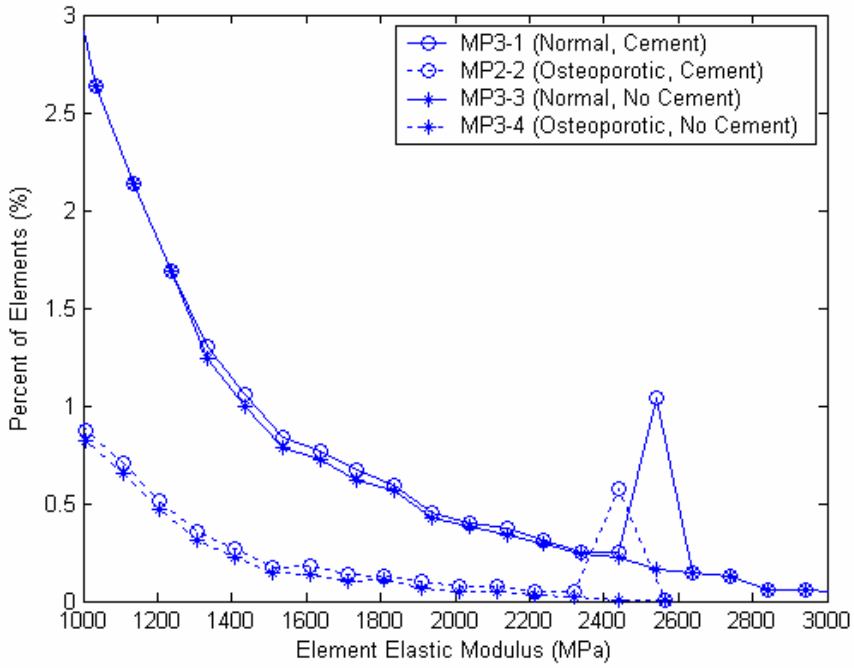

(b)

Figure 2.8: Element Property Distributions. The percentage of elements assigned to each material property is plotted against elastic modulus for Male Post 03 models. (a) Note that the osteoporotic case has the peak (mode) percentage at a lower modulus and drops off more quickly . (b) The small peaks near 2500 MPa are from the elements representing cement.

material properties initially produced contained cement. To create models for comparison, the cement was “removed”. It was manually determined which elements were cement, and their material properties were reassigned to the mode of the element moduli. The removal of cement can be seen in Figure 2.9, which shows material properties in the same cross section of model MP3-1 (with cement) and model MP3-3 (cement removed). To create a homogeneous model with cement, the cement elements determined from the non-homogeneous model were assigned a single modulus representing cement. Thus homogeneous models with cement had two materials.

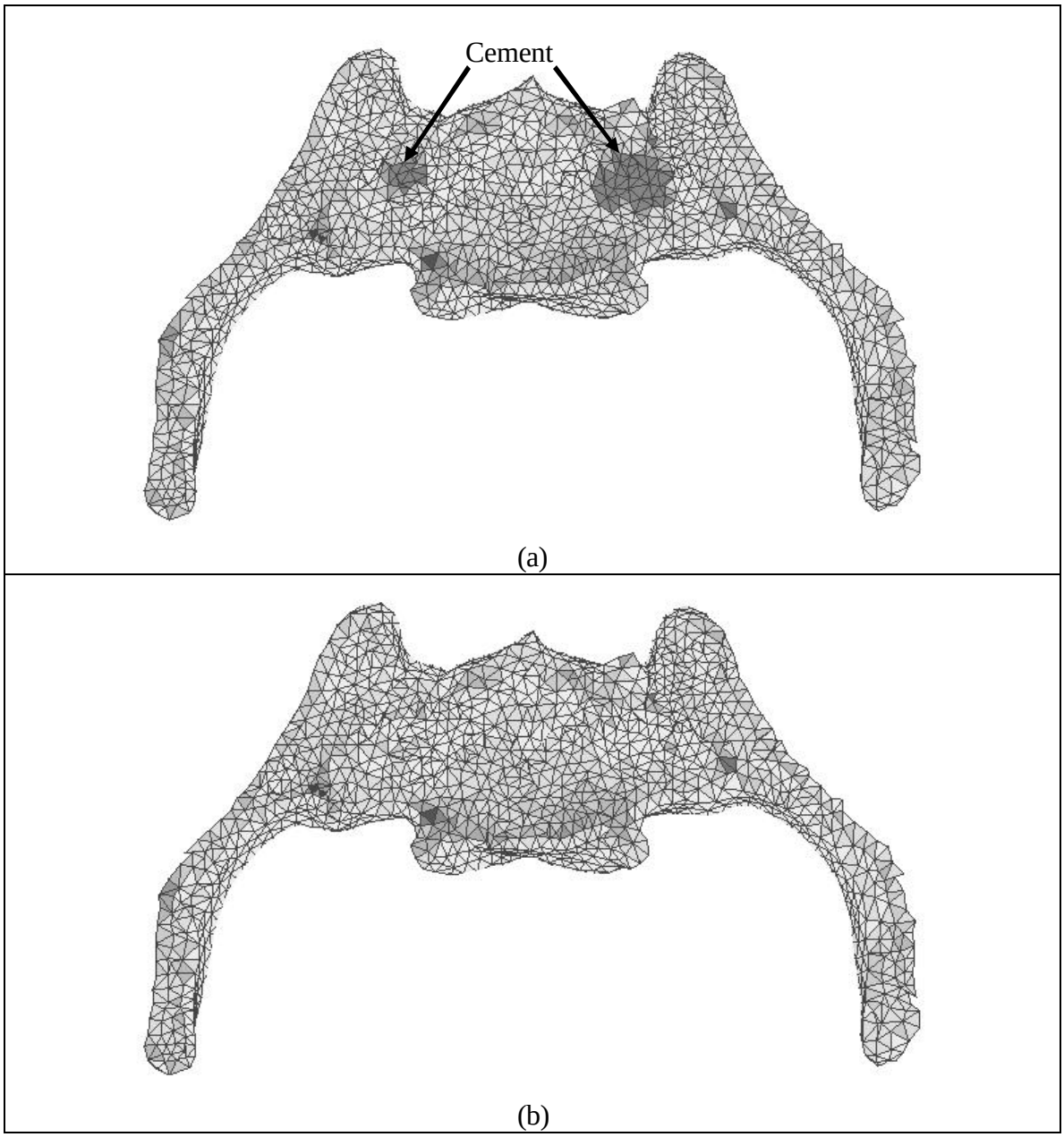

Figure 2.9: Cement Removal. (a) The presence of cement can be seen clearly in this cross section of model MP3-1, in which darker element color indicates higher modulus. (b) In the same cross section of model MP3-3, the cement has been removed by changing the modulus values of the ‘cement’ elements.

2.4 Analysis Performed

Several studies were performed using the models outlined in the previous section. The effect of each parameter of interest was examined by comparing results from models in which that parameter differed. ABAQUS (ABAQUS, Inc., Providence, Rhode Island, USA) was used to solve the models. For the given loads and boundary conditions, the models were solved for stresses, strains and displacements at the nodes. The solver used a single matrix decomposition to solve for the unknowns directly. When a model was ready for analysis, an ABAQUS input file was written by Patran. After the analysis was complete, the results were read back into Patran for post-processing.

MODEL COMPARISONS

Model results were compared both on a whole model level, and at specific locations within the models. The deflection at the sacral promontory was usually the greatest deflection in the model, and always a local maximum. Deflections at this location were one way of comparing the overall models. In models that used the same mesh, the results could be compared on a node by node basis. Comparing principal strains throughout the models provided another way of comparing whole models.

The location of the cement was of particular interest in comparing the models. It has been hypothesized that cement serves to reduce the micromotion at a crack in the bone. Even without a crack present, it was expected that the higher stiffness of the cement would reduce the local deformations in the bone. Thus, the principal strains in the locations of the cement were examined.

Regions of interest (ROI) were created within the volumes of the injected cement, as determined from the CT images. Because cement was injected bilaterally, there was a

ROI on both the left and the right. Each ROI was comprised of a grid, with nominal point spacing of 3 mm, created in a transverse plane. The ROIs for the Male Post 3 models had 45 points in the left grid and 24 points in the right grid. (Note that the right ROI is smaller because there is less cement on the right.) The ROIs in the Pelvis Post 5 models had 42 points on the left and 48 points on the right.

Patran was used to extrapolate results data to the ROI grid points. Model results could be examined at the ROI points, which were independent of the model mesh. This allowed local comparisons in the convergence tests, which used different meshes. In a few cases, Patran failed to extrapolate to a particular ROI point in a particular mesh. It was found that by slightly adjusting the point location, extrapolation could be made to succeed. The adjusted point locations were all less than 0.09 mm from the original point locations. Because this is much less than the grid spacing of the ROIs, the error introduced by the movement of these points was assumed to be negligible.

To compare the results, the change, or percent difference, between two values was calculated using the following equation:

$$Diff = \left(\frac{Result_2 - Result_1}{Result_1} \right) * 100 \qquad (2)$$

In each comparison, $Result_1$ comes from the model chosen as the baseline, and $Result_2$ from the other model. For strains, Equation 2 was evaluated at each point in the regions of interest. To determine the overall magnitude of the difference in the region of interest, the root-mean-square of the percent difference was calculated as

$$RMS_{Diff} = \left(\frac{\sum_{i=1}^{n} Diff_i^{\,2}}{n} \right)^{1/2} \qquad (3)$$

where n is the number of points in the region of interest. RMS_{Diff} was used as a measure of the overall difference in strains in the regions of interest.

CONVERGENCE CHECK

Convergence of the finite element mesh was checked by comparisons of models MP3-7, MP3-9 and MP3-10, as indicated in Table 2.3. The models were identical except for the mesh used. Rather than being distributed between multiple nodes, the load was applied at a single node for the convergence study. This was to reduce differences in the force distribution that could arise between different meshes. The location of the loaded node in each model was nearly the same, with less than 1 mm difference between the meshes. Identical homogeneous material properties were used to reduce any differences that could arise from applying non-homogeneous properties to dissimilar meshes. Between two models, the results of the finer mesh were used as the baseline for comparison.

Table 2.3: Comparisons made for convergence test

Comparison	Model 1 (Finer Mesh)	Model 2 (Coarser Mesh)	Model Notes
1	MP3-9	MP3-7	Homogeneous, No Cement, Point loads
2	MP3-10	MP3-9	Homogeneous, No Cement, Point loads
3	MP3-10	MP3-7	Homogeneous, No Cement, Point loads

MATERIAL HOMOGENEITY

In this examination, the parameter of interest was whether the material properties of the model were homogeneous or not. A total of eight comparisons, shown in Table 2.4, were made between non-homogeneous models (MP3-1 to 4, PP5-1 to 4) and homogeneous models (MP3-5 to 8, PP5-5 to 8). Each homogeneous model was compared

with the corresponding non-homogeneous model, in which all other parameters were the same. As the more realistic representation, the non-homogeneous models were used as the baseline model in each comparison.

Table 2.4: Comparisons between homogeneous and non-homogeneous models

Comparison	Model 1 (Non-homogeneous)	Model 2 (Homogeneous)	Model Notes
1	MP3-1	MP3-5	Normal density, with cement
2	MP3-2	MP3-6	Osteoporotic, with cement
3	MP3-3	MP3-7	Normal density, no cement
4	MP3-4	MP3-8	Osteoporotic, no cement
5	PP5-1	PP5-5	Normal density, with cement
6	PP5-2	PP5-6	Osteoporotic, with cement
7	PP5-3	PP5-7	Normal density, no cement
8	PP5-4	PP5-8	Osteoporotic, no cement

BONE DENSITY

The difference between normal and osteoporotic bone was evaluated by comparing the models with normal material density inputs to models with reduced material density. The normal density models were chosen to be the baseline for comparison, and thus the difference in the results represents the variation of osteoporotic from normal bone. Table 2.5 shows the eight comparisons made.

Table 2.5: Comparisons between normal and reduced density (osteoporotic) models

Comparison	Model 1 (Normal density)	Model 2 (Osteoporotic)	Model Notes
1	MP3-1	MP3-2	Non-homogeneous, with cement
2	MP3-3	MP3-4	Non-homogeneous, no cement
3	MP3-5	MP3-6	Homogeneous, with cement
4	MP3-7	MP3-8	Homogeneous, no cement
5	PP5-1	PP5-2	Non-homogeneous, with cement
6	PP5-3	PP5-4	Non-homogeneous, no cement
7	PP5-5	PP5-6	Homogeneous, with cement
8	PP5-7	PP5-8	Homogeneous, no cement

EFFECTS OF CEMENT

The effects of cement injection on the sacrum were examined by comparing models containing cement to the corresponding models that did not contain cement. The eight comparisons made are shown in Table 2.6. Although the models without cement were created by removing cement from the models with cement, the procedure of interest is adding cement to the sacrum. Thus, the models without cement were used as the baseline case, and the different results represent changes caused by adding cement.

Table 2.6: Comparisons between models with and without cement

Comparison	Model 1 (No Cement)	Model 2 (Cement)	Model Notes
1	MP3-3	MP3-1	Non-homogeneous, Normal density
2	MP3-4	MP3-2	Non-homogeneous, Osteoporotic
3	MP3-7	MP3-5	Homogeneous, Normal density
4	MP3-8	MP3-6	Homogeneous, Osteoporotic
5	PP5-3	PP5-1	Non-homogeneous, Normal density
6	PP5-4	PP5-2	Non-homogeneous, Osteoporotic
7	PP5-7	PP5-5	Homogeneous, Normal density
8	PP5-8	PP5-6	Homogeneous, Osteoporotic

Chapter 3: Results

In this chapter, results from the finite element models are presented and compared. In Section 3.1 the outcome of the convergence study is presented, justifying the use of the normal size finite meshes in the subsequent models. Section 3.2 presents comparisons between homogeneous and non-homogeneous models. The effects of bone density are shown in Section 3.3, which compares models simulating normal and osteoporotic bone. Finally, the effects of sacroplasty are examined in section 3.4 by comparing models with cement to models without.

3.1 Model Convergence

Results for convergence testing show that the normal mesh size compares reasonably well with the finer meshes. The models tested for convergence were subjected to a single point load, rather than distributing the load across the base of the sacrum. Although large variations in the deflections occurred at the loading point, this can be ignored because the point load represents a singularity in the model. At the sacral promontory, the differences in deflection were less than 7%. Table 3.1 compares the deflections at the sacral promontory for the convergence models. The two finer models compare much more closely to each other than to the normal model.

Table 3.1: Comparisons of deflections at sacral promontory in convergence testing

Comparison	Mesh	Deflection (mm)	Mesh	Deflection (mm)	Difference
1	Fine (MP3-9)	0.444	Normal (MP3-7)	0.414	-6.85%
2	Very Fine (MP3-10)	0.436	Fine (MP3-9)	0.444	1.86%
3	Very Fine (MP3-10)	0.436	Normal (MP3-7)	0.414	-5.11%

Figure 3.1 shows plots of the maximum principal, maximum shear, and minimum principal strains in the regions of interest. It can be seen qualitatively that all three models generally gave the same results. These results were compared, and the RMS_{Diff} calculated for each case. With the exception of the maximum principal strain in the left region of interest, RMS_{Diff} was below 5% (see Appendix 3).

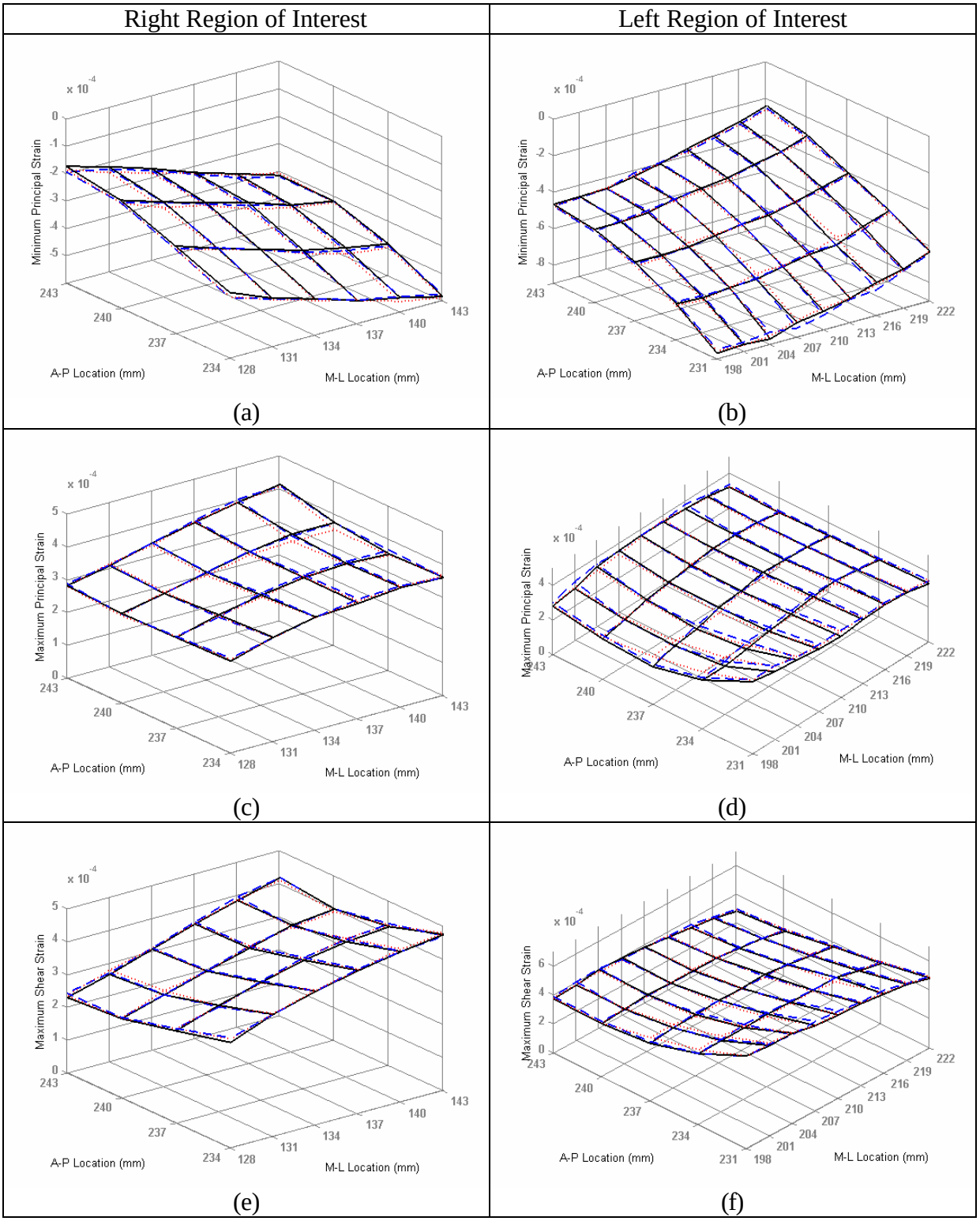

Figure 3.1: Convergence test strains in regions of interest. Comparison of various strains in regions of interest, for normal (red dotted line), fine (blue dashed line), and very fine (solid line) mesh sizes. The minimum principal (a, b), maximum principal (c, d), and maximum shear (e, f) strains are shown respectively for Right and Left regions of interest.

As the magnitude of the minimum principal strain is the largest in the regions of interest, it provides the best measure of model convergence. Figure 3.2 shows the mean values of minimum principal strain in the regions of interest. The RMS_{Diff} values for the minimum principal strains are given in Table 3.2. Note that the RMS_{Diff} does not exhibit a significant decrease when comparing the two finer models.

Table 3.2: ROI Differences in convergence test. RMS_{Diff} is given for minimum principal strains in models using different mesh sizes.

Coarser Mesh	Normal (MP3-7)	Fine (MP3-9)	Normal (MP3-7)
Finer Mesh	Fine (MP3-9)	Very Fine (MP3-10)	Very Fine (MP3-10)
RMS_{Diff} (Left ROI)	2.66%	2.56%	3.05%
RMS_{Diff} (Right ROI)	2.71%	3.27%	4.13%

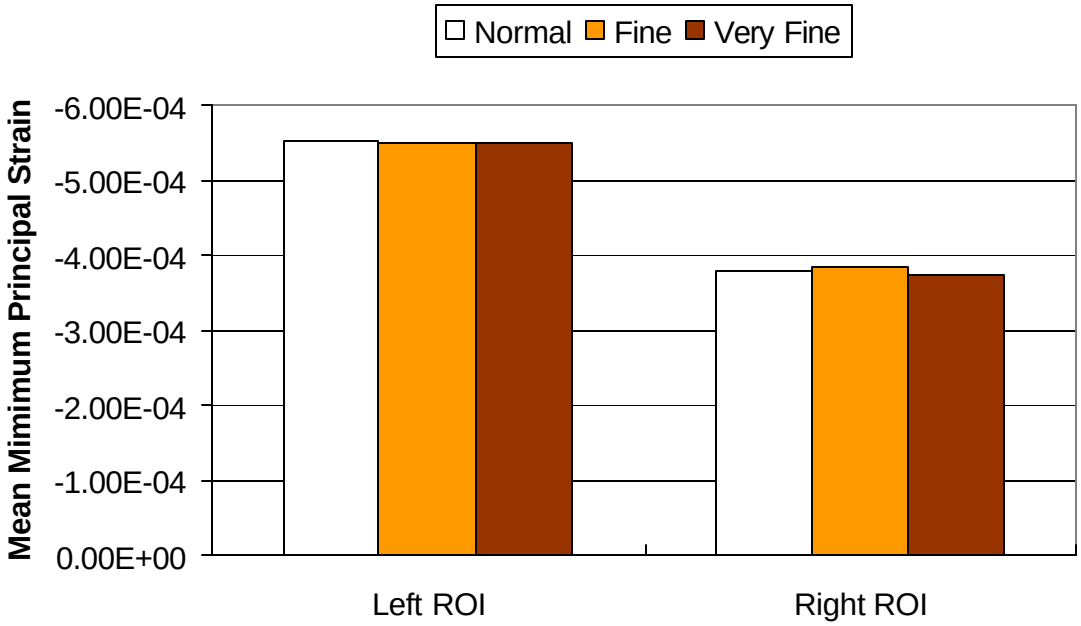

Figure 3.2: Mean minimum principal strains in convergence test. The mean values in the regions of interest are shown, and compare quite well.

For the region of interest strains, reduction in element size did not reduce the differences to zero. This suggests that some errors may be present that are unrelated to mesh size. For example, some error could be introduced during extrapolation of results to

the region of interest grids. That is to say, the model is as converged as it will get, and the level of error in the strain results is known.

The convergence test provides an idea of the error that may be present in the results. However, since the models to be compared in this study use identical meshes, loads and boundary conditions, the errors introduced should be similar, if not identical. Thus, the major effect seen in each comparison should be due to the parameters of interest, such as material homogeneity, presence of cement, and bone density. Although the convergence test used only homogeneous models, it should still be valid if non-homogeneous properties are applied. According to Taddei (2004), the introduction of inhomogeneous material properties did not worsen the convergence behavior of models of the femur.

3.2 Material Homogeneity

Comparisons of homogeneous models with non-homogeneous were performed. Table 3.3 presents comparisons of the sacral promontory deflections in homogeneous and non-homogeneous cases. The homogeneous models underwent larger deflections than the non-homogeneous, which indicates that they were less stiff. The differences in the Male Post 3 models are larger than in the Pelvis Post 5 models. This could be due to the actual differences in bone geometry and material distribution.

The principal strains in the regions of interest show significant variations. The value of RMS_{Diff} varies from about 12% to 37% (see Appendix 3). In the regions of interest, minimum principal strains were generally of greater magnitude than maximum principal strains. Figure 3.3 illustrates the principal strains in the regions of interest for

models MP3-3 (non-homogeneous) and MP3-7 (homogeneous), which are normal density models without cement. It can be seen that the homogeneous model strains tend to be smaller in the regions of interest.

Table 3.3: Deflections at sacral promontory for homogeneous and non-homogeneous models. The difference is given for each comparison made. (N = normal density, O = osteoporotic, C = cement, NC = no cement)

	Non-Homogeneous		Homogeneous		Difference
	Model	Deflection (mm)	Model	Deflection (mm)	
Comparison 1: (N, C)	MP3-1	0.404	MP3-5	0.457	12.9%
Comparison 2: (O, C)	MP3-2	0.759	MP3-6	0.837	10.3%
Comparison 3: (N, NC)	MP3-3	0.414	MP3-7	0.461	11.4%
Comparison 4: (O, NC)	MP3-4	0.772	MP3-8	0.848	9.8%
Comparison 5: (N, C)	PP5-1	0.386	PP5-5	0.406	5.1%
Comparison 6: (O, C)	PP5-2	0.730	PP5-6	0.748	2.5%
Comparison 7: (N, NC)	PP5-3	0.402	PP5-7	0.412	2.6%
Comparison 8: (O, NC)	PP5-4	0.753	PP5-8	0.766	1.7%

For models without cement, the mean value of the non-homogeneous strains is larger than the homogeneous strains. Cement seems to reduce the difference. Figure 3.4 shows mean minimum principal strains in normal density models with cement and normal density models without cement. The RMS_{Diff} values for these cases, shown in Table 3.4, provide a better indication of the magnitude of the differences in the ROI. Appendix 3 tabulates region of interest principal strains for comparisons between homogeneous and non-homogeneous models.

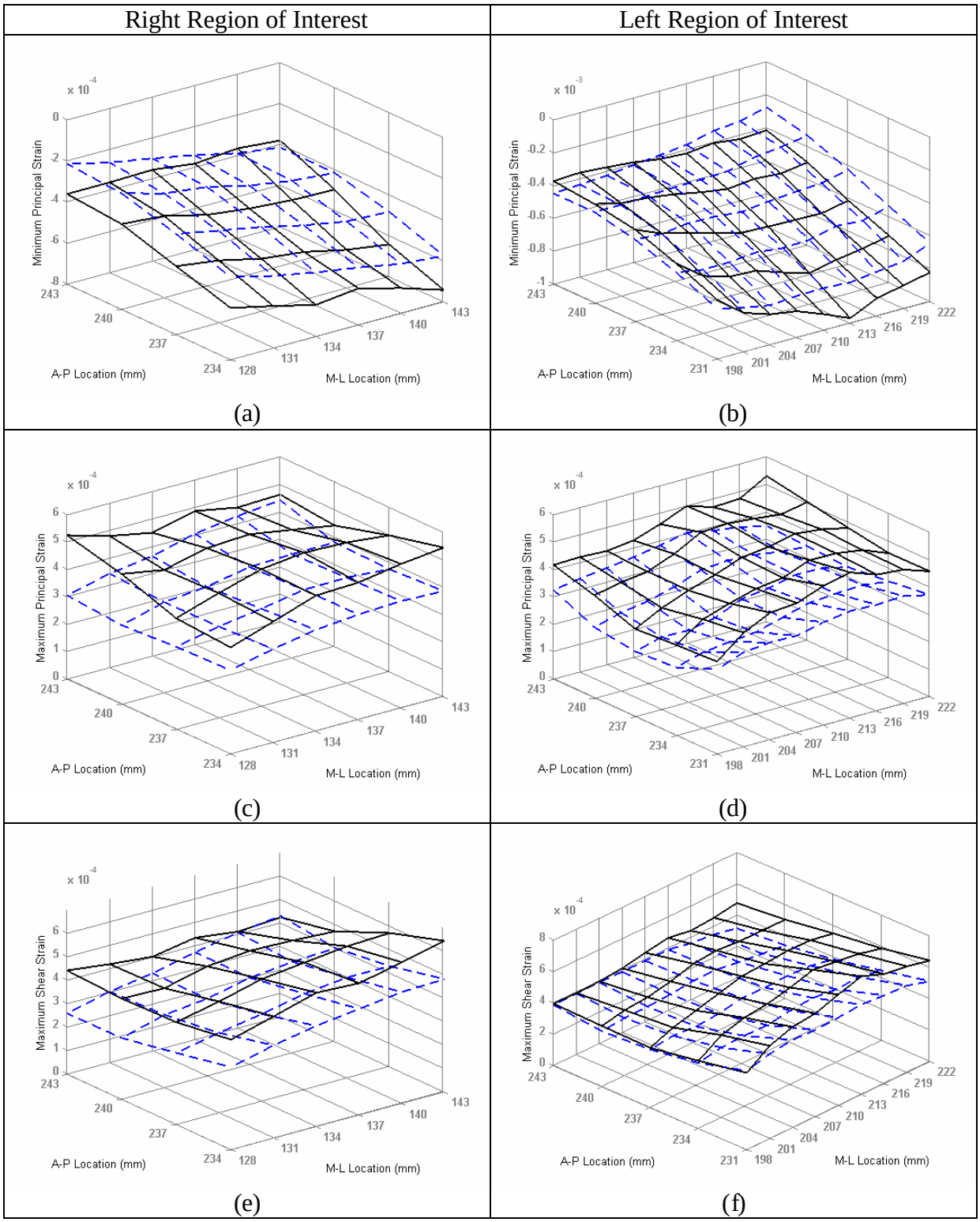

Figure 3.3: Region of interest principal strains in homogeneous and non-homogeneous models. Region of interest strains in non-homogeneous (solid line, model MP3-3) and homogeneous (dashed line, model MP3-7) models used in Comparison 3 (Normal density, no cement). The minimum principal (a, b), maximum principal (c, d), and maximum shear (e, f) strains are shown for Right and Left ROIs respectively. Note that the homogeneous strains tend to be smaller.

The differences in homogeneity are not limited to the regions of interest, but extend throughout the model. To examine the effects of homogeneity throughout the entire model, minimum principal strains from homogeneous models were plotted node by node against the minimum principal strains from non-homogeneous models. These strain versus strain plots, one from Male Post 3 and one from Pelvis Post 5, are shown in Figure 3.5. A slope of 1 in Figure 3.5 would indicate the homogeneous and non-homogenous models are essentially the same stiffness. The values of 0.982 and 0.958 indicate that the homogeneous models are slightly stiffer, but also that reasonably good values were chosen for the homogeneous elastic moduli. The coefficients of determination indicate that the homogeneous models accounts for 86% and 79%, respectively, of the variation in the non-homogeneous model. This is consistent with Dalstra's (1995) assertion that while homogeneous material properties are not a bad simplifying assumption, they do not capture all of the behavior.

Table 3.4: ROI Differences between non-homogeneous and homogeneous models. RMS_{Diff} is given for minimum principal strains in normal density models with and without cement.

	Normal, Cement		Normal, No Cement	
Non-homogeneous	MP3-1	PP5-1	MP3-3	PP5-3
Homogeneous	MP3-5	PP5-5	MP3-7	PP5-5
RMS_{Diff} (Left ROI)	28.0%	14.3%	18.9%	31.7%
RMS_{Diff} (Right ROI)	20.1%	12.7%	24.6%	31.2%

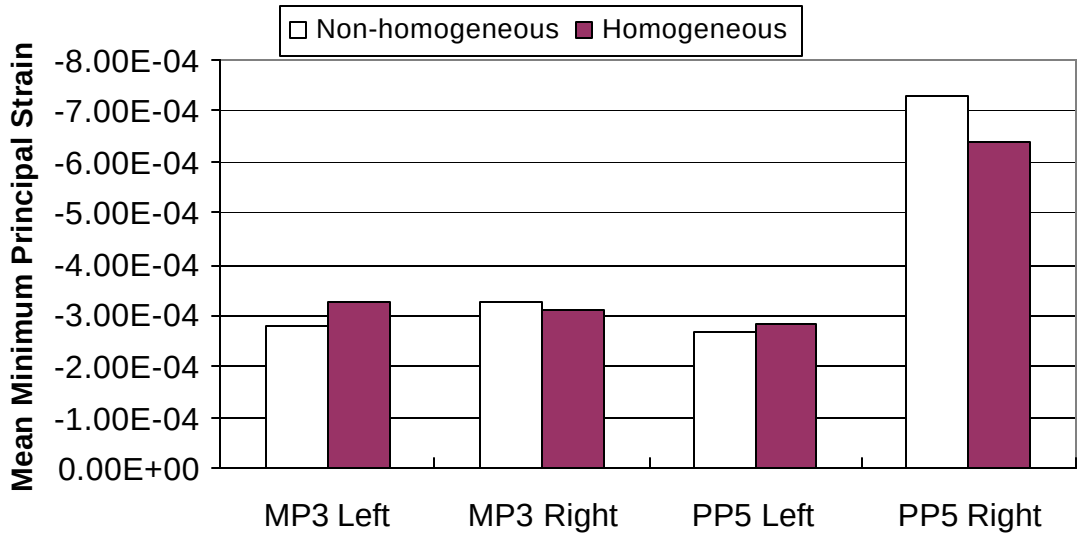

a) Normal Density, Cement

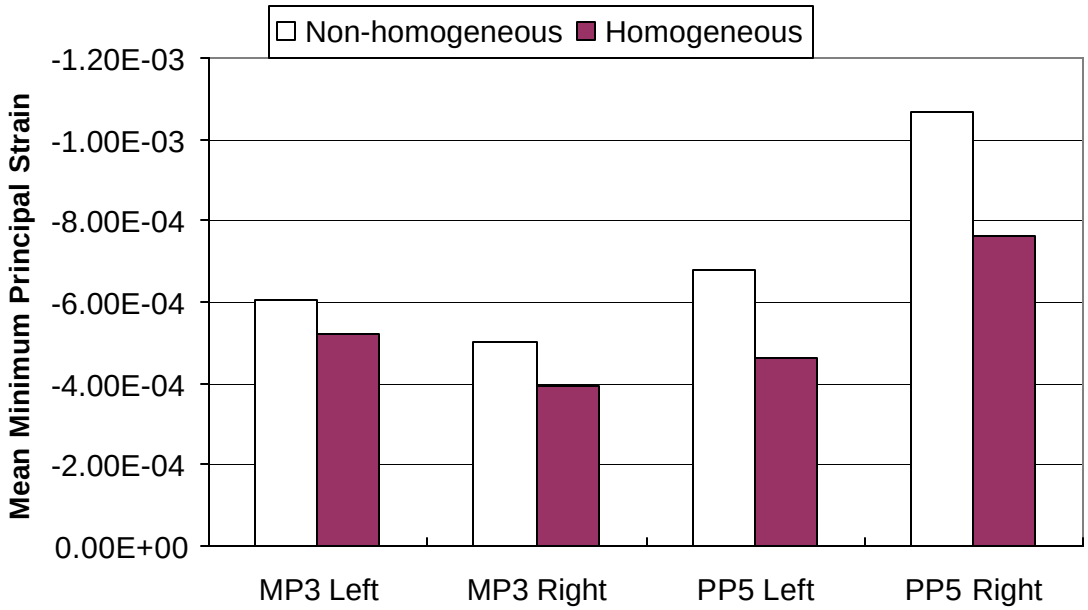

b) Normal Density, No Cement

Figure 3.4: Mean ROI strains in non-homogeneous and homogeneous models. (a) Mean minimum principal strains in regions of interest for non-homogeneous (MP3-1, PP5-1) and homogeneous (MP3-5, PP5-5) normal density models with cement. (b) Non-homogeneous (MP3-3, PP5-3) and homogeneous (MP3-7, PP5-7) normal density models without cement. Without cement, the homogeneous strain is less than non-homogeneous. Cement seems to reduce the difference.

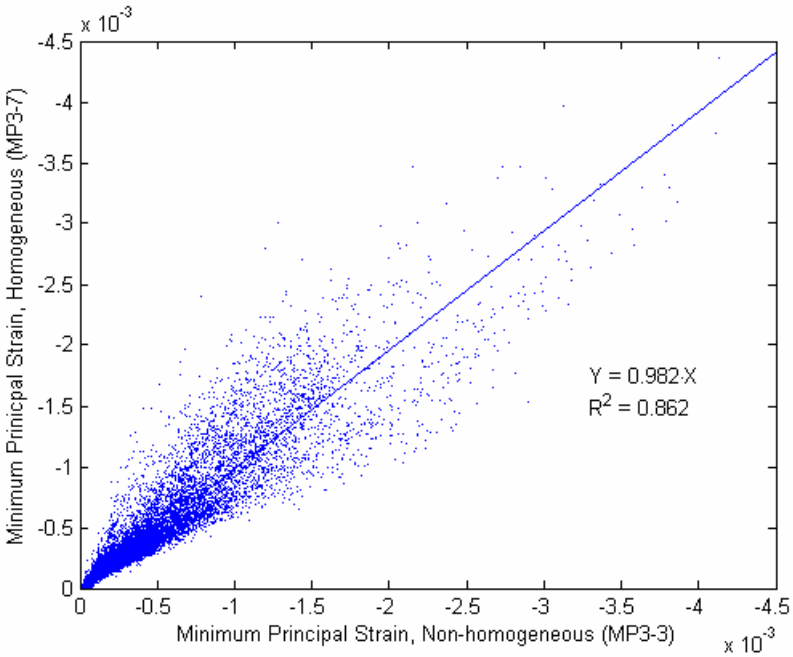

(a)

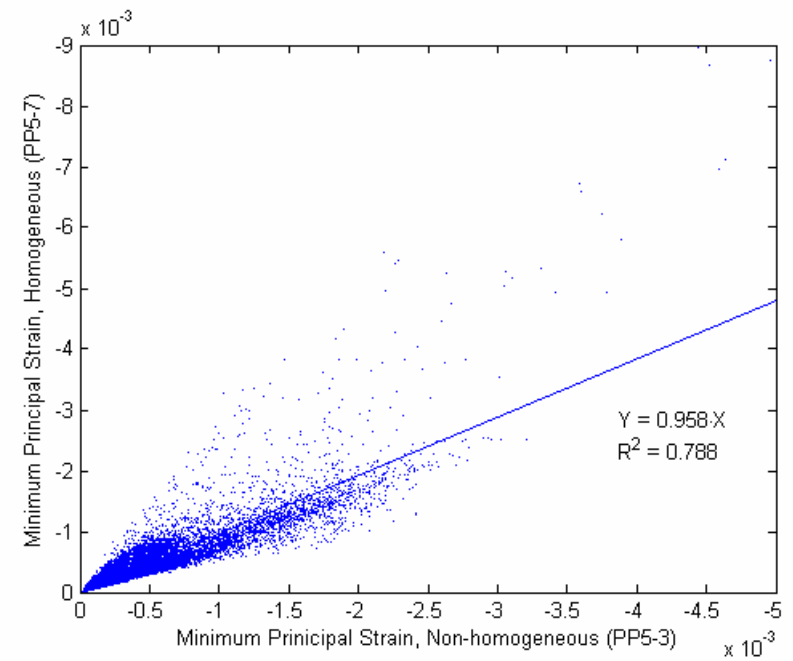

(b)

Figure 3.5: Whole model strain comparisons, homogeneous and non-homogeneous models. The minimum principal strains from a non-homogeneous and homogeneous (MP3-7) model are plotted against each other for each node in the mesh. For the Male Post 3 models (a), the best fit line shows that the homogeneous model accounts for 86% of the variation of the non-homogeneous model, while the Pelvis Post 5 models (b) show more variation. The slopes of the lines show the homogeneous elastic moduli were well chosen, as the optimum value would produce a slope of exactly 1.

3.3 Bone Density

The effect of bone density was very apparent, as the models with reduced bone density were considerably less stiff. As Table 3.5 shows, the models that simulated osteoporosis by reduced bone density had a significant increase in sacral promontory deflection over the normal density models. The increase was relatively consistent across the different comparisons made, ranging from 83 to 89%.

Table 3.5: Deflections at sacral promontory for normal and osteoporotic (reduced density) models. The difference is given for each comparison made. (NH = non-homogeneous, H = homogeneous, C = cement, NC = no cement)

	Normal Density		Osteoporotic		Difference
	Model	Deflection (mm)	Model	Deflection (mm)	
Comparison 1: (NH, C)	MP3-1	0.404	MP3-2	0.759	87.6%
Comparison 2: (NH, NC)	MP3-3	0.414	MP3-4	0.772	86.7%
Comparison 3: (H, C)	MP3-5	0.457	MP3-6	0.837	83.2%
Comparison 4: (H, NC)	MP3-7	0.461	MP3-8	0.848	84.0%
Comparison 5: (NH, C)	PP5-1	0.386	PP5-2	0.730	89.0%
Comparison 6: (NH, NC)	PP5-3	0.402	PP5-4	0.753	87.4%
Comparison 7: (H, C)	PP5-5	0.406	PP5-6	0.748	84.2%
Comparison 8: (H, NC)	PP5-7	0.412	PP5-8	0.766	85.8%

The increases in region of interest strains in the osteoporotic cases were significant, although not as consistent as the model deflections. The RMS_{Diff} values ranged from 39 to 86% (see Appendix 3). For example, Figure 3.6 illustrates the principal strains at the regions of interest for models MP3-3 (normal) and MP3-4 (osteoporotic), which are non-homogeneous models without cement. It can be seen that the strain in the osteoporotic model is larger throughout.

Figure 3.7 shows the mean values of the minimum principal strains in homogeneous and non-homogeneous models without cement. It is apparent that the strains of the osteoporotic model are significantly larger. The values of RMS_{Diff} in these cases, shown in Table 3.6, are also significant. Note that in the homogeneous cases, the

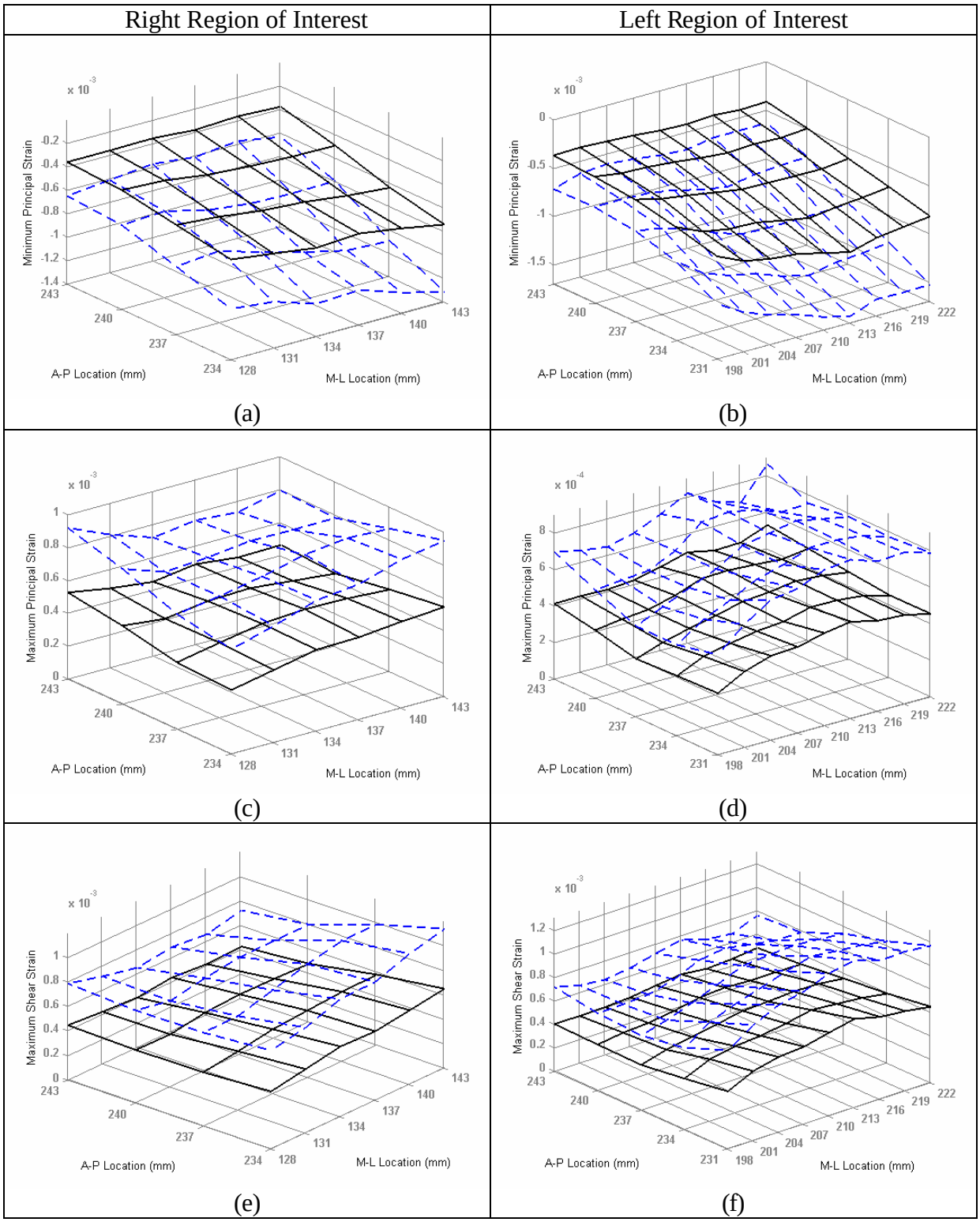

Figure 3.6: Region of interest principal strains in normal and osteoporotic models. Comparison 2 region of interest strains in normal (solid line, model MP3-3) and osteoporotic (dashed line, model MP3-4) models. The minimum principal (a, b), maximum principal (c, d), and maximum shear (e, f) strains are shown respectively for Right and Left regions of interest.

differences are identical to the changes in sacral promontory deflection. Because these are purely homogeneous models, the changes in strain are linear and equivalent to the changes in the elastic moduli. See Appendix 3 for results from all comparisons made.

As with material homogeneity, the material differences between normal and osteoporotic models extend throughout the model. Thus, the differences between them are not limited to the regions of interest. Strain-strain plots of minimum principal strains from normal and osteoporotic models are shown in Figure 3.8. The linear regressions for both Male Post 3 models and Pelvis Post 5 models show that the strain in the osteoporotic case is significantly larger than the normal case. The increase is about 86%, similar to the sacral promontory deflection. The coefficients of determination (R^2 = 0.997 and 0.989, respectively) are high, showing that the osteoporotic strains are nearly a direct scaling of the normal density strains. Thus, the material variations introduced from the CT images are represented similarly, regardless of the density level introduced.

Table 3.6: ROI Differences between normal and osteoporotic models. RMS_{Diff} is given for minimum principal strains in non-homogeneous and homogeneous models without cement.

	Non-homogeneous, No Cement		Homogeneous, No Cement	
Normal	MP3-3	PP5-3	MP3-7	PP5-3
Osteoporotic	MP3-4	PP5-4	MP3-8	PP5-5
RMS_{Diff} (Left ROI)	68.8%	39.0%	84.0%	85.8%
RMS_{Diff} (Right ROI)	69.9%	59.7%	84.0%	85.8%

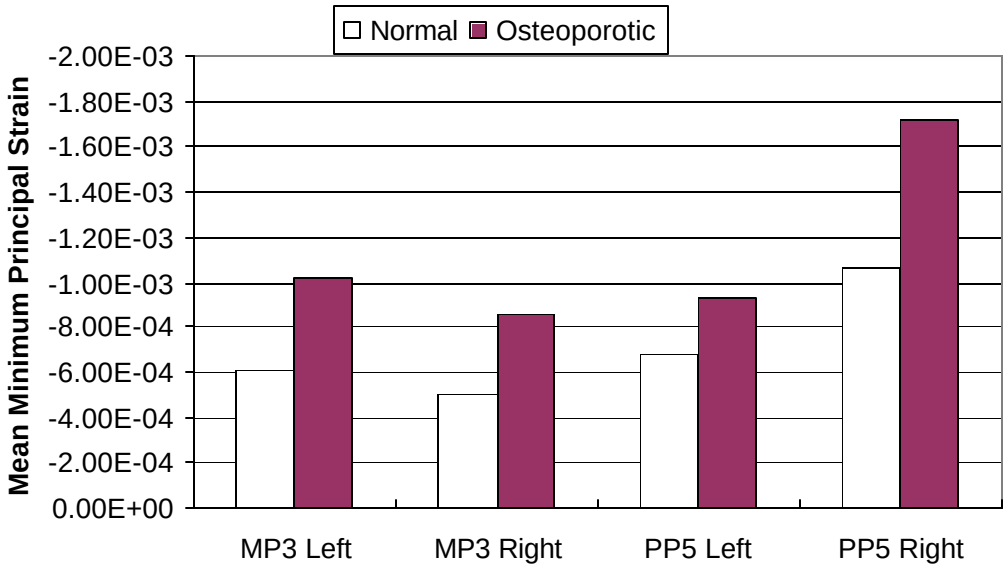

a) Non-homogeneous, No Cement

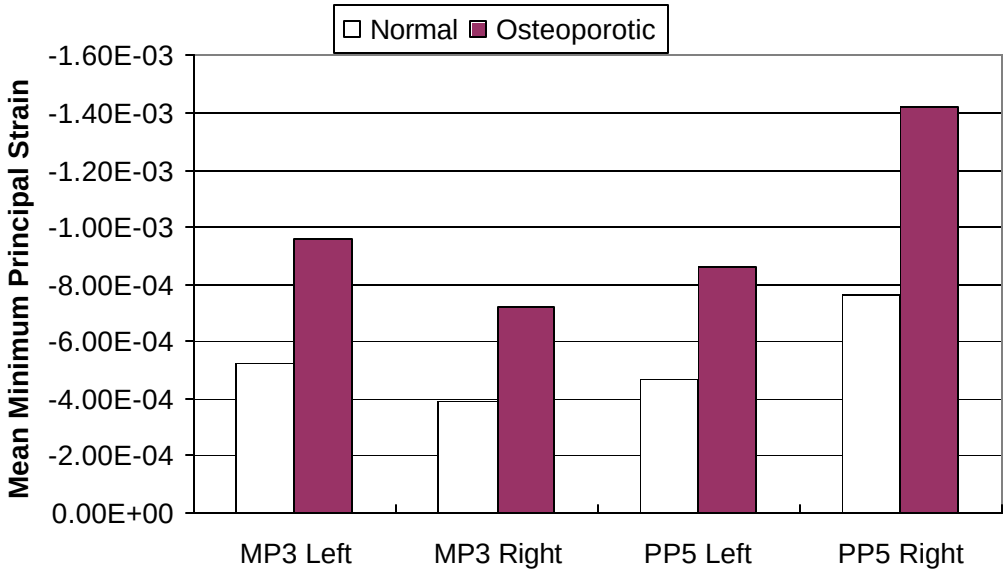

b) Homogeneous , No Cement

Figure 3.7: Mean ROI strains in normal and osteoporotic models. (a) Mean minimum principal strains in regions of interest for normal (MP3-3, PP5-3) and osteoporotic (MP3-4, PP5-4) non-homogeneous models without cement. (b) Normal (MP3-7, PP5-8) and osteoporotic (MP3-8, PP5-8) homogeneous models without cement. The osteoporotic models have significantly higher strains.

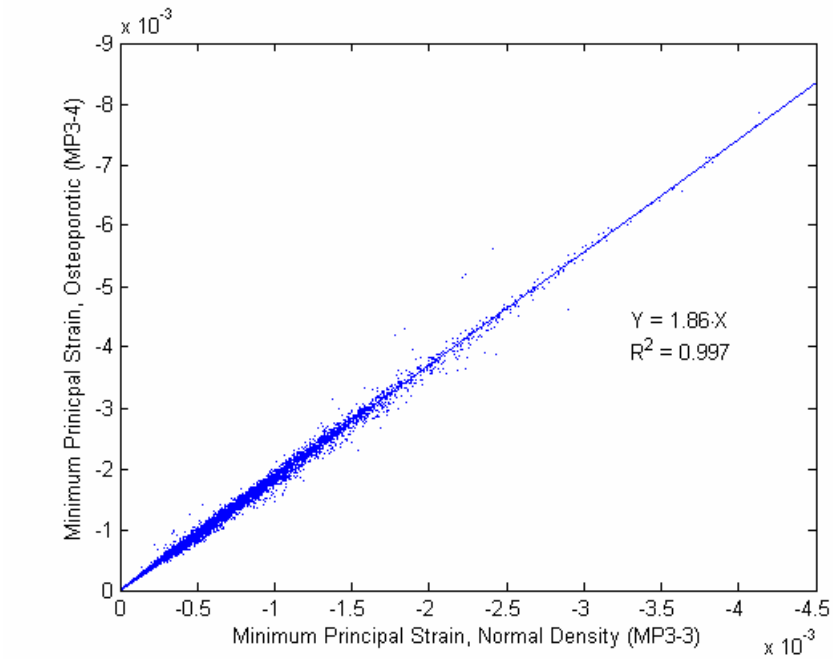

(a)

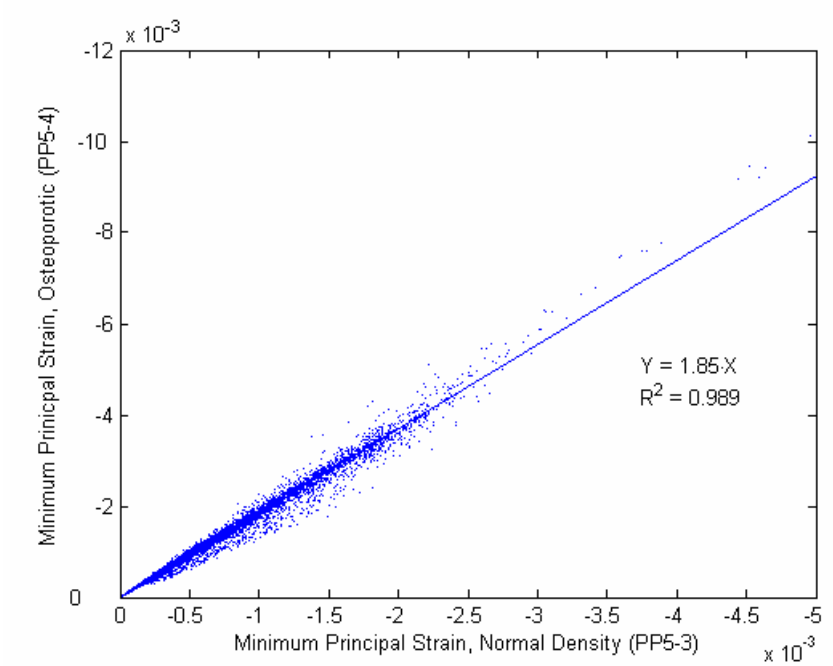

(b)

Figure 3.8: Whole model strain comparisons, normal density and osteoporotic models. The minimum principal strains from normal and osteoporotic models are plotted against each other for each node in the mesh. The best-fit lines for Male Post 3 (a) and Pelvis Post 5 (b) models show that the osteoporotic strains are about 86% larger than the normal density model. The high coefficients of determination indicate that the material variations introduced from the CT images effect the results similarly, despite the differences in the absolute values.

3.4 Effect of Cement

Models with cement were compared to those without. The deflections at the sacral promontory were reduced in all cases by the inclusion of cement. However, the reduction was small, ranging from -0.89% to -3.90% as shown in Table 3.7. Thus, the effect of cement on the overall model stiffness was relatively minor.

Table 3.7: Deflections at sacral promontory for models with and without cement. The difference is given for each comparison made. (NH = non-homogeneous, H = homogeneous, N = normal density, O = osteoporotic)

	No Cement		Cement		Difference
	Model	Deflection (mm)	Model	Deflection (mm)	
Comparison 1: (NH, N)	MP3-3	0.414	MP3-1	0.404	-2.27%
Comparison 2: (NH, O)	MP3-4	0.772	MP3-2	0.759	-1.79%
Comparison 3: (H, N)	MP3-7	0.461	MP3-5	0.457	-0.89%
Comparison 4: (H, O)	MP3-8	0.848	MP3-6	0.837	-1.33%
Comparison 5: (NH, N)	PP5-3	0.402	PP5-1	0.386	-3.90%
Comparison 6: (NH, O)	PP5-4	0.753	PP5-2	0.730	-3.08%
Comparison 7: (H, N)	PP5-7	0.412	PP5-5	0.406	-1.52%
Comparison 8: (H, O)	PP5-8	0.766	PP5-6	0.748	-2.37%

Contrary to the effect on the overall model, the inclusion of cement had a significant local impact. The strain magnitudes in the regions of interest were reduced by the inclusion of cement. The values of RMS_{Diff} varied from 25 to 60% (See Appendix 3). Figure 3.9 shows the region of interest principal strains for model MP3-1 (cement) and model MP3-3 (no cement), which are non-homogeneous normal density models. It can be seen in Figure 3.9 that the effect tends to be greatest at the center of the region of interest. As the cement is nominally centered in these regions, it seems that toward the edges, moving away from the cement, the effect of the cement drops off.

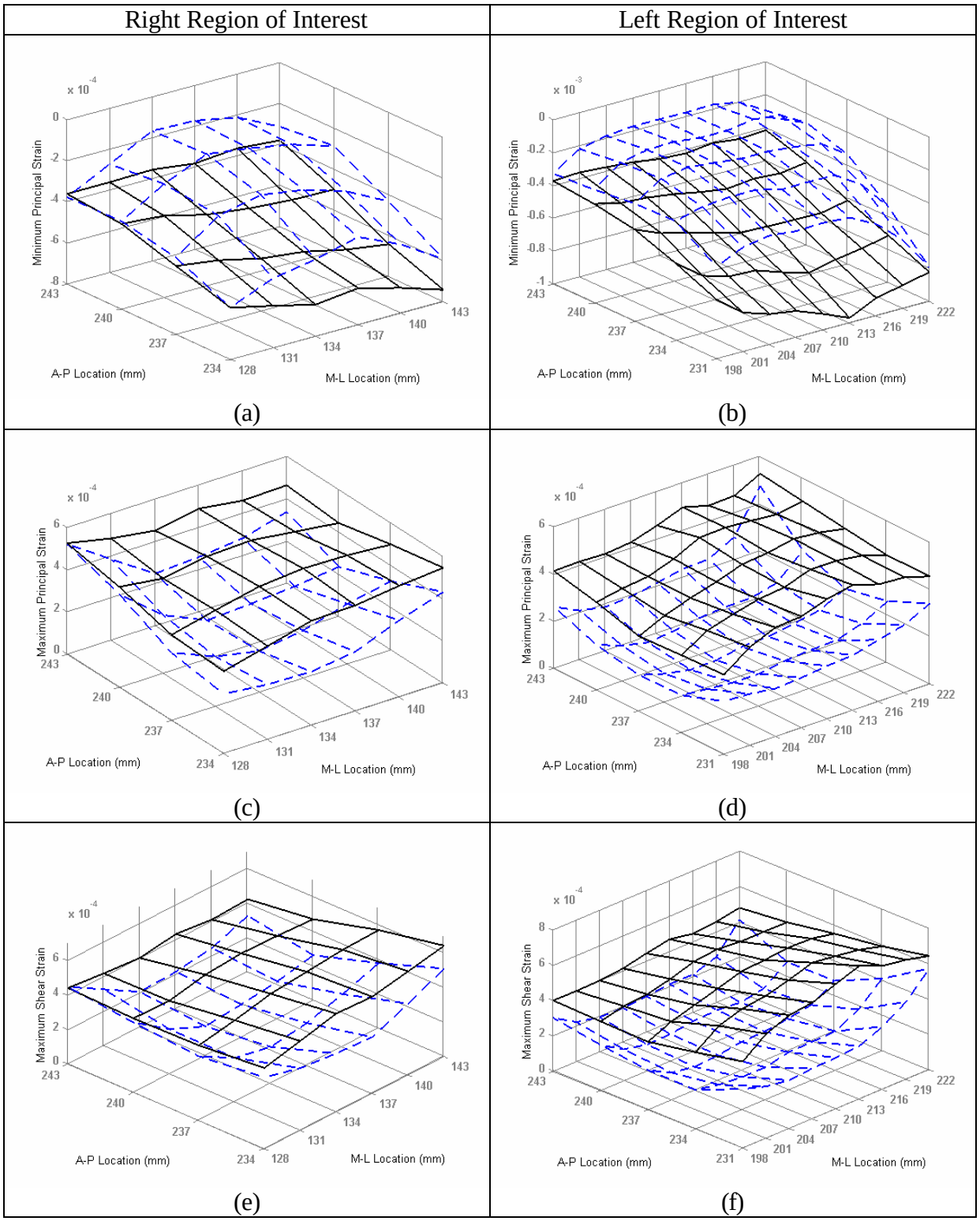

Figure 3.9: Region of interest principal strains in models with and without cement. Comparison 1 region of interest strains in No Cement (solid line, model MP3-3) and Cement (dashed line, model MP3-1) models. The minimum principal (a, b), maximum principal (c, d), and maximum shear (e, f) strains are shown respectively for Right and Left regions of interest.

The cement causes a significant reduction in the region of interest strain. Figure 3.10 shows the mean minimum principal strains for normal and osteoporotic non-homogeneous models. For the non-homogeneous case, it does not appear that the effect of cement differs between the normal and osteoporotic models. Figure 3.11 shows the mean minimum principal strains for normal and osteoporotic homogeneous models. In the homogeneous models, the effect of cement is less in normal density models than in the osteoporotic models. RMS_{Diff} values for all of these cases are presented in Table 3.8. See Appendix 3 for results for all comparisons made.

Unlike material homogeneity and bone density, the effects of cement appear to be mostly localized. This is confirmed by Figure 3.12, which compares whole model strains in models with and without cement. The strain variations introduced by the cement are visible as the scattering of points off the line. Since these are mostly below the line, the effect on the overall model is one of reducing strain. The slopes of the best fit lines indicate the cement models are 2 – 5 % stiffer. This is comparable to the differences seen in the sacral promontory deflections.

Table 3.8: ROI Differences between models with and without cement. RMS_{Diff} is given for minimum principal strains in normal and osteoporotic non-homogeneous models.

	Non-homogeneous, Normal		Non-homogeneous, Osteoporotic	
No Cement	MP3-3	PP5-3	MP3-4	PP5-4
Cement	MP3-1	PP5-1	MP3-2	PP5-2
RMS_{Diff} (Left ROI)	56.4%	59.6%	58.1%	54.4%
RMS_{Diff} (Right ROI)	40.0%	42.2%	40.3%	40.2%
	Homogeneous, Normal		Homogeneous, Osteoporotic	
No Cement	MP3-7	PP5-7	MP3-8	PP5-8
Cement	MP3-5	PP5-5	MP3-6	PP5-6
RMS_{Diff} (Left ROI)	40.8%	39.6%	51.7%	54.2%
RMS_{Diff} (Right ROI)	25.5%	25.0%	34.4%	35.3%

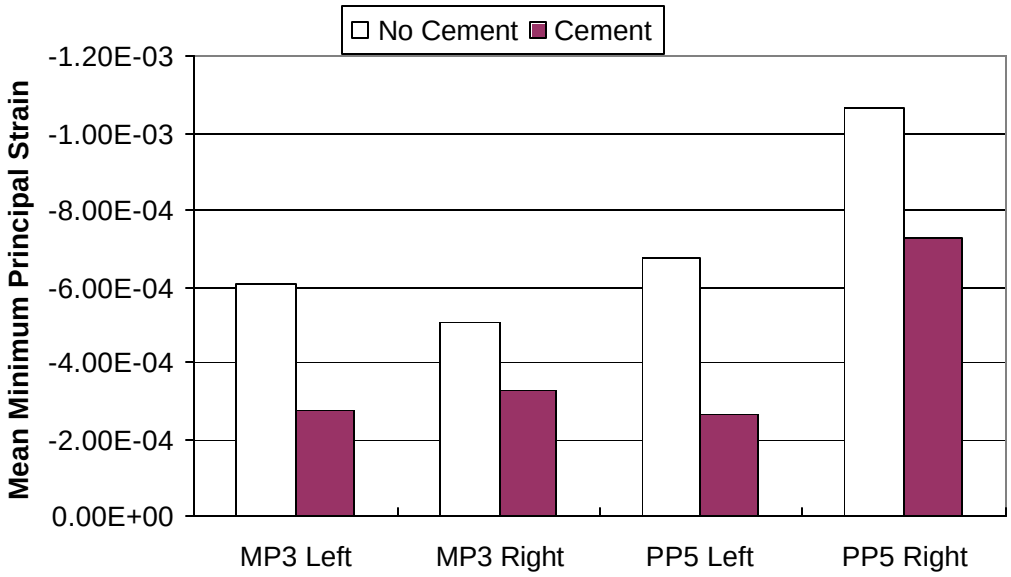

a) Non-homogeneous, Normal Density

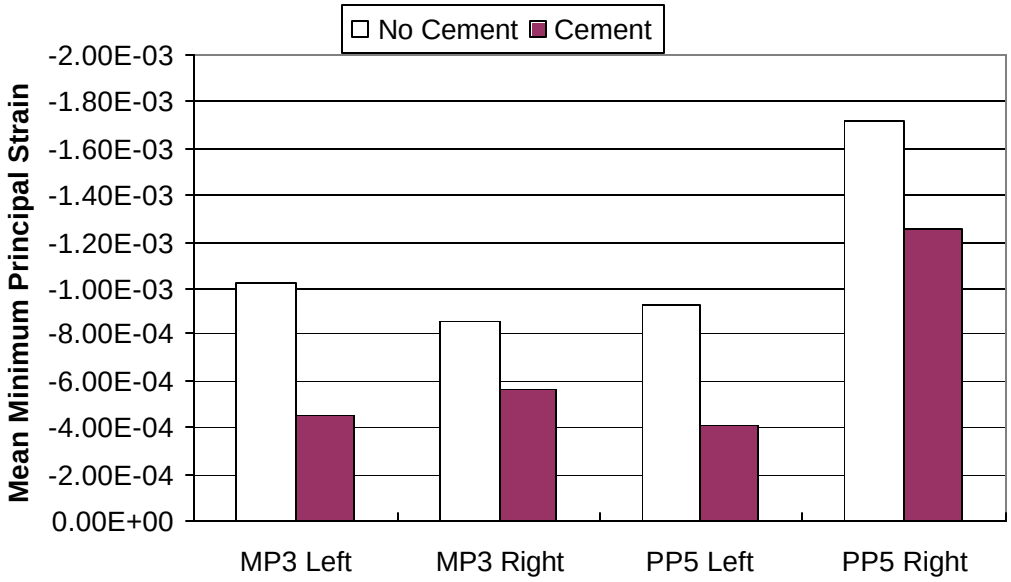

b) Non-homogeneous, Osteoporotic

Figure 3.10: Mean ROI strains in non-homogeneous models for cement comparison. (a) Mean minimum principal strains in regions of interest for non-homogeneous normal density models with (MP3-1, PP5-1) and without (MP3-3, PP5-3) cement. (b) Non-homogeneous osteoporotic models with (MP3-2, PP5-2) and without (MP3-4, PP5-4) cement.

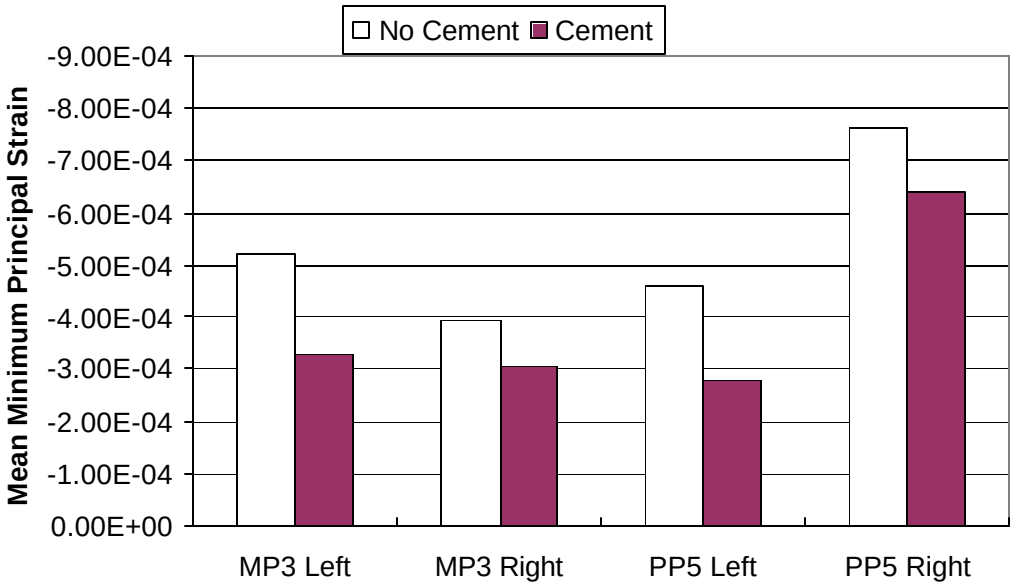

a) Homogeneous, Normal Density

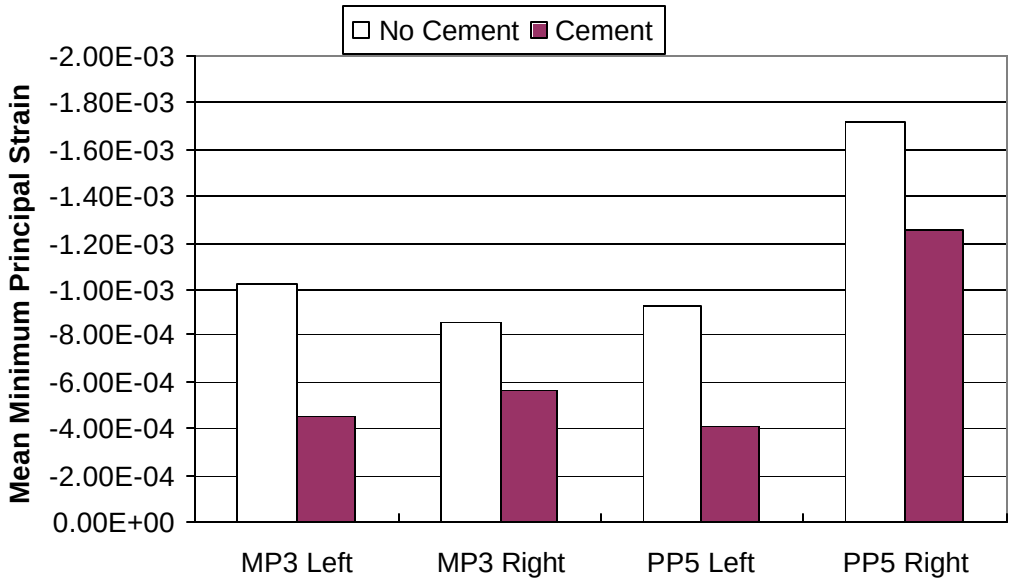

b) Homogeneous, Osteoporotic

Figure 3.11: Mean ROI strains in homogeneous models for cement comparison. (a) Mean minimum principal strains in regions of interest for homogeneous normal density models with (MP3-5, PP5-5) and without (MP3-7, PP5-7) cement. (b) Homogeneous osteoporotic models with (MP3-6, PP5-6) and without (MP3-8, PP5-8) cement. The strain reduction from cement is less in the normal density case.

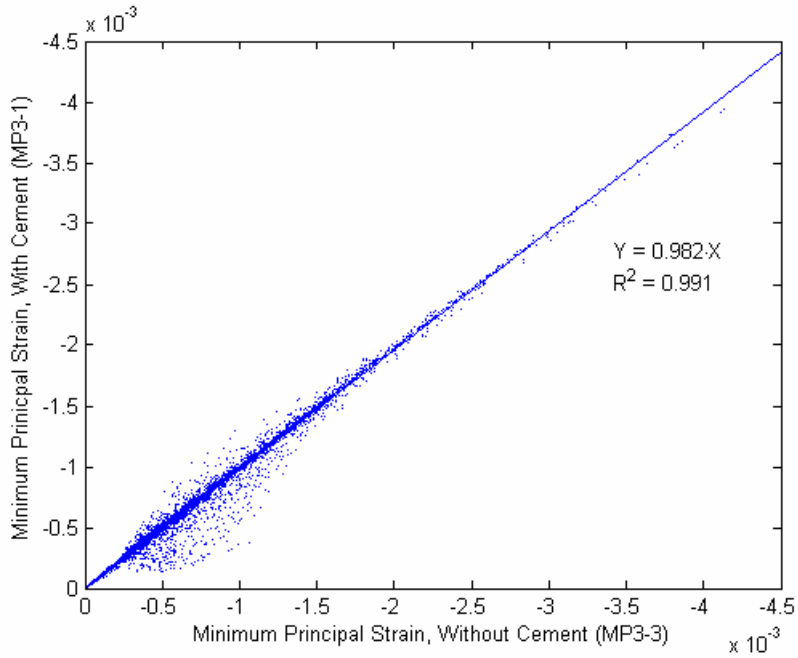

(a)

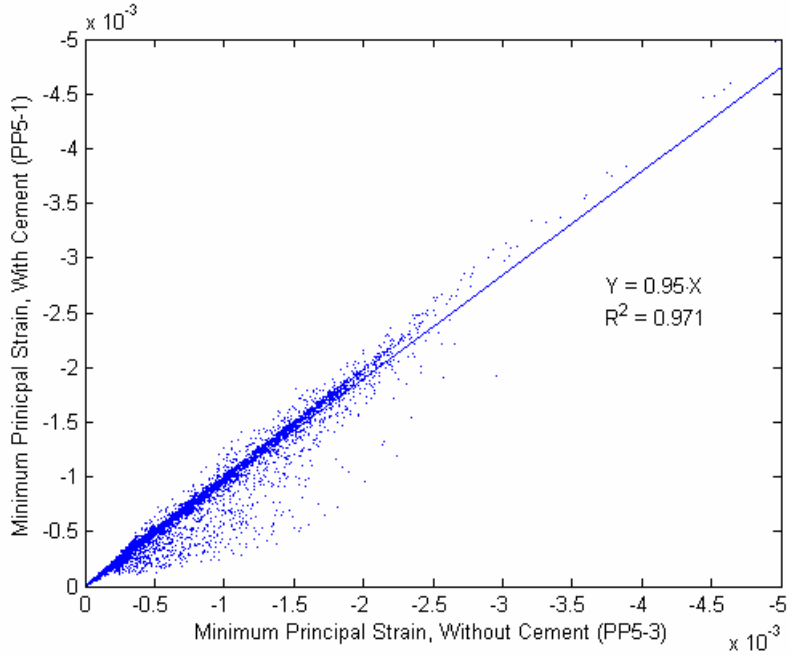

(b)

Figure 3.12: Whole model strain comparisons, models with and without cement. The minimum principal strains from models with cement and models without cement are plotted against each other for each node in the mesh. For both Male Post 3 (a) and Pelvis Post 5 (b), the cement produces only a slight decrease in the strain overall. However, the cement greatly reduced strains at some points, which appear well below the line.

Chapter 4: Discussion

In Chapter 4, the outcomes of the finite element models are discussed. In Section 4.1, the significance of the strains observed in the sacrum is highlighted. Several effects of the material homogeneity are discussed in Section 4.2, showing the importance of non-homogeneous properties. Section 4.3 discusses the differences seen between normal and osteoporotic models. Sacroplasty is discussed in Section 4.4, based on the results of the models with and without cement. Some thoughts on the differences seen between individuals are given in Section 4.5. Finally, a summary of the important conclusions is given in Section 4.6.

4.1 Sacral Strains

Both compressive and tensile principal strains were significant in the regions of interest. The minimum principal (compressive) strains in the regions of interest were generally of larger magnitude than the maximum principal (tensile) strains. However, the magnitude of the tensile strains was significant, generally about 50 – 90% of the magnitude of the compressive strain. Because significant tensile and compressive principal strains were present, shear strains were also significant at the regions of interest. The presence of significant tensile strains is important because the strength of cancellous bone in tension is thought to be less than in compression.

It is generally accepted that cancellous bone is weaker in tension than compression. According to Kaplan (1985) the tensile strength of cancellous bone is about 7.6 MPa, 60% of the compressive strength of 12.4 MPa. Keaveny (2001) indicates that the difference between tensile and compressive yield stress is a linear function of the elastic modulus. However, the tensile yield strain does not appear to depend on the elastic

modulus, and was found to be less than the compressive yield strain (Kopperdahl, 1998). Thus, the strain is actually better than stress as an indicator of failure risks in cancellous bone.

Compared to the yield strain of cancellous bone, the strains found in the regions of interest appear to be low. The maximum region of interest strains occur in model PP5-4, which is non-homogeneous, osteoporotic, and without cement. These peak strains are 0.156% for tension and 0.344% for compression. Kopperdahl (1998) found yield strains for tension and compression to be 0.78% and 0.84% respectively in human vertebral bone. Although the region of interest strains are not this large, they almost certainly do not represent the largest strains in the model. Additionally, different loading could change the strains significantly, leading to failure in the cancellous bone.

Although stresses were not examined explicitly, the stress state should be similar to the strain state. That is to say that both compressive and tensile stresses will be significant. The presence of significant tensile stress and strain is could affect the risks of sacral insufficiency fractures. Because of the lower strength in tension, tensile stresses or strains in the sacral ala might be the deciding factor in the beginning and/or propagation of a crack. Confirmation of this might be possible by introducing material damage to a model of the sacrum.

4.2 Material Properties

The use of non-homogeneous materials had a significant effect on the results, as homogeneous properties only accounted for about 80% of the strain variation predicted by non-homogeneous models. It was assumed that the non-homogeneous case is more correct than the homogeneous, because the non-homogeneous case corresponds more

closely to the actual physiology. Compared to the homogeneous case, a non-homogeneous model causes some strains to increase and some to decrease. In some locations, the stiffness in the non-homogeneous model is higher than the homogeneous stiffness, causing a decrease in strains. Likewise, in some locations the non-homogeneous stiffness is lower, causing an increase in strains.

Based on the sacral promontory deflections, the non-homogeneous models were 2-14% stiffer. However, based on the whole model strain comparisons, the homogeneous models were 1-4% stiffer. This discrepancy is probably a result of local differences in the material properties. In non-homogeneous models, the base of the sacrum is cortical bone, about twice the stiffness of cancellous bone. Thus, the local stiffness of the base of the sacrum (where the loads are applied) is smaller in the homogeneous models, even though overall the homogeneous model is stiffer.

The regions of interest provide another example of how the local effects of non-homogeneous models may be different than homogeneous models. For models without cement, the material in the regions of interest is simply cancellous bone, with roughly half the stiffness of the homogeneous model. One possible consequence of this is that a non-homogeneous model's region of interest strains will be higher than region of interest strains in the corresponding homogeneous model. In fact, this effect is seen in the results of models without cement. Another possible consequence is that the stresses could be redistributed around the lower stiffness cancellous bone. In this case, the strains would be similar in the homogeneous and non-homogeneous cases, but the regions of interest would carry different loads.

Some elements in the non-homogeneous model will have greater stiffness than the homogeneous case. In actual bone, an important region of higher stiffness is the cortical shell. However, in the models created there is no cortical shell, *per se*. As can be seen in the CT image shown in Figure 4.1(a), the actual cortical shell is thin, though significantly denser than the cancellous bone. In the model, the cortical shell is not as clearly present. Since Bonemat V2 averages the pixels within the volume of each element to determine the element modulus, the element size reduces the visible "cortical shell" in the model. Because most elements containing cortical bone also contain a significant fraction of cancellous bone, the element modulus is less than cortical bone stiffness.

Although the cortical shell was not modeled explicitly, I believe this had little effect on the results because this study does not present stresses or strains in the cortical shell. According to Bayraktar (2003), the cortical shell of the vertebral body serves primarily to provide load transfer paths to trabeculae at the edges. This was determined by modeling the cancellous core of the vertebral body at the trabecular level. When the cortical shell was removed, many trabeculae on the outer part of the model were not loaded, increasing the loads on others. In this study, I did not model actual trabeculae, so a cortical shell was not needed to transfer loads to trabeculae. The stiffness contributed by the cortical shell was averaged into the elements that included it.

If it was desired to examine results at the surface, it could be worth creating a model that better defined the cortical shell. With the method used in this study, reducing the element size could better represent the cortical shell. This is illustrated by Figure 4.1(c), in which non-homogeneous properties were applied to the finer mesh used for model MP3-9. Alternatively, some finite element models of bone, for example

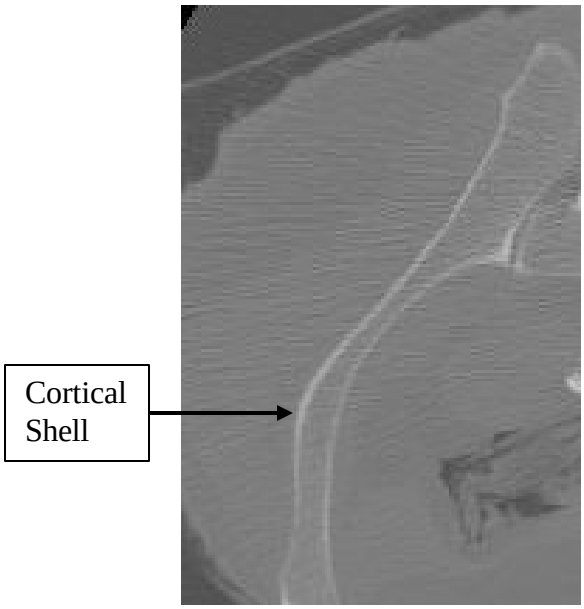

(a)

(b)

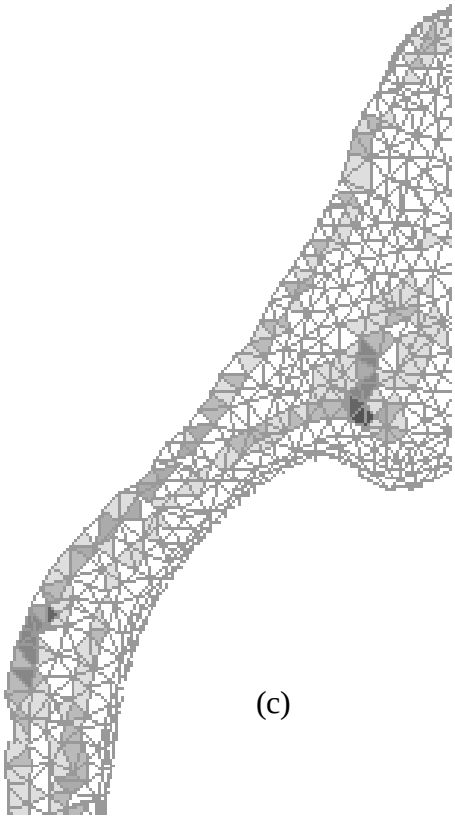

(c)

Figure 4.1: Representation of cortical shell. (a) In the CT image, the cortical shell is thin, but distinctly different than cancellous bone. (b) In the models used, the cortical shell is not seen as clearly, as the stiffness is averaged into the larger elements. (c) As element size is reduced, the cortical shell appears more clearly.

Liebschner (2001), Polikeit (2003), and Garcia (2000), have created specific elements representing the cortical shell. This method explicitly defines the cortical shell, but adds complexity in creating the mesh, especially with regards to applying non-homogeneous material properties from a CT image. This complexity was not deemed necessary in this study, as the focus was not on the cortical shell.

One assumption made in this study is that the cancellous bone of the sacrum is isotropic. However, it is possible that the anisotropy of the sacrum would have a significant effect. The addition of anisotropy could be an important addition to future models, but would require better information on the anisotropy of sacral bone. Augat (1998) pointed out that a high resolution CT image could be used to determine the directionality of trabeculae, and thus give some idea of the anisotropic properties of the bone in the image. However, such a method would require higher resolution images than were used in this case.

4.3 Osteoporosis

A reduction in bone density was used to model osteoporosis. This had the effect of reducing the elastic moduli applied to the model. In a similar manner, Polikeit (2003) modeled osteoporosis by directly reducing the elastic modulus, by 33% for cortical bone and 66% for cancellous bone. However, beyond simple density reduction, bone loss with aging includes thinning of the cortical shell and loss of trabeculae, reducing trabecular connectivity (Jee, 2001). Thus, a simple density change may not fully capture the effects of osteoporosis. It would be of interest to know how well a simple density reduction models the effect of osteoporosis. By using CT images of osteoporotic bones to create

finite element models, the effects of actual osteoporosis could be compared with the effects of density reduction.

The results showed that a reduction in bone density caused the strains to increase. In purely homogeneous models, the increase was exactly linear, proportional to the amount of density reduction. This was to be expected. However, even in non-homogeneous models, the change was still highly linear, and proportional to the density reduction. This was somewhat surprising. It indicates that the variation of the material properties within the model is relatively insensitive to the level of density used. The relative variation of the material properties was the same, independent of the magnitude of the actual elastic moduli. This is shown in Figure 4.2. The actual element property distributions (Figure 4.2(a)) of the normal and osteoporotic models are different. However, each curve shows the same variation when normalized about its mean elastic modulus, as shown in Figure 4.2(b).

The percent strain increase in osteoporotic models was about 86% overall. The increase was lower, from 40 to 70%, in the regions of interest. Although there is some scatter in the non-homogeneous cases, it is interesting that the strain increase due to density reduction was uniformly lower in these locations. This effect could be explained by the presence of cement in models containing cement. Cement increases the stiffness in the regions of interest, which would resist the increase in strain.

The osteoporotic models are at greater risk of developing fractures than the normal models. The maximum strains in the regions of interest were 35 to 88% greater in osteoporotic models. For example, in the models MP3-3 and MP3-4 (non-homogeneous, without cement,) the maximum compressive strains in the Left regions of interest are

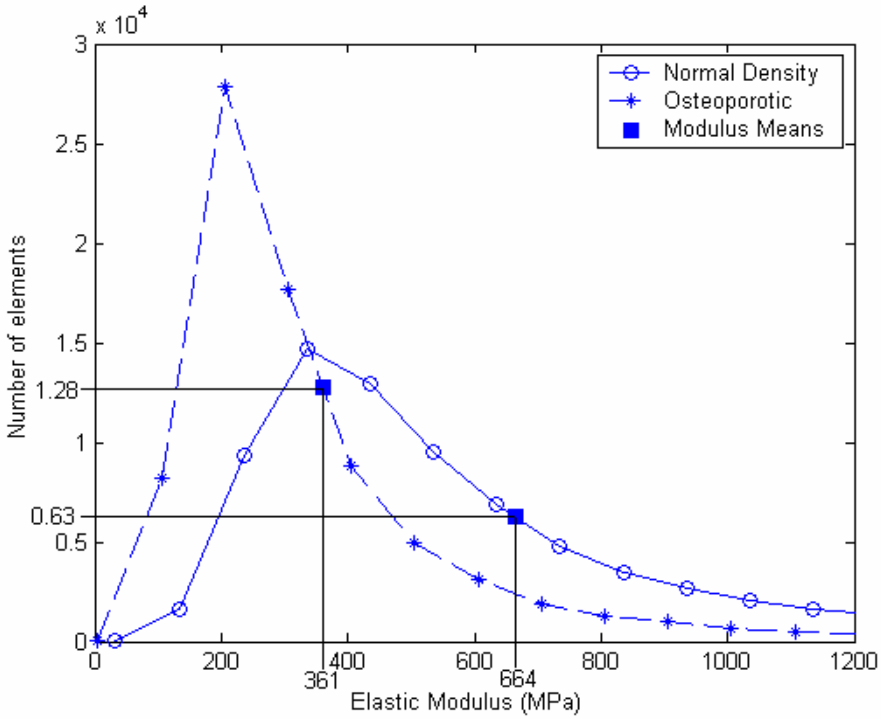

(a)

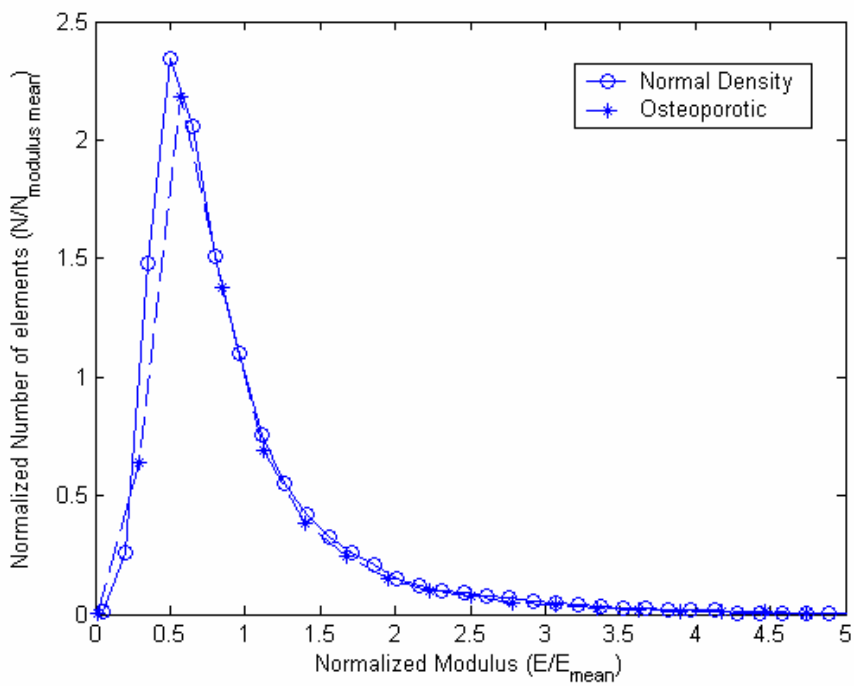

(b)

Figure 4.2: Similarity of Normal and Osteoporotic Modulus Distributions. (a) The element modulus distributions are significantly different, representing lower modulus values for the osteoporotic case. (b) When normalized about the mean modulus points, the two curves closely coincide. Thus, normal and osteoporotic material properties represent the same material variation, but scaled to different magnitudes.

0.097% and 0.163%. Recall the compressive yield strain of 0.84% (Kopperdahl, 1998). Based on these strains, with the loads used, the normal model has a safety factor of 8.7 while the osteoporotic model has a safety factor of 5.2. This indicates that the osteoporotic models will reach yield more easily, and thus are at greater risk of cancellous bone failure.

4.4 Effect of Cement

The introduction of cement reduced local (region of interest) strains 40 to 60% in the non-homogeneous models. However, the overall models experienced only slight strain reductions. Based on the deflections at the sacral promontory, the model stiffness increased about 1 to 4% with the addition of cement.

Liebschner (2001) predicted that cement could increase vertebral body stiffness by almost 50% over the intact stiffness, and Heini (2001) showed stiffness increases of 174% in osteoporotic vertebrae. However, the volume of cement used in these cases was between 25 and 50% of the whole vertebral body volume. The stiffness increase depends on the amount of cement injected (Liebschner, 2001). From the finite element models, a rough estimate of the cement fill of the sacrum is about 3%. As the sacrum is larger than a vertebral body, achieving comparable percent fill would require considerably more cement. This could increase the risks of the procedure, specifically the possibility of cement leakage from the sacrum. If the sacrum is limited to small percent fills, the effects of sacroplasty will be primarily limited to the local areas around the cement.

In the homogeneous models, the strain reductions due to cement in the regions of interest were greater in the osteoporotic cases (about 50% reduction) than in the normal density cases (about 40% reduction). For the non-homogeneous models, the strain

reductions were similar in the normal and osteoporotic cases. Thus, it appears that non-homogeneous models react differently to the inclusion of cement than homogeneous models. While the nature of the difference was not well defined by this study, this again shows that non-homogeneous material properties are an important aspect of modeling bone.

Although this model helps quantify the effects of cement injection in the sacrum, it does not directly address the case of sacral insufficiency fractures. No fracture was included in the model, nor was damage introduced. Sacral fractures were not believed to be present in the cadavers on which sacroplasty was performed. Even if sacral fractures were present, the bone density in the CT scan would be about the same. Thus, the material properties created for the models would be similar. To better study the effects of cement on sacral fractures, future modeling efforts could include an explicit representation of a crack in the finite element model.

4.5 Variations between Individuals

CT images from two different cadavers were used to create finite element models. As expected, there were some differences in the results. The sacral promontory deflections were from 2.5 – 11% less in the Pelvis Post 5 models. This is probably in part due to the sacral geometry differences between the two. The sacral promontory protrudes more in the Male Post 3 models, which means it will deflect more if there is a rotation of the sacrum about a medial-lateral axis.

In comparing non-homogeneous and homogeneous models, the Pelvis Post 5 models showed somewhat more variation (R^2 = 0.79, versus 0.86 for Male Post 3). In

addition, the maximum compressive strain in the Pelvis Post 5 homogeneous model, about 0.9%, was nearly twice that in the Male Post 3 homogeneous model. Between normal and osteoporotic models, the strain variation was small for both Pelvis Post 5 and Male Post 3 models, R^2 = 0.989 and 0.997 respectively. Also, the strain increases due to osteoporosis were nearly identical, 86% and 85% respectively. The inclusion of cement had a greater effect on the Pelvis Post 5 models. Model stiffness increased by about 5%, as compared to about 2% for the Male Post 3 models. The difference is likely due to the amount of cement. From the CT images, it appears that more cement was injected into the sacrum in the Pelvis Post 5 cadaver. Given the differences in the sacrum geometry and material distributions, the results were quite similar.

4.6 Summary

- The sacrum has a 3D multi-axial state of strain. Tensile, compressive, and shear strains are all significant.
- Homogeneous models can account for about 80% of the variation of non-homogeneous models.
- Simulating osteoporosis by reducing the bone density applied to the model increases the resulting strains nearly linearly, even in non-homogeneous cases.
- Cement in the sacrum reduced strains 40-60% locally. However, model stiffness only increased 1-4%.

References:

An, Y.H., Barfield, W.R., and Knets, I., "Methods of Evaluation for Bone Dimensions, Densities, Contents, Morphology and Structures," pp. 103-118 in: An, Y.H., and Draughn, R.A. (eds.), 2000, *Mechanical Testing of Bone and the Bone-Implant Interface*, CRC Press, Boca Raton.

Ashman, R.B, Turner, C.H., and Cowin, S.C., 1986, "Ultrasonic Technique for the Measurement of the Structural Elastic Modulus of Cancellous Bone," Trans. Orth. Res. Soc., pp. 43.

Augat, P., Link, T., Lang, T.F., Lin, J.C., Majumdar, S., and Genant, H.K., 1998, "Anisotropy of the Elastic Modulus of Trabecular Bone Specimens from Different Anatomical Locations," Med. Eng. & Phys., **20**, pp. 124–131.

Babayev, M., Lachmann, E., and Nagler, W., 2000, "The Controversy Surrounding Sacral Insufficiency Fractures: To Ambulate or Not To Ambulate?," Am. J. Phys. Med. Rehabil., **79**(4), pp. 404-409.

Baroud, G., Wu, J.Z., Bohner, M., Sponagel, S., and Steffen, T., 2003, "How to Determine the Permeability for Cement Infiltration of Osteoporotic Cancellous Bone," Med. Eng. Phys., **25**, pp. 283-288.

Barr, J.D., Barr, M.S., Lemley, T.J., et al, 2000, "Percutaneous Vertebroplasty for Pain Relief and Spinal Stabilization," SPINE **25**(8) pp. 923-928.

Bascoulergue, Y., Duquesnel, J., Leclercq, R., Mottolese, C., and Lapras, C., 1977, "Percutaneous Injection of Methyl Methacrylate in the Vertebral Body for the Treatment of Various Diseases: Percutaneous Vertebroplasty (abstract)." Radiology, **169P**, pp. 372.

Bayraktar, H.H., Buckley, J.M., Adams, M.F., Gupta, A., Hoffmann, P.F., Lee, D.C., Papadopoulos, P., and Keaveny, T.M., 2003, "Cortical Shell Thickness and its Contribution to Vertebral Body Stiffness," ASME 2003 Summer Bioengineering Conference, Key Biscayne, Florida, pp. 115-116.

Belkoff, S.M., Mathis, J.M., Jasper, L.E., et al, 2001, "The Biomechanics of Vertebroplasty - The Effect of Cement Volume on Mechanical Behavior," SPINE **26** (14), pp. 1537-1541.

Berlemann, U., Ferguson, S.J., Nolte, L.P., et al, 2002, "Adjacent Vertebral Failure After Vertebroplasty - A Biomechanical Investigation," J. Bone Joint Surg. Br., **84B**(5), pp. 748-752.

Brown, T.D., and Ferguson, A.B., 1980, "Mechanical Property Distribution in the Cancellous Bone of the Human Proximal Femur," Acta Orthop. Scand., **51**, pp. 429-437.

Carter, D.R., and Hayes, W.C., 1977, “The Compressive Behavior of Bone as a Two-Phase Porous Structure,” J. Bone Joint Surg., **59-A**(7), pp. 954-962.

Cattaneo, P.M., Dalstra, M., Frich, L.H., 2001, “A Three-Dimensional Finite Element Model from Computed Tomography Data: A Semi-Automated Method,” Proc. Inst. Mech. Eng. [H], **215**(2), pp. 203-213.

Charriere, E., Sirey, F., and Zysset, P.K., 2003, “A Finite Element Model of the L5–S1 Functional Spinal Unit: Development and Comparison with Biomechanical Tests In Vitro,” Comp. Methods Biomech. Biomed. Eng., **6**(4), pp. 249–261.

Ciarelli, M.J., Goldstein, S.A., Dickie, D., Ku, J.L, Kapper, M., Stanley, J., Flynn, M.J., and Matthews, L.S., 1986, “Experimental Determination of the Orthogonal Mechanical Properties, Density, and Distribution of Human Trabecular Bone from the Major Metaphyseal Regions Utilizing Materials Testing and Computed Tomography,” Trans. Orth. Res. Soc., pp. 42.

Ciarelli, M.J., Goldstein, S.A., Kuhun, J.L., Cody, D.D., and Brown, M.B., 1991, “Evaluation of Orthogonal Mechanical Properties and Density of Human Trabecular Bone from the Major Metaphyseal Regions with Materials Testing and Computed Tomography,” J. Orthop. Res., **9**(5), pp. 674–682.

Dalstra, M., Huiskes, R., Odgaard, A., and van Erning, L., 1993, “Mechanical and Textural Properties of Pelvic Trabecular Bone,” J. Biomech., **26**(4-5), pp. 523-535.

Dalstra, M., Huiskes, R., and van Erning, L., 1995, “Development and Validation of a Three-Dimensional Finite Element Model of the Pelvic Bone,” J. Biomech. Eng., **117**(3), pp. 272-278.

Dawson, J.M., Khmelniker, B.V., and McAndrew, M.P., 1999, “Analysis of the Structural Behavior of the Pelvis during Lateral Impact using the Finite Element Method,” Accid. Anal. Prev., **31**(1-2), pp. 109-119.

Dehdashti, A.R., Martin, J.B., Jean, B., and Rufenacht, D.A., 2000, “PMMA Cementoplasty in Symptomatic Metastatic Lesions of the S1 Vertebral Body,” Cardiovasc. Intervent. Radiol., **23**(3), pp. 235-237.

Evans, F.G., and King, A.L., , “Regional Differences in some Physical Properties of Human Spongy Bone,” pp. 49-67 in: Evans, F.G. (ed.), 1961, *Biomechanical Studies of the Musculo-Skeletal System*, C.C. Thomas, Springfield.

Ezquerro, F., Simón, A., Prado, M., and Pérez, A., 2004, “Combination of Finite Element Modeling and Optimization for the Study of Lumbar Spine Biomechanics Considering the 3D Thorax–Pelvis Orientation,” Med. Eng. & Phys., **26**, pp. 11–22.

Galibert, P., Deramond, H., Rosat, P., and Le Gars, D., 1987, "Preliminary Note on the Treatment of Vertebral Angioma by Percutaneous Acrylic Vertebroplasty [in French]," Neurochirurgie, **33**, pp. 166–168.

Garant, M., 2002, "Sacroplasty: A New Treatment for Sacral Insufficiency Fracture," J. Vasc. Interv. Radiol., **13**, pp. 1265-1267.

Garcia, J.M., Doblare, M., Seral, B., Seral, F., Palanca, D., and Gracia, L., 2000, "Three-Dimensional Finite Element Analysis of Several Internal and External Pelvis Fixations," J. Biomech. Eng., **122**(5), pp. 516-522.

Giddings, V.L., Kurtz, S.M., Jewett, C.W., Foulds, J.R., and Edidin, A.A., 2001, "A Small Punch Test Technique for Characterizing the Elastic Modulus and Fracture Behavior of PMMA Bone Cement used in Total Joint Replacement," Biomaterials, **22**(13), pp. 1875-1881.

Goldstein, S.A., 1987, "The Mechanical Properties of Trabecular Bone: Dependence on Anatomic Location and Function," J. Biomech., **20**(11/12), pp. 1055-1061.

Goodenough, D.J., "Tomographic Imaging," pp. 511-54, in: Beutel, J., Kundel, H.L., and Van Metter, R.L. (eds.), 2000, *Handbook of Medical Imaging, Volume 1. Physics and Psychophysics*, SPIE Press, Bellingham.

Grasland, A., Pouchot, J., Mathieu, A., Paycha, F., and Vinceneux, P., 1996, "Sacral Insufficiency Fractures: An Easily Overlooked Cause of Back Pain in Elderly Women," Arch. Intern. Med., **156**(6): pp. 668-674.

Harper, C.M., and Lyles, Y.M., 1988, "Physiology and Complications of Bed Rest," JAGS, **36**, pp. 1047-1054.

Heini, P.F., Berlemann, U., Kaufmann, M., Lippuner, K., Fankhauser, C., and van Landuyt, P., 2001, "Augmentation of Mechanical Properties in Osteoporotic Vertebral Bones – A Biomechanical Investigation of Vertebroplasty Efficacy with Different Bone Cements," Eur. Spine. J., **10**, pp.164–171.

Heini, P.F., Walchli, B., Berlemann, U., 2000, "Percutaneous Transpedicular Vertebroplasty with PMMA: Operative Technique and Early Results. A Prospective Study for the Treatment of Osteoporotic Compression Fractures," Eur. Spine J., **9**, pp. 445–450.

Hodgskinson, R., and Currey, J.D., 1992, "Young's Modulus, Density and Material Properties in Cancellous Bone over a Large Density Range," J. Mat. Sci. Mat. Med., **3**(5), pp. 377-381.

Jee, W.S.S., “Integrated Bone Tissue Physiology: Anatomy and Physiology,” pp. 1-1 – 1-68 in: Cowin, S.C. (ed.), 2001, *Bone Biomechanics Handbook, Second Edition,* CRC Press, Boca Raton.

Kaplan, S.J., Hayes, W.C., Stone, J.L., and Beaupre, G.S., 1985, “Tensile Strength of Bovine Trabecular Bone,” J. Biomech., **18**, pp. 723-727.

Keaveny, T.M., “Strength of Trabecular Bone,” pp. 16-1 – 16-42, in: Cowin, S.C. (ed.), 2001, *Bone Biomechanics Handbook, Second Edition,* CRC Press, Boca Raton.

Keller, T.S., Hansson, T.H., Panjabi, M.M., and Spengler, D.M., 1987, “Regional Variations in the Compressive Properties of Lumbar Trabeculae,” Trans. Orth. Res. Soc., pp. 378.

Knapp, K.M., Blake, G.M., Spector, T.D., and Fogelman, I., 2004, “Can the WHO Definition of Osteoporosis be Applied to Multi-Site Axial Transmission Quantitative Ultrasound?,” Osteoporos. Int., **15**(5), pp. 367-74.

Kosmopoulos, V., and Keller, T.S., 2004, “Damage-Based Finite-Element Vertebroplasty Simulations,” Eur. Spine J., **13**(7), pp. 617-625.

Kopperdahl, D.L., and Keaveny, T.M., 1998, “Yield strain behavior of trabecular bone,” J. Biomech., **31**, pp. 601-608.

Liebschner, M.A.K., Rosenberg, W.S., and Keaveny, T.M., 2001, “Effects of Bone Cement Volume and Distribution on Vertebral Stiffness After Vertebroplasty,” SPINE **26** (14), pp. 1547-1554.

Lindahl, O., 1976, “Mechanical Properties of Dried Defatted Spongy Bone,” Acta Orthop. Scand., **47**, pp. 11-19.

Linden, U., 1991, “Mechanical Properties of Bone Cement – Importance of the Mixing Technique,” Clin. Orth. Rel. Res., **272**, pp. 274-278.

Lourie, H., 1982, “Spontaneous Osteoporotic Fracture of the Sacrum,” JAMA, **248**, pp. 715-717.

Marcy, P.Y., Palussiere, J., Descamps, B., Magne, N., Bondiau, P.Y., Ciais, C., and Bruneton, J.N., 2000, “Percutaneous Cementoplasty for Pelvic Bone Metastasis,” Support Care Cancer, **8**(6), pp. 500-503.

Marom, S.A., and Linden, M.J., 1990, “Computer Aided Stress Analysis of Long Bones Utilizing Computed Tomography,” J. Biomech., **23**(5), pp. 399–404.

Martens, M., VanAudekercke, R., Delport, P., DeMeester, P., and Muelier, J.C., 1983, "The Mechanical Characteristics of Cancellous Bone at the Upper Femoral Region," J. Biomech., **16**, pp. 971-983.

Martin, R.B., 1991, "Determinants of the Mechanical Properties of Bones," J. Biomech., **24**(Suppl. 1), pp. 79-88. Erratum in: J. Biomech., 1992, **25**(10), pp. 1251.

Mathis, J.M., Barr, J.D., Belkoff, S.M., Barr, M.S., Jensen, M.E., and Deramond, H., 2001, "Percutaneous Vertebroplasty: A Developing Standard of Care for Vertebral Compression Fractures," Am. J. Neuroradiol. **22**, pp. 373-381.

McBroom, R.J., Hayes, W.C., Edwards, W.T., Goldberg, R.P., and White, A.A., 1985, "Prediction of Vertebral Body Compressive Fracture using Quantitative Computed Tomography," J. Bone Joint Surg., **67A**, pp. 1206-1214.

McElhaney, J.H., Fogle, J.L, Melvin, J.W., Haynes, R.R., Roberts, V.L., and Alem, N.M., 1970, "Mechanical Properties of Cranial Bone," J. Biomech., **3**, pp. 495-511.

Merz, B., Niederer, P., Muller, R., and Ruegsegger, P., 1996, "Automated Finite Element Analysis of Excised Human Femora Based on Precision-QCT," J. Biomech. Eng., **118**(3), pp. 387–90.

Morris, P.P., Associate Professor, Division of Radiologic Sciences, Wake Forest University School of Medicine, Personal communication, February 7, 2005.

Newhouse, K.E., el-Khoury, G.Y., and Buckwalter, J.A., 1992, "Occult Sacral Fractures in Osteopenic Patients," J. Bone Joint Surg. Am., **74**, pp. 1472 - 1477.

Pentecost, R.L., Murray, R.A., and Brindley, H.H., 1964, "Fatigue, Insufficiency and Pathologic Fractures," JAMA, **187**(13), pp. 1001-1004.

Polikeit, A., Nolte, L.P., and Ferguson, S.J., 2003, "The Effect of Cement Augmentation on the Load Transfer in an Osteoporotic Functional Spinal Unit: Finite-Element Analysis," Spine, **28**(10), pp. 991-996.

Pommersheim, W., Huang-Hellinger, F., Baker, M., and Morris, P., 2003, "Sacroplasty: A Treatment for Sacral Insufficiency Fractures," Am. J. Neuroradiol., **24**(5), pp. 1003-1007.

Saha, S., and Pal, S., 1984, "Mechanical Properties of Bone Cement: A Review," J. Biomed. Mat. Res., **18**, pp. 435-462.

San Millan, R.D., Burkhardt, K., Jean, B., et al, 1999, "Pathology Findings with Acrylic Implants," Bone, **25**, pp. 85S–90S.

Schoenfeld, C.M., Lautenschlager, E.P., and Meyer, P.R., 1974, "Mechanical Properties of Human Cancellous Bone in the Femoral Head," Med. Biol. Eng., **12**, pp. 313-317.

Simonian, P.T., Routt, M.L., Harrington, R.M., and Tencer, A.F., 1996, "Internal Fixation for the Transforaminal Sacral Fracture," Clin. Orth., **323**, pp. 202-209.

Stolk, J., Verdonschot, N., and Huiskes, R., 2001, "Hip-joint and Abductor-Muscle Forces Adequately Represent In Vivo Loading of a Cemented Total Hip Reconstruction," J. Biomech., **34**, pp. 917-926.

Struhl, S., Goldstein, S.A., Dickie, D.L., Flynn, M.J., and Matthews, L.S., 1987, "The Distribution of Mechanical Properties of Trabecular Bone within Vertebral Bodies and Iliac Crest: Correlation with Computed Tomography Density," Trans. Orth. Res. Soc., pp. 262.

Sun, K., and Liebschner, M.A., 2004, "Evolution of Vertebroplasty: A Biomechanical Perspective," Annals Biomed. Eng., **32**(1), pp. 77-91.

Tack, G.R., Lee, S.Y., Lee, S.J., et al, 2001, "Prediction of Cement Volume for Vertebroplasty Based on Imaging and Biomechanical Results," KSME Int. J., **15**(7), pp. 1041-1050.

Taddei, F., Pancanti, A., and Viceconti, M., 2004, "An Improved Method for the Automatic Mapping of Computed Tomography Numbers onto Finite Element Models," Med. Eng. & Phys., **26**(1), pp. 61-69.

Taillandier, J., Langue, F., Alemanni, M., and Taillandier-Heriche, E., 2003, "Mortality and Functional Outcomes of Pelvic Insufficiency Fractures in Older Patients," Joint Bone Spine, **70**(4), pp. 287-289.

Tohmeh, A.G., Mathis, J.M., Fenton, D.C., Levine, A.M., and Belkoff, S.M., 1999, "Biomechanical Efficacy of Unipedicular Versus Bipedicular Vertebroplasty for the Management of Osteoporotic Compression Fractures," SPINE **24**(17), pp. 1771-1776.

Tortora, G.J., and Anagnostakos, N.P., 1984, *Principles of Anatomy and Physiology, 4th Edition*, Harper & Row, New York.

Wasnich, R.D., 1996, "Vertebral Fracture Epidemiology," Bone, **18**, pp. S179 – S183.

Watts, N.B., Harris, S.T., and Genant, H.K., 2001, "Treatment of Painful Osteoporotic Vertebral Fracture with Percutaneous Vertebroplasty or Kyphoplasty," Osteoporos. Int., **12**, pp. 429–437.

Weber, M., Hasler, P., and Gerber, H., 1993, "Insufficiency Fractures of the Sacrum, Twenty Cases and Review of the Literature," SPINE, **18**(16), pp. 2507-2512.

Wilcox, R.K., 2004, “The Biomechanics of Vertebroplasty: A Review,” Proc. Inst. Mech. Eng. [H], **218**(1), pp. 1-10.

Williams, P.L., Warwick, R., Dyson, M., and Bannister, L.H. (eds.), 1989, *Gray’s Anatomy, 37th Edition*, Churchill Livingstone, New York.

World Health Organization Study Group, 1994, “Assessment of Fracture Risk and its Application to Screening for Postmenopausal Osteoporosis,” WHO Technical Report Series 843, Geneva.

Zannoni, C., Mantovani, R., and Viceconti, M., 1998, “Material Properties Assignment to Finite Element Models of Bone Structures: A New Method,” Med. Eng. Phys., **20**(10), pp. 735–40.

Appendix 1: Bonemat Parameter File

The Bonemat parameter file is a text file called "param_file.txt" that contains inputs to the Bonemat program. This appendix shows an example of the parameter file with line-by-line explanation:

```
mesh.out image.vtk newmesh.out materials.frq
120 0.15 200 1.7
2
1E6  0.981      0 2875    3
0.981    0      0 2818 1.96
100
4
```

1) Lists four filenames in this order: input FE mesh, input CT image, output mesh with materials added, output text file listing the material values created.

2) Lists two points to define the CT brightness - bone density line in the order CT 1, Density 1, CT 2, Density 2. The different values used are:

Image Male Post 03, normal density:	120	0.15	200	1.7
Image Male Post 03, osteoporotic:	120	0.105	200	1.19
Image Pelvis Post 05, normal density:	130	0.345	200	1.7
Image Pelvis Post 05, osteoporotic:	130	0.2415	200	1.19

3) Number of density – elastic modulus equations used.

4, 5) Define density – elastic modulus equations. For example,

```
1E6  0.981     0   2875    3
```

means between densities of 1E6 and 0.981, modulus = 0 + 2875*density^3.

6) Modulus step size: controls spacing of elastic moduli created.

7) Order of numerical integration to be used.

Appendix 2: Model Material Properties

Each elastic modulus applied to the various models is listed, along with the number and percentage elements it was applied to.

Model MP3 – 1, Non-homogeneous, Normal Density, With Cement

Modulus (MPa)	# Elements	%
31.775	53	0.07%
135.28	1628	2.11%
235.35	9327	12.08%
335.35	13694	17.74%
435.36	12960	16.78%
535.36	9492	12.29%
635.37	6925	8.97%
735.38	4759	6.16%
835.38	3482	4.51%
935.52	2642	3.42%
1035.5	2033	2.63%
1135.6	1651	2.14%
1235.6	1306	1.69%
1335.6	1009	1.31%
1435.7	819	1.06%
1535.8	649	0.84%
1636	594	0.77%
1736.5	517	0.67%
1836.5	459	0.59%
1937	351	0.45%
2037.6	307	0.40%
2138.3	288	0.37%
2238.6	242	0.31%
2339.3	194	0.25%
2440.4	190	0.25%
2540.5	806	1.04%
2640.5	113	0.15%
2741.1	99	0.13%
2841.2	46	0.06%
2941.7	41	0.05%
3042.4	40	0.05%
3147.9	33	0.04%
3250.8	36	0.05%
3351.2	35	0.05%
3451.9	29	0.04%

Modulus (MPa)	# Elements	%
3553.6	30	0.04%
3655.9	20	0.03%
3763.3	22	0.03%
3863.9	26	0.03%
3966.3	30	0.04%
4067.2	22	0.03%
4174	25	0.03%
4274.7	22	0.03%
4379.7	21	0.03%
4486	10	0.01%
4590.2	14	0.02%
4697	12	0.02%
4801	8	0.01%
4922.7	15	0.02%
5023.9	9	0.01%
5129.7	8	0.01%
5238.5	11	0.01%
5341.6	13	0.02%
5442.1	4	0.01%
5551.3	5	0.01%
5674	7	0.01%
5797.7	8	0.01%
5900.2	3	0.00%
6009.6	6	0.01%
6127.4	4	0.01%
6231.9	2	0.00%
6427.4	1	0.00%
6587.6	1	0.00%
6718	1	0.00%
6940.5	1	0.00%
7717.5	1	0.00%
8166.2	2	0.00%
11843	1	0.00%
14662	1	0.00%

Model MP3 – 2, Non-homogeneous, Osteoporotic, With Cement

Modulus (MPa)	# Elements	%
4.35	47	0.06%
105.74	8162	10.57%
205.75	27032	35.01%
305.75	17639	22.84%
405.76	8848	11.46%
505.76	4941	6.40%
605.84	3084	3.99%
705.85	1914	2.48%
805.86	1271	1.65%
906.24	1004	1.30%
1006.40	672	0.87%
1106.60	545	0.71%
1206.70	393	0.51%

Modulus (MPa)	# Elements	%
1306.70	272	0.35%
1406.90	205	0.27%
1506.90	130	0.17%
1610.00	137	0.18%
1710.80	107	0.14%
1810.90	97	0.13%
1911.70	81	0.10%
2013.00	58	0.08%
2113.70	58	0.08%
2214.90	36	0.05%
2321.90	39	0.05%
2438.70	442	0.57%
2566.10	1	0.00%

Model MP3 – 3, Non-homogeneous, Normal Density, No Cement

Modulus (MPa)	# Elements	%
31.775	53	0.07%
135.28	1628	2.11%
235.35	9327	12.08%
335.35	14730	19.08%
435.36	12960	16.78%
535.36	9492	12.29%
635.37	6925	8.97%
735.38	4759	6.16%
835.38	3482	4.51%
935.52	2642	3.42%
1035.5	2033	2.63%
1135.6	1651	2.14%
1235.6	1306	1.69%
1335.6	956	1.24%
1435.7	771	1.00%
1535.8	603	0.78%
1636	561	0.73%
1736.5	477	0.62%
1836.5	434	0.56%
1937	328	0.42%
2037.6	292	0.38%
2138.3	261	0.34%
2238.6	230	0.30%
2339.3	183	0.24%
2440.4	170	0.22%
2540.5	123	0.16%
2640.5	113	0.15%
2741.1	99	0.13%
2841.2	46	0.06%
2941.7	41	0.05%
3042.4	40	0.05%
3147.9	33	0.04%
3250.8	36	0.05%
3351.2	35	0.05%
3451.9	29	0.04%

Modulus (MPa)	# Elements	%
3553.6	30	0.04%
3655.9	20	0.03%
3763.3	22	0.03%
3863.9	26	0.03%
3966.3	30	0.04%
4067.2	22	0.03%
4174	25	0.03%
4274.7	22	0.03%
4379.7	21	0.03%
4486	10	0.01%
4590.2	14	0.02%
4697	12	0.02%
4801	8	0.01%
4922.7	15	0.02%
5023.9	9	0.01%
5129.7	8	0.01%
5238.5	11	0.01%
5341.6	13	0.02%
5442.1	4	0.01%
5551.3	5	0.01%
5674	7	0.01%
5797.7	8	0.01%
5900.2	3	0.00%
6009.6	6	0.01%
6127.4	4	0.01%
6231.9	2	0.00%
6427.4	1	0.00%
6587.6	1	0.00%
6718	1	0.00%
6940.5	1	0.00%
7717.5	1	0.00%
8166.2	2	0.00%
11843	1	0.00%
14662	1	0.00%

Model MP3 – 4, Non-homogeneous, Osteoporotic, No Cement

Modulus (MPa)	# Elements	%
4.35	47	0.06%
105.74	8162	10.57%
205.75	27845	36.06%
305.75	17639	22.84%
405.76	8848	11.46%
505.76	4941	6.40%
605.84	3084	3.99%
705.85	1914	2.48%
805.86	1271	1.65%
906.24	1004	1.30%
1006.40	632	0.82%
1106.60	504	0.65%
1206.70	360	0.47%

Modulus (MPa)	# Elements	%
1306.70	242	0.31%
1406.90	175	0.23%
1506.90	113	0.15%
1610.00	107	0.14%
1710.80	78	0.10%
1810.90	84	0.11%
1911.70	53	0.07%
2013.00	36	0.05%
2113.70	36	0.05%
2214.90	22	0.03%
2321.90	15	0.02%
2438.70	2	0.00%
2566.10	1	0.00%

Model MP3 – 5, Homogeneous, Normal Density, With Cement

Modulus (MPa)	# Elements	%
664.45	76534	99.12%
2540.5	681	0.88%

Model MP3 – 6, Homogeneous, Osteoporotic, With Cement

Modulus (MPa)	# Elements	%
361.05	76534	99.12%
2438.70	681	0.88%

Model MP3 – 7, Homogeneous, Normal Density, No Cement

Modulus (MPa)	# Elements	%
664.45	77215	100.00%

Model MP3 – 8, Homogeneous, Osteoporotic, No Cement

Modulus (MPa)	# Elements	%
361.05	77215	100.00%

Model MP3 – 9, Homogeneous, Normal Density, No Cement

Modulus (MPa)	# Elements	%
664.45	241462	100.00%

Model MP3 – 10, Homgeneous, Normal Density, No Cement

Modulus (MPa)	# Elements	%
664.45	596472	100.00%

Model PP5 – 1, Non-homogeneous, Normal Density, With Cement

Modulus (MPa)	# Elements	%
36.482	160	0.24%
136.67	304	0.45%
236.74	5564	8.17%
336.75	13122	19.28%
436.76	10536	15.48%
536.79	7715	11.33%
636.79	5946	8.73%
736.82	4684	6.88%
836.84	3495	5.13%
936.86	2646	3.89%
1036.9	2003	2.94%
1137.1	1484	2.18%
1237.1	1264	1.86%
1337.2	984	1.45%
1437.3	848	1.25%
1537.4	689	1.01%
1637.4	622	0.91%
1737.5	519	0.76%
1837.5	502	0.74%
1937.6	480	0.71%
2037.9	388	0.57%
2138.1	354	0.52%
2238.2	318	0.47%
2338.3	285	0.42%
2438.4	274	0.40%
2538.5	1176	1.73%
2640.1	207	0.30%
2740.8	154	0.23%
2841.3	127	0.19%
2942	96	0.14%
3042.1	98	0.14%
3142.3	108	0.16%
3242.9	62	0.09%
3345.3	73	0.11%
3447.9	52	0.08%

Modulus (MPa)	# Elements	%
3548.2	61	0.09%
3651.8	57	0.08%
3754	59	0.09%
3854.4	44	0.06%
3957.6	41	0.06%
4057.8	42	0.06%
4164.5	34	0.05%
4266.5	35	0.05%
4366.6	38	0.06%
4469.1	31	0.05%
4570	21	0.03%
4676.9	26	0.04%
4791.8	30	0.04%
4891.9	23	0.03%
4992.8	18	0.03%
5097.1	25	0.04%
5205.3	25	0.04%
5305.5	15	0.02%
5406.8	16	0.02%
5513.3	13	0.02%
5615.8	14	0.02%
5720.4	12	0.02%
5833.1	13	0.02%
5950.2	7	0.01%
6053.9	6	0.01%
6158.5	4	0.01%
6274.4	8	0.01%
6382.5	4	0.01%
6510.5	4	0.01%
6612.7	1	0.00%
6742.5	2	0.00%
6872.2	1	0.00%
7010	2	0.00%
7129.1	1	0.00%
7236.2	1	0.00%

Model PP5 – 2, Non-homogeneous, Osteoporotic, With Cement

Modulus (MPa)	# Elements	%
60.094	328	0.48%
160.35	16964	24.92%
260.36	19169	28.16%
360.36	11087	16.29%
460.36	6377	9.37%
560.42	3593	5.28%
660.44	2312	3.40%
760.52	1566	2.30%
860.59	1168	1.72%
960.61	980	1.44%
1060.7	749	1.10%
1160.8	618	0.91%
1261.1	495	0.73%
1361.2	457	0.67%
1461.4	402	0.59%
1561.6	302	0.44%

Modulus (MPa)	# Elements	%
1661.6	243	0.36%
1761.9	185	0.27%
1862.2	155	0.23%
1962.4	134	0.20%
2062.5	108	0.16%
2163.8	86	0.13%
2264.4	64	0.09%
2367.2	35	0.05%
2469.4	484	0.71%
2571.1	4	0.01%
2677.1	1	0.00%
2890.6	2	0.00%
3431.8	1	0.00%
3882.3	1	0.00%
4456.1	1	0.00%
4937.5	2	0.00%

Model PP5 – 3, Non-homogeneous, Normal Density, No Cement

Modulus (MPa)	# Elements	%
36.482	160	0.24%
136.67	304	0.45%
236.74	5564	8.17%
336.75	14520	21.33%
436.76	10536	15.48%
536.79	7715	11.33%
636.79	5946	8.73%
736.82	4684	6.88%
836.84	3495	5.13%
936.86	2646	3.89%
1036.9	2003	2.94%
1137.1	1484	2.18%
1237.1	1264	1.86%
1337.2	984	1.45%
1437.3	785	1.15%
1537.4	609	0.89%
1637.4	563	0.83%
1737.5	462	0.68%
1837.5	460	0.68%
1937.6	433	0.64%
2037.9	342	0.50%
2138.1	309	0.45%
2238.2	290	0.43%
2338.3	253	0.37%
2438.4	246	0.36%
2538.5	307	0.45%
2640.1	207	0.30%
2740.8	154	0.23%
2841.3	126	0.19%
2942	96	0.14%
3042.1	98	0.14%
3142.3	107	0.16%
3242.9	62	0.09%
3345.3	73	0.11%
3447.9	52	0.08%

Modulus (MPa)	# Elements	%
3548.2	61	0.09%
3651.8	57	0.08%
3754	59	0.09%
3854.4	44	0.06%
3957.6	41	0.06%
4057.8	42	0.06%
4164.5	34	0.05%
4266.5	35	0.05%
4366.6	38	0.06%
4469.1	31	0.05%
4570	21	0.03%
4676.9	26	0.04%
4791.8	30	0.04%
4891.9	23	0.03%
4992.8	18	0.03%
5097.1	25	0.04%
5205.3	25	0.04%
5305.5	15	0.02%
5406.8	16	0.02%
5513.3	13	0.02%
5615.8	14	0.02%
5720.4	12	0.02%
5833.1	13	0.02%
5950.2	7	0.01%
6053.9	6	0.01%
6158.5	4	0.01%
6274.4	8	0.01%
6382.5	4	0.01%
6510.5	4	0.01%
6612.7	1	0.00%
6742.5	2	0.00%
6872.2	1	0.00%
7010	2	0.00%
7129.1	1	0.00%
7236.2	1	0.00%

Model PP5 – 4, Non-homogeneous, Osteoporotic, No Cement

Modulus (MPa)	# Elements	%
60.094	328	0.48%
160.35	16964	24.92%
260.36	20104	29.53%
360.36	11087	16.29%
460.36	6377	9.37%
560.42	3593	5.28%
660.44	2312	3.40%
760.52	1566	2.30%
860.59	1168	1.72%
960.61	980	1.44%
1060.7	749	1.10%
1160.8	618	0.91%
1261.1	427	0.63%
1361.2	399	0.59%
1461.4	349	0.51%
1561.6	250	0.37%

Modulus (MPa)	# Elements	%
1661.6	202	0.30%
1761.9	150	0.22%
1862.2	127	0.19%
1962.4	100	0.15%
2062.5	84	0.12%
2163.8	58	0.09%
2264.4	40	0.06%
2367.2	20	0.03%
2469.4	9	0.01%
2571.1	4	0.01%
2677.1	1	0.00%
2890.6	2	0.00%
3431.8	1	0.00%
3882.3	1	0.00%
4456.1	1	0.00%
4937.5	2	0.00%

Model PP5 – 5, Homogeneous, Normal Density, With Cement

Modulus (MPa)	# Elements	%
772.71	67183	98.69%
2538.5	890	1.31%

Model PP5 – 6, Homogeneous, Osteoporotic, With Cement

Modulus (MPa)	# Elements	%
415.8852	67183	98.69%
2469.4	890	1.31%

Model PP5 – 7, Homogeneous, Normal Density, No Cement

Modulus (MPa)	# Elements	%
772.71	68073	100.00%

Model PP5 – 8, Homogeneous, Osteoporotic, No Cement

Modulus (MPa)	# Elements	%
415.8852	68073	100.00%

Appendix 3: Results of Model Comparisons

This appendix presents results from the different model comparisons made in the study. Maximum principal, minimum principal, and maximum shear strains are compared in each region of interest. The mean and maximum values of strain in the ROI are presented, along with the comparison RMS_{Diff} value.

Comparisons made in Convergence Test

		Left ROI			Right ROI		
	Strain	Max Princ.	Min. Princ.	Max. Shear	Max Princ.	Min. Princ.	Max. Shear
Comparison 1:							
Fine	Mean	3.42E-04	-5.52E-04	4.47E-04	3.39E-04	-3.80E-04	3.59E-04
(MP3-9)	Max	4.29E-04	-8.50E-04	6.38E-04	4.06E-04	-5.78E-04	4.68E-04
Normal	Mean	3.35E-04	-5.51E-04	4.43E-04	3.33E-04	-3.84E-04	3.58E-04
(MP3-7)	Max	4.25E-04	-8.63E-04	6.43E-04	4.05E-04	-5.90E-04	4.76E-04
	RMS_{Diff}	6.16%	2.66%	3.27%	2.48%	2.71%	1.73%
Comparison 2:							
Very Fine	Mean	3.31E-04	-5.50E-04	4.40E-04	3.36E-04	-3.74E-04	3.55E-04
(MP3-10)	Max	4.17E-04	-8.70E-04	6.43E-04	4.11E-04	-5.87E-04	4.72E-04
Fine	Mean	3.42E-04	-5.52E-04	4.47E-04	3.39E-04	-3.80E-04	3.59E-04
(MP3-9)	Max	4.29E-04	-8.50E-04	6.38E-04	4.06E-04	-5.78E-04	4.68E-04
	RMS_{Diff}	5.49%	2.56%	2.87%	1.78%	3.27%	2.08%
Comparison 3:							
Very Fine	Mean	3.31E-04	-5.50E-04	4.40E-04	3.36E-04	-3.74E-04	3.55E-04
(MP3-10)	Max	4.17E-04	-8.70E-04	6.43E-04	4.11E-04	-5.87E-04	4.72E-04
Normal	Mean	3.35E-04	-5.51E-04	4.43E-04	3.33E-04	-3.84E-04	3.58E-04
(MP3-7)	Max	4.25E-04	-8.63E-04	6.43E-04	4.05E-04	-5.90E-04	4.76E-04
	RMS_{Diff}	6.97%	3.05%	3.19%	2.33%	4.13%	2.10%

Comparisons between Non-homogeneous (NH) and Homogeneous (H) Models

		Left ROI			Right ROI		
	Strain	Max Princ.	Min. Princ.	Max. Shear	Max Princ.	Min. Princ.	Max. Shear
Comparison 1: Normal Density, With Cement							
NH	Mean	1.97E-04	-2.76E-04	2.37E-04	2.89E-04	-3.26E-04	3.08E-04
(MP3-1)	Max	4.75E-04	-7.98E-04	5.69E-04	5.17E-04	-5.93E-04	5.09E-04
H	Mean	2.21E-04	-3.26E-04	2.73E-04	2.69E-04	-3.06E-04	2.88E-04
(MP3-5)	Max	3.47E-04	-6.61E-04	4.96E-04	3.74E-04	-4.96E-04	4.14E-04
	RMS_{Diff}	18.14%	27.96%	23.47%	15.97%	20.09%	17.60%
Comparison 2: Osteoporotic, With Cement							
NH	Mean	3.28E-04	-4.57E-04	3.93E-04	4.87E-04	-5.65E-04	5.26E-04
(MP3-2)	Max	8.94E-04	-1.48E-03	1.07E-03	9.29E-04	-1.03E-03	8.86E-04
H	Mean	3.44E-04	-5.03E-04	4.23E-04	4.33E-04	-5.06E-04	4.70E-04
(MP3-6)	Max	6.47E-04	-1.22E-03	9.16E-04	6.32E-04	-8.52E-04	7.11E-04
	RMS_{Diff}	11.79%	17.90%	14.99%	15.16%	18.00%	16.34%
Comparison 3: Normal Density, No Cement							
NH	Mean	4.51E-04	-6.05E-04	5.28E-04	4.74E-04	-5.03E-04	4.89E-04
(MP3-3)	Max	5.29E-04	-9.72E-04	7.51E-04	5.41E-04	-7.42E-04	6.41E-04
H	Mean	3.34E-04	-5.21E-04	4.27E-04	3.59E-04	-3.91E-04	3.75E-04
(MP3-7)	Max	3.99E-04	-7.61E-04	5.72E-04	4.38E-04	-5.76E-04	4.79E-04
	RMS_{Diff}	26.60%	18.92%	20.46%	25.37%	24.64%	24.86%
Comparison 4: Osteoporotic, No Cement							
NH	Mean	7.28E-04	-1.03E-03	8.77E-04	7.88E-04	-8.57E-04	8.23E-04
(MP3-4)	Max	8.68E-04	-1.63E-03	1.25E-03	9.43E-04	-1.32E-03	1.13E-03
H	Mean	6.14E-04	-9.59E-04	7.86E-04	6.61E-04	-7.20E-04	6.91E-04
(MP3-8)	Max	7.34E-04	-1.40E-03	1.05E-03	8.07E-04	-1.06E-03	8.82E-04
	RMS_{Diff}	16.88%	15.96%	13.94%	18.57%	20.66%	19.36%
Comparison 5: Normal Density, With Cement							
NH	Mean	2.29E-04	-2.66E-04	2.48E-04	3.70E-04	-7.27E-04	5.48E-04
(PP5-1)	Max	3.64E-04	-5.01E-04	4.09E-04	7.92E-04	-1.80E-03	1.28E-03
H	Mean	2.01E-04	-2.80E-04	2.40E-04	3.13E-04	-6.39E-04	4.76E-04
(PP5-5)	Max	3.35E-04	-6.03E-04	4.69E-04	6.52E-04	-1.49E-03	1.07E-03
	RMS_{Diff}	16.31%	14.26%	12.74%	15.61%	12.69%	13.46%
Comparison 6: Osteoporotic, With Cement							
NH	Mean	3.76E-04	-4.13E-04	3.94E-04	6.18E-04	-1.25E-03	9.36E-04
(PP5-2)	Max	6.52E-04	-8.03E-04	6.45E-04	1.42E-03	-3.31E-03	2.34E-03
H	Mean	3.15E-04	-3.89E-04	3.52E-04	5.05E-04	-1.07E-03	7.89E-04
(PP5-6)	Max	5.00E-04	-8.44E-04	6.72E-04	1.17E-03	-2.74E-03	1.96E-03
	RMS_{Diff}	17.42%	12.28%	14.38%	17.94%	13.88%	15.13%
Comparison 7: Normal Density, No Cement							
NH	Mean	4.47E-04	-6.78E-04	5.63E-04	6.19E-04	-1.07E-03	8.43E-04
(PP5-3)	Max	7.18E-04	-1.24E-03	9.77E-04	8.76E-04	-1.86E-03	1.35E-03
H	Mean	2.81E-04	-4.63E-04	3.72E-04	4.09E-04	-7.64E-04	5.86E-04
(PP5-7)	Max	4.91E-04	-9.24E-04	7.08E-04	6.93E-04	-1.52E-03	1.11E-03
	RMS_{Diff}	37.03%	31.73%	33.80%	35.40%	31.21%	32.80%
Comparison 8: Osteoporotic, No Cement							
NH	Mean	6.58E-04	-9.33E-04	7.95E-04	9.74E-04	-1.72E-03	1.35E-03
(PP5-4)	Max	9.75E-04	-1.67E-03	1.32E-03	1.56E-03	-3.44E-03	2.47E-03
H	Mean	5.21E-04	-8.61E-04	6.91E-04	7.60E-04	-1.42E-03	1.09E-03
(PP5-8)	Max	9.13E-04	-1.72E-03	1.32E-03	1.29E-03	-2.83E-03	2.06E-03
	RMS_{Diff}	22.47%	11.89%	16.12%	22.97%	18.48%	20.21%

Comparisons between Normal Density and Osteoporotic Models

		Left ROI			Right ROI		
Strain		Max Princ.	Min. Princ.	Max. Shear	Max Princ.	Min. Princ.	Max. Shear
Comparison 1: Non-homogeneous, With Cement							
Normal	Mean	1.97E-04	-2.76E-04	2.37E-04	2.89E-04	-3.26E-04	3.08E-04
(MP3-1)	Max	4.75E-04	-7.98E-04	5.69E-04	5.17E-04	-5.93E-04	5.09E-04
Osteo.	Mean	3.28E-04	-4.57E-04	3.93E-04	4.87E-04	-5.65E-04	5.26E-04
(MP3-2)	Max	8.94E-04	-1.48E-03	1.07E-03	9.29E-04	-1.03E-03	8.86E-04
	RMS_{Diff}	64.10%	64.60%	64.22%	66.86%	71.69%	69.44%
Comparison 2: Non-homogeneous, No Cement							
Normal	Mean	4.51E-04	-6.05E-04	5.28E-04	4.74E-04	-5.03E-04	4.89E-04
(MP3-3)	Max	5.29E-04	-9.72E-04	7.51E-04	5.41E-04	-7.42E-04	6.41E-04
Osteo.	Mean	7.28E-04	-1.03E-03	8.77E-04	7.88E-04	-8.57E-04	8.23E-04
(MP3-4)	Max	8.68E-04	-1.63E-03	1.25E-03	9.43E-04	-1.32E-03	1.13E-03
	RMS_{Diff}	61.46%	68.78%	65.68%	66.46%	69.93%	68.23%
Comparison 3: Homogeneous, With Cement							
Normal	Mean	2.21E-04	-3.26E-04	2.73E-04	2.69E-04	-3.06E-04	2.88E-04
(MP3-5)	Max	3.47E-04	-6.61E-04	4.96E-04	3.74E-04	-4.96E-04	4.14E-04
Osteo.	Mean	3.44E-04	-5.03E-04	4.23E-04	4.33E-04	-5.06E-04	4.70E-04
(MP3-6)	Max	6.47E-04	-1.22E-03	9.16E-04	6.32E-04	-8.52E-04	7.11E-04
	RMS_{Diff}	54.50%	53.71%	53.83%	60.71%	65.63%	63.31%
Comparison 4: Homogeneous, No Cement							
Normal	Mean	3.34E-04	-5.21E-04	4.27E-04	3.59E-04	-3.91E-04	3.75E-04
(MP3-7)	Max	3.99E-04	-7.61E-04	5.72E-04	4.38E-04	-5.76E-04	4.79E-04
Osteo.	Mean	6.14E-04	-9.59E-04	7.86E-04	6.61E-04	-7.20E-04	6.91E-04
(MP3-8)	Max	7.34E-04	-1.40E-03	1.05E-03	8.07E-04	-1.06E-03	8.82E-04
	RMS_{Diff}	84.03%	84.03%	84.03%	84.03%	84.03%	84.03%
Comparison 5: Non-homogeneous, With Cement							
Normal	Mean	2.29E-04	-2.66E-04	2.48E-04	3.70E-04	-7.27E-04	5.48E-04
(PP5-1)	Max	3.64E-04	-5.01E-04	4.09E-04	7.92E-04	-1.80E-03	1.28E-03
Osteo.	Mean	3.76E-04	-4.13E-04	3.94E-04	6.18E-04	-1.25E-03	9.36E-04
(PP5-2)	Max	6.52E-04	-8.03E-04	6.45E-04	1.42E-03	-3.31E-03	2.34E-03
	RMS_{Diff}	63.49%	58.46%	60.79%	63.08%	66.56%	65.37%
Comparison 6: Non-homogeneous, No Cement							
Normal	Mean	4.47E-04	-6.78E-04	5.63E-04	6.19E-04	-1.07E-03	8.43E-04
(PP5-3)	Max	7.18E-04	-1.24E-03	9.77E-04	8.76E-04	-1.86E-03	1.35E-03
Osteo.	Mean	6.58E-04	-9.33E-04	7.95E-04	9.74E-04	-1.72E-03	1.35E-03
(PP5-4)	Max	9.75E-04	-1.67E-03	1.32E-03	1.56E-03	-3.44E-03	2.47E-03
	RMS_{Diff}	52.36%	38.97%	44.99%	57.98%	59.67%	59.10%
Comparison 7: Homogeneous, With Cement							
Normal	Mean	2.01E-04	-2.80E-04	2.40E-04	3.13E-04	-6.39E-04	4.76E-04
(PP5-5)	Max	3.35E-04	-6.03E-04	4.69E-04	6.52E-04	-1.49E-03	1.07E-03
Osteo.	Mean	3.15E-04	-3.89E-04	3.52E-04	5.05E-04	-1.07E-03	7.89E-04
(PP5-6)	Max	5.00E-04	-8.44E-04	6.72E-04	1.17E-03	-2.74E-03	1.96E-03
	RMS_{Diff}	58.22%	43.09%	50.30%	58.25%	62.68%	61.18%
Comparison 8: Homogeneous, No Cement							
Normal	Mean	2.81E-04	-4.63E-04	3.72E-04	4.09E-04	-7.64E-04	5.86E-04
(PP5-7)	Max	4.91E-04	-9.24E-04	7.08E-04	6.93E-04	-1.52E-03	1.11E-03
Osteo.	Mean	5.21E-04	-8.61E-04	6.91E-04	7.60E-04	-1.42E-03	1.09E-03
(PP5-8)	Max	9.13E-04	-1.72E-03	1.32E-03	1.29E-03	-2.83E-03	2.06E-03
	RMS_{Diff}	85.80%	85.80%	85.80%	85.80%	85.80%	85.80%

Comparisons between Models Without (NC) and With (C) Cement

		Left ROI			Right ROI		
	Strain	Max Princ.	Min. Princ.	Max. Shear	Max Princ.	Min. Princ.	Max. Shear
Comparison 1: Non-homogeneous, Normal Density							
NC	Mean	4.51E-04	-6.05E-04	5.28E-04	4.74E-04	-5.03E-04	4.89E-04
(MP3-3)	Max	5.29E-04	-9.72E-04	7.51E-04	5.41E-04	-7.42E-04	6.41E-04
C	Mean	1.97E-04	-2.76E-04	2.37E-04	2.89E-04	-3.26E-04	3.08E-04
(MP3-1)	Max	4.75E-04	-7.98E-04	5.69E-04	5.17E-04	-5.93E-04	5.09E-04
	RMS_{Diff}	57.84%	56.39%	56.84%	42.27%	40.03%	40.72%
Comparison 2: Non-homgeneous, Osteoporotic							
NC	Mean	7.28E-04	-1.03E-03	8.77E-04	7.88E-04	-8.57E-04	8.23E-04
(MP3-4)	Max	8.68E-04	-1.63E-03	1.25E-03	9.43E-04	-1.32E-03	1.13E-03
C	Mean	3.28E-04	-4.57E-04	3.93E-04	4.87E-04	-5.65E-04	5.26E-04
(MP3-2)	Max	8.94E-04	-1.48E-03	1.07E-03	9.29E-04	-1.03E-03	8.86E-04
	RMS_{Diff}	57.69%	58.09%	57.78%	42.58%	40.30%	40.98%
Comparison 3: Homgeneous, Normal Density							
NC	Mean	3.34E-04	-5.21E-04	4.27E-04	3.59E-04	-3.91E-04	3.75E-04
(MP3-7)	Max	3.99E-04	-7.61E-04	5.72E-04	4.38E-04	-5.76E-04	4.79E-04
C	Mean	2.21E-04	-3.26E-04	2.73E-04	2.69E-04	-3.06E-04	2.88E-04
(MP3-5)	Max	3.47E-04	-6.61E-04	4.96E-04	3.74E-04	-4.96E-04	4.14E-04
	RMS_{Diff}	36.87%	40.77%	39.07%	27.32%	25.51%	26.05%
Comparison 4: Homogeous, Osteoporotic							
NC	Mean	6.14E-04	-9.59E-04	7.86E-04	6.61E-04	-7.20E-04	6.91E-04
(MP3-8)	Max	7.34E-04	-1.40E-03	1.05E-03	8.07E-04	-1.06E-03	8.82E-04
C	Mean	3.44E-04	-5.03E-04	4.23E-04	4.33E-04	-5.06E-04	4.70E-04
(MP3-6)	Max	6.47E-04	-1.22E-03	9.16E-04	6.32E-04	-8.52E-04	7.11E-04
	RMS_{Diff}	47.69%	51.66%	49.98%	37.36%	34.40%	35.46%
Comparison 5: Non-homogeneous, Normal Density							
NC	Mean	4.47E-04	-6.78E-04	5.63E-04	6.19E-04	-1.07E-03	8.43E-04
(PP5-3)	Max	7.18E-04	-1.24E-03	9.77E-04	8.76E-04	-1.86E-03	1.35E-03
C	Mean	2.29E-04	-2.66E-04	2.48E-04	3.70E-04	-7.27E-04	5.48E-04
(PP5-1)	Max	3.64E-04	-5.01E-04	4.09E-04	7.92E-04	-1.80E-03	1.28E-03
	RMS_{Diff}	49.08%	59.56%	54.41%	45.85%	42.15%	43.44%
Comparison 6: Non-homogeneous, Osteoporotic							
NC	Mean	6.58E-04	-9.33E-04	7.95E-04	9.74E-04	-1.72E-03	1.35E-03
(PP5-4)	Max	9.75E-04	-1.67E-03	1.32E-03	1.56E-03	-3.44E-03	2.47E-03
C	Mean	3.76E-04	-4.13E-04	3.94E-04	6.18E-04	-1.25E-03	9.36E-04
(PP5-2)	Max	6.52E-04	-8.03E-04	6.45E-04	1.42E-03	-3.31E-03	2.34E-03
	RMS_{Diff}	44.65%	54.40%	49.79%	44.76%	40.23%	41.88%
Comparison 7: Homogeneous, Normal Density							
NC	Mean	2.81E-04	-4.63E-04	3.72E-04	4.09E-04	-7.64E-04	5.86E-04
(PP5-7)	Max	4.91E-04	-9.24E-04	7.08E-04	6.93E-04	-1.52E-03	1.11E-03
C	Mean	2.01E-04	-2.80E-04	2.40E-04	3.13E-04	-6.39E-04	4.76E-04
(PP5-5)	Max	3.35E-04	-6.03E-04	4.69E-04	6.52E-04	-1.49E-03	1.07E-03
	RMS_{Diff}	30.00%	39.62%	35.29%	29.31%	25.00%	26.47%
Comparison 8: Homogeneous, Osteoporotic							
NC	Mean	5.21E-04	-8.61E-04	6.91E-04	7.60E-04	-1.42E-03	1.09E-03
(PP5-8)	Max	9.13E-04	-1.72E-03	1.32E-03	1.29E-03	-2.83E-03	2.06E-03
C	Mean	3.15E-04	-3.89E-04	3.52E-04	5.05E-04	-1.07E-03	7.89E-04
(PP5-6)	Max	5.00E-04	-8.44E-04	6.72E-04	1.17E-03	-2.74E-03	1.96E-03
	RMS_{Diff}	41.60%	54.21%	48.54%	40.68%	35.32%	37.19%

Vita:

Dennis Earl Anderson was born to James and Darla Anderson in Kettering, Ohio in 1980. He spent his childhood in several different parts of the United States, living in Illinois, Oregon, California and Wyoming. In 1998, he graduated from Campion Academy in Loveland, Colorado. The same year, he entered the engineering program at Texas A&M University in College Station, Texas. While at A&M, he participated in the co-operative education program, working for 3M Company. His first exposure to bone biomechanics came from participating in an undergraduate summer research program in 2002. In May of 2003, Dennis graduated from Texas A&M with his Bachelor of Science in Mechanical Engineering and a minor in History. Following graduation, he came to Virginia Tech in Blacksburg, Virginia, and began graduate studies in the Department of Engineering Science and Mechanics. Dennis intends to remain at Virginia Tech for doctoral work.